Energy-based control approaches in human-robot collaborative disassembly

Hjorth, Sebastian

DOI (link to publication from Publisher):
10.54337/aau561827516

Publication date:
2023

Document Version
Publisher's PDF, also known as Version of record

ENERGY-BASED CONTROL APPROACHES IN HUMAN-ROBOT COLLABORATIVE DISASSEMBLY

BY
SEBASTIAN HJORTH

DISSERTATION SUBMITTED 2023

AALBORG UNIVERSITY
DENMARK

Energy-based control approaches in human-robot collaborative disassembly

Ph.D. Dissertation

Sebastian Hjorth

Dissertation submitted July 26, 2023

Dissertation submitted:	July 26, 2023
PhD supervisor::	Assoc. Prof. Dimitris Chrysostomou Aalborg University
PhD committee:	Associate Professor Shahab Heshmati-alamdari Aalborg University
	Senior Research Associate Andrej Gams Jožef Stefan Institute, Slovenia
	Associate Professor, Roel Pieters Tampere University
PhD Series:	Faculty of Engineering and Science, Aalborg University
Department:	Department of Materials and Production

ISSN (online): 2446-1636
ISBN (online): 978-87-7573-663-8

Published by:
Aalborg University Press
Kroghstræde 3
DK – 9220 Aalborg Ø
Phone: +45 99407140
aauf@forlag.aau.dk
forlag.aau.dk

Printed in Denmark by Stibo Complete, 2023

Acknowledgments

My journey in robotics started at Aalborg University as part of the newly opened robotics education in 2014. Back then, I could never have imagined that this would arise to such a passion that I ended up pursuing a PhD.
I would like to thank Prof. Dr. Ole Madsen, who introduced me to this specific PhD position under the guidance of Assoc. Prof. Dr. Dimitrios Chrysostomou; to whom I want to give special thanks for providing me with this unique opportunity, the trust in me, and the guidance during this journey. Thank you for supporting me. A big thank you to my colleagues from AAU's Robotics and Automation Group, who supported me and made the tough days at the office endurable.
My gratitude also goes to Dr. Arash Ajoudani from the Italian Institute of Technology for the unique opportunity to spend seven months at his Human Robot interfaces and physical interaction Lab (HRII-lab). I am honored to be able to work with you in the future; I also want to thank all the members of the HRII-lab for all the support you gave me, the engaging discussion we had, as well as the fun times we had together in and outside of the lab.
I am deeply indebted to my friends Felipe, Odete, Fabri, and Jack, who have been crucial in making this journey a more enjoyable and enriching experience through our friendship. Thank you for being such great friends.
A special thanks goes to Clémence, for your indescribable support, your patients, and for being an anchor point during the final stretch of this journey.
Lastly and most importantly, I want to thank my most significant source of support, motivation, and inspiration, my Dad. *Far, tak for alt!*

Abstract

Climate change and the scarcity of natural resources are forcing us as a society to rethink how we utilize already extracted and manipulated/manufactured resources with the push towards a more efficient usage of our natural resources as well as a sustainable business model, the reuse of already manufactured products that have reached their end-of-life present companies with a multitude of new opportunities and methods to optimize their business.
However, the implementation of such changes also brings challenges with it, especially when it comes to extracting components from end-of-life products in such a way that they can be reintroduced in the production stream. This disassembly process is often impossible for fully automated systems, especially if it comes to non-destructive disassembly. Hence, research has started to focus on human-robot-collaborative solutions.
This PhD thesis focuses on enabling a closer interaction between humans and robots during disassembly tasks. Firstly, a literature review on human-robot collaborative disassembly and its sub-fields was conducted. It discovered various gaps within the current research and presented a framework for evaluating future contributions within this field. Secondly, based on this investigation, the thesis proposes an energy-based method that enables physical human-robot interaction in restricted workspaces through the combination of a Cartesian impedance controller with an artificial potential field approach. Thirdly, the energy-aware Cartesian impedance controller utilized in this method is extended through the introduction of an augmented energy tank to ensure the passivity of the impedance controller as well as compared to control approaches currently used in the field of human-robot collaborative disassembly on a faulty unscrewing task. Lastly, the two previously described approaches were combined and extended by presenting two approaches for ensuring the passivity of control action of the workspace restrictions. Additionally, the two approaches were evaluated on a faulty extraction/separation task.
In summary, the key method of this thesis took basis in energy-based approaches in order to monitor and manipulate the energy stored in the system and exchanged with the environment to facilitate the physical human-robot interaction during human-robot-collaborative disassembly processes.

Resumé

Klimaforandringerne og knapheden på naturressourcer tvinger os som samfund til at gentænke, hvordan vi udnytter allerede udvundne og manipulerede/fremstillede ressourcer med henblik på en mere effektiv udnyttelse af vores naturressourcer samt en bæredygtig forretningsmodel. Genbrug af allerede fremstillede produkter, der har nået deres end-of-life, giver virksomhederne et væld af nye muligheder og metoder til at optimere deres forretning.
Implementeringen af sådanne ændringer bringer dog også udfordringer med sig, især når det kommer til at udvinde komponenter fra udtjente produkter på en sådan måde, at de kan genindføres i produktionsstrømmen. Denne demonteringsproces er ofte umulig for fuldautomatiske systemer, især hvis det kommer til ikke-destruktiv demontering. Derfor er forskningen begyndt at fokusere på menneske-robot-samarbejdsløsninger.
Denne ph.d.-afhandling fokuserer på at muliggøre en tættere interaktion mellem mennesker og robotter under demonteringsopgaver. Først blev der gennemført en litteraturgennemgang om menneske-robot-sam-arbejdet vedrørende demontering og dens underområder. Den opdagede forskellige huller i den aktuelle forskning og præsenterede en ramme til evaluering af fremtidige bidrag inden for feltet. For det andet, baseret på denne undersøgelse, foreslår afhandlingen en energibaseret metode, som muliggør fysisk menneske-robot-interaktion i begrænsede arbejdsområder ved at kombinere en kartesisk impedanscontroller med en kunstig potentialfelttilgang.For det tredje udvides den energibevidste kartesiske impedanscontroller, der anvendes i denne metode. Dette gøres ved at introducere en forstærket energitank for at sikre passiviteten af impedanscontrolleren og sammenligne den med kontrolmetoder, der i øjeblikket anvendes inden for menneske-robot-samarbejdet ved demontering af en defekt udskruningsopgave. Til sidst blev de to tidligere beskrevne tilgange kombineret og udvidet ved at præsentere to metoder til at sikre passiviteten af kontrolhandlingen i arbejdsområdebegrænsninger. Derudover blev de to tilgange evalueret på en defekt ekstraktions-/separationsopgave.
Samlet set tog denne afhandling udgangspunkt i energibaserede tilgange for at overvåge og manipulere den energi, der er lagret i systemet og udvekslet med omgivelserne for at lette den fysiske menneske-robot-interaktion under menneske-robot-samarbejdet i adskillelsesprocesserne.

Thesis Details

Thesis Title:	Energy-based control approaches in human-robot collaborative disassembly
PhD Student:	Sebastian Hjorth
Supervisors:	Assoc. Prof. Dimitrios Chrysostomou, Aalborg University

The main body of this thesis consists of the following papers.

[Paper A | [1]] Hjorth S, Chrysostomou D; Human–robot collaboration in industrial environments: A literature review on non-destructive disassembly (2021) *Robotics and Computer-Integrated Manufacturing*.

[Paper B | [2]] Hjorth S, Lachner J, Stramigioli S, Madsen O, Chrysostomou D; An Energy-based Approach for the Integration of Collaborative Redundant Robots in Restricted Work Environments (2020) *IEEE International Conference on Intelligent Robots and Systems*.

[Paper C | [3]] Hjorth S, Lamon E, Chrysostomou D, Ajoudani A; Design of an Energy-Aware Cartesian Impedance Controller for Collaborative Disassembly (2023) *IEEE International Conference on Robotics and Automation*.

[Paper D | [4]] Hjorth S, Lachner J, Ajoundani A , and Chrysostomou D, Enabling passivity for Cartesian workspace restrictions, Submitted to (2024) *IEEE International Conference on Robotics and Automation*.

In addition to the main papers, the following publication has also been made.

- Mobedi E, Hjorth S, Wansoo K, De Momi E, Tsagarakis N and Ajoudani A, A Power-Aware Control Strategy for an Elbow Effort-Compensation Device, (2023) *IEEE Robotic and Automation Letter*.

The thesis has been presented for evaluation as a partial requirement for obtaining a PhD degree. It relies on the scientific papers mentioned above, which have either been submitted or published. The chapters of the thesis incorporate certain sections directly or indirectly from these papers. In order to assess

the thesis, co-author statements have been provided to the evaluation committee and are accessible to the faculty. It is important to note that the thesis is currently unsuitable for open publication in its current form due to potential copyright concerns.

List of Symbols and Abbreviations

List of Abbreviations

AAU	Aalborg University
CE	circular economy
CEBM	circular economic buisness model
EOL	end-of-life
EOLP	end-of-life product
HRC	human-robot collaboration
HRCD	human-robot collaborative disassembly
HRI	human-robot interaction
pHRI	physical human-robot interaction
TCP	tool-center-point

Contents

CHAPTER 1

General Introduction

1.1 Motivation

As the world's population exponentially grows, consumption rates and the demand for new products also increase dramatically. Climate change and the scarcity of natural resources create one of the biggest challenges, today's society has to face.
To tackle these challenges, it is no longer enough to only focus on improving the efficiency of new products; therefore, it is essential to focus on handling the products when they have reached their end-of-life (EOL). Currently, a great number of EOL products (EOLPs) are continuously being disposed of, leading to several environmental problems [5]; this can be unnecessary since new products from the same company often share the same or slightly modified sub-components with their previous iteration. Hence, responsible EOL treatment, which would be more resource and climate-friendly, focuses on extracting sub-assemblies or components to requalify and remanufacture them such that they can be reused in new products. The assessment done in [6] by Ardente et al. highlighted that the implementation of such a remanufacturing/requalification process might result in (i) a reduction in the production/use of non-environmental friendly chemicals, (ii) decreased energy consumption, (iii) as well as in a more economically viable process than recycling the products' raw materials. This assessment was further supported by the following report from the Ellen MacArthur Foundation [7], where it was highlighted that manufacturing companies that apply a circular economy business model (CEBM) could capitalize on benefits such as:

- substantial net material savings,
- a reduction in exposure to price volatility,
- an increase in economic development,
- an increase in its potential within the areas of innovation and job creation,
- an increase in resilience towards variation in living systems and the economy.

Therefore, as mentioned in [Paper A | [1]] policy providers have discussed and promoted CEBMs in UN- and EU- summits, such as the First Vice-President of the European Commission Frans Timmermans [8], responsible for sustainable development, who said: "Circular economy is key to putting our economy onto a sustainable path and delivering on the global Sustainable Development Goals." An abstract illustration of the concept of this circular economic business model can be seen in Figure 1.1. As previously mentioned, a CEBM provides several benefits for manufacturers; however, it is of the essence that the disassembly process is automated to become a financially viable option.

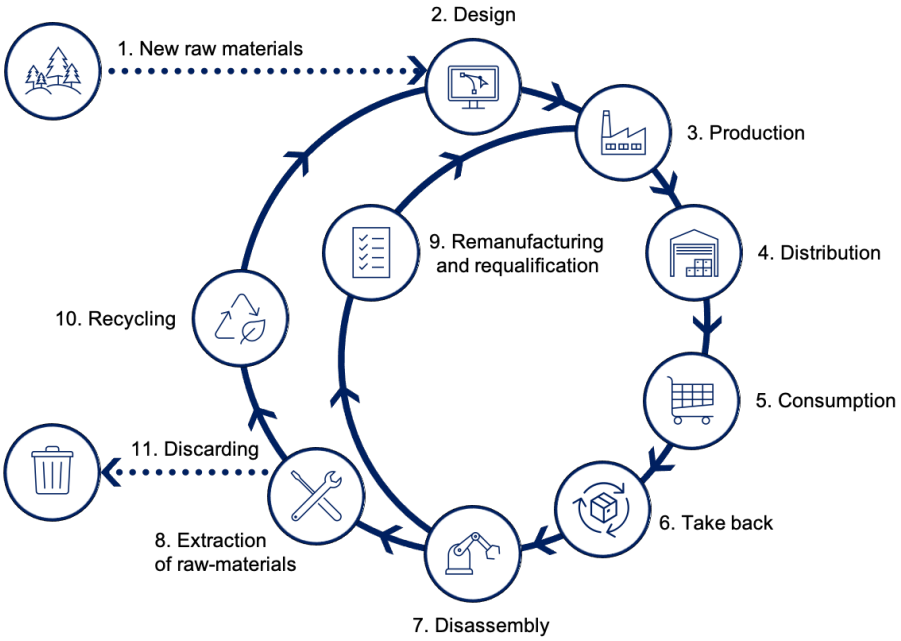

Figure 1.1: Abstract visualization representing the life cycle of resources based on the circular economy business model. Step 1: Introduction of new raw materials into production; Step 2: Sub-component design and manufacturing; Step 3: Production of the final product; Step4: Distribution of the product to customers; Step5: Consumption of the product; Step6: Retrieval of the end-of-life product (EOLP); Step7: Disassembly of the EOLP; Step 8: Extraction of raw materials; Step 9: Remanufacturing and requalification of extracted sub-components; Step 10: Recycling of raw materials; 11: Disposal of non-recyclable raw materials.[Paper A | [1]]

Therefore, one has to look at various technological solutions that enable manufacturers to implement such CEBM. According to [9], one of these technological enablers for the automation of the majority of modern manufacturing processes is the industrial manipulator.
As aforementioned, the general process of disassembling EOLPs in a non-destructive manner such that their sub-components can be reused in new products is desirable due to economic factors. However, it is not as trivial as following their assembly process in reverse order. Even though the main design characteristics of the process itself, such as task definition and task planning, between assembly and disassembly processes are related. This is partially due to how sub-components of a product are joined together (e.g., Snap fittings, gluing, riveting). Hence, robotics disassembly systems utilize various technological enablers, such as image processing, object detection, and decision-making algorithms, to identify and classify not only the product itself but also the product's sub-components and their individual state.
The information collected from these systems is then used to guide the robotic

system during the disassembly of the EOLP. An example of such a system was presented in [10], in which the focus is on the recycling and reuse of cell phones. The robotic disassembly system utilized in this work consisted of a robotic arm, a vision system, and a decision-making system. The latter detects the current state of the cellphone based on the captured images of the vision system and utilizes this information to handle multiple types of uncertainties associated with the cellphone's condition. Besides correctly identifying products, components, and their respective states, another common challenge within disassembly is associated with the extraction of components from their fixtures; during this operation, it can occur that the component gets jammed or wedged and thereby applying unnecessary forces and strain on the components. This can lead to the components getting damaged or even braking and, therefore, being unable to pass the re-qualification process. To address this, researchers [11] have developed methods that utilize active compliance control schemes for the extraction of components. However, as aforementioned, the process of disassembling EOLPs in a non-destructive manner such that their sub-components can be reused in new products is not as trivial as following their assembly process in its reverse order. This is partially due to how subcomponents of a product are joined together (e.g., Snap fittings, gluing, riveting). Additionally, the disassembly processes of EOLPs face a variety of challenges which, according to Elo et al. [12] and Tolio et al. [13], are related but not limited to: (i) high variability in the conditions of post-use parts; (ii) poor information about the returned products; (iii) increasing product complexity; (iv) short life-cycle of products and high product variety; (v) increasing quality requirements on recovered materials and components, (vi) pressure on costs and efficiency. Based on these investigations, it can be seen that the main challenges for a disassembly system are related to the variability and uncertainties of the product state (e.g., the mixture of materials, non-homogeneous materials, component location, and the variation of the structural rigidity of its individual components), making it impossible for a fully automated system to complete the process in an economically viable time or even complete it at all [Paper A | [1]]. Hence, the conclusion can be drawn that it is still necessary to keep humans in the loop when it comes to the non-destructive disassembly of ELOPs.

1.2 Research Questions

The motivation and background described earlier describe the starting point from which the thesis will outline the research questions for this thesis.

The challenges that robotic systems face during the disassembly and especially non-destructive disassembly of EOLPs, are numerous and complex. This complexity can make it time-consuming, if not impossible, for fully automated state-of-the-art robotic setups. Resulting in the introduction of hu-

mans into the disassembly process. However, it was first possible to approach tasks through the collaboration between humans and robots through the commercialization of collaborative-enabled manipulators nearly two decades ago. Hence, the field of human-robot collaborative disassembly (HRCD) is relatively new. Therefore, it is necessary to first evaluate the current state-of-the-art of these HRCD solutions based on the current state of the art of its subfields. To identify the technical challenges associated with implementing a HRCD system. This leads to the first research question tackled in this thesis.

Q1: What are the main technological hurdles HRCD applications face? (Discussed in chapter 3.)

In general, safety is always a concern when it comes to physical human-robot interaction (pHRI); this holds especially true when robotic systems are deployed in physically restricted spaces. Therefore, it should always be possible for human operators to manipulate the execution of the manipulator's task within the manipulators' workspace without compromising their safety. However, in places where the manipulator workspace is physically restricted, there is also a need for virtual Cartesian workspace restrictions to prevent unintended collisions with other machinery or human operators who may not be aware of the manipulator's task. Additionally, there are other constraints, such as singularities, self-collisions, and joint limits, which, if violated, force the manipulator to halt its motion and require a reinitialization of the system. This leads to the second research question tackled in this thesis.

Q2: How can the workspaces of kinematically redundant manipulators be restricted while ensuring safe pHRI? (Discussed in chapter 4.)

Disassembly processes present several challenges for robotic solutions, particularly those associated with product variability and uncertainties. Hence, a possible solution to these challenges are HRCD cells, where the human operator remains in the loop. Due to the increased risk of unpredictable events associated with product variability and uncertainties occurring while the robot works in unstructured environments, safety is paramount in such applications. Consequently, the question arises if energy-aware control strategies are suitable for disassembly tasks and how they perform compared to current control strategies utilized in state-of-the-art disassembly applications. This leads to the third research question tackled in this thesis.

Q3: How does an energy-aware Cartesian Impedance control strategy perform on disassembly tasks? (Discussed in chapter 5).

In robotic solutions incorporating humans in close approximation (i.e., HRCD

cells), safety is paramount due to the increased risk of unpredictable events associated with product variability and uncertainties occurring while the robot works in unstructured environments. Hence, in order to ensure that unintended collisions with other machinery or human operators during collaborative tasks such as HRCD tasks do not occur, virtual workspace restrictions are necessary. However, enforcing such virtual workspace restrictions, especially when excessive forces are acting on the robot, can lead to unstable behavior. Consequently, it is essential to ensure that the system stays passive in order to guarantee the stability of the system when subjected to virtual workspace restrictions. This leads to the forth research question tackled in this thesis.

Q4: How can virtual workspace restrictions be enforced without violating the system's passivity? (Discussed in chapter 6.)

1.3 Thesis outline

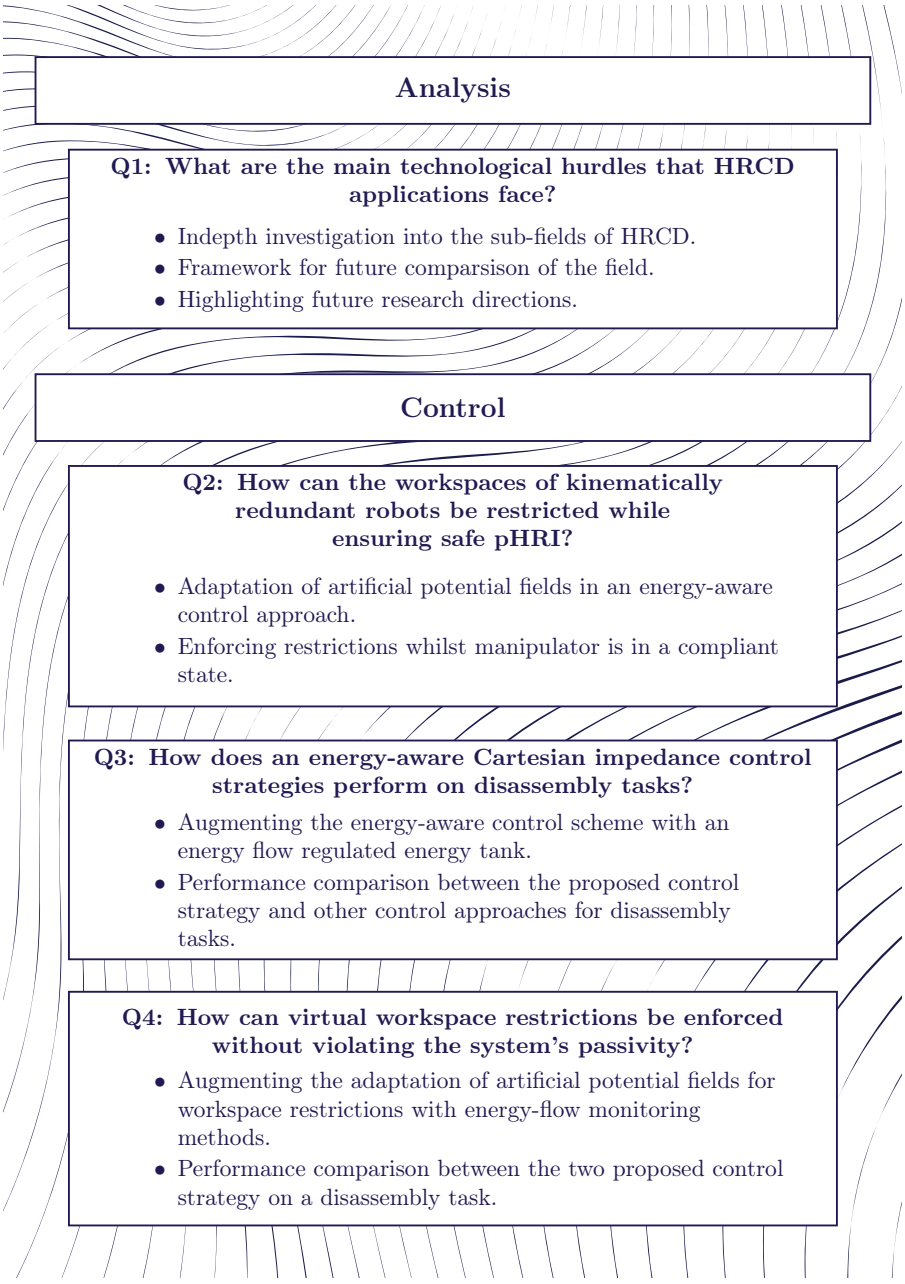

CHAPTER 2

Fundamentals

2.1 Introduction

This chapter aims to provide the reader with a solid understanding of the key concepts related to human-robot collaboration (HRC) and passivity, which will be relevant for the rest of the thesis. Section 2.2 introduces the reader to the various sub-categories of HRC. Additionally, the reader is introduced to the general concept of passivity in section 2.3.

2.2 Human-robot Collaboration

Human-robot collaboration is currently a necessity when it comes to the implementation of non-destructive disassembly processes. Even though the precise interpretation of the term HRC is not defined, HRC generally refers to the working relationship between humans and robots in which they cooperate/collaborate to accomplish a task. From this general definition, it can easily be seen that the implementation of such collaborative tasks incorporates various fields. In order to give the reader a brief overview of the various fields in HRC, this work splits into two main areas: Robot Safety in subsection 2.2.1 and Communication in subsection 2.2.2. In subsection 2.2.1, the reader is first introduced to the relevant ISO standards currently governing the implementation of HRC-application safety as well as giving a general overview of the types of control schemes which enable the various forms of HRC applications. In subsection 2.2.2, an overview of the various ways humans can communicate with robots is presented.

2.2.1 Robot safety

For the safe implementation of robots, the International Organization for Standardization (ISO) created various standards that provide guidelines and requirements with the aim of ensuring their safety and effectiveness. Additionally, the various ISO standards serve the purpose of classifying HRC in a general way and in a robot safety related context. It thereby enables the categorization of the various kinds of collaboration and interaction based on their type (e.g., verbal, non-verbal), severity, as well as control modes. In a manufacturing-based context, the ISO standards ISO 8373 standard [14], ISO 10218-1/2 standard [15, 16], and ISO 15066 standard [17] are the most important ones. The ISO 8373 standard outlines the vocabulary used in the area of HRC. It covers the terms concerning the interaction between humans and robots, control systems, strategies, and other relevant terms related to the robots. The ISO 10218-1/2 standard provides a general description of collaborative-enabled robots, workspaces, and operations. Specifically, it focuses on specifying requirements and limitations for the behavior of robots when interacting with human operators. It also addresses the safety require-

ments that robot systems must meet when applied in an HRC context. Building upon the ISO 10218 standard, the ISO 15066 standard further elaborates on the requirements and guidelines for HRC. It defines the appropriate procedure for restricting speed values to ensure that force and pressure values remain within humans' defined pain sensitivity threshold during collisions with robots. Derived from these specifications, the four-level of control modes *Safety-rated Monitored Speed (SMS)*, *Hand-Guidance (HG)*, *Speed and Separation Monitoring (SSM)* and *Power and Force limitation (PFL)*.

Control strategies

Looking at control strategies from the perspective of human-robot collaboration and safety, one can in general differentiate them based on the following two categories: *pre-collision* and *post-collision control strategies*.

Pre-collision control strategies

The primary objective of pre-collision control strategies is to proactively prevent any detrimental contact between the robot and its surroundings. These strategies adapt the manipulator's motion by adapting its trajectory or velocity based on its distance to autonomous quantities and their behavior with the help of sensory input from, for example camera, laser sensors. Even though pre-collision control schemes enable manipulators to avoid collisions, they can not guarantee that no harmful contact between humans and robots will occur. As pointed out in [18,19], this is due to the fact that predicting the relative motions between the robot and human with exteroceptive sensors can be challenging. Furthermore, solely adjusting the robot's movement may not be adequate for the prevention of the occurrence of (harmful) collisions. Consequently, in order to enable collaboration between humans and robots that occur in close proximity to each other, it is important that contact forces between humans and robots are limited to a desirable ("safe") level. Thus, it is a necessity to implement a post-collision control strategy that has the capability to limit the contact forces between humans and robots to a desirable level.

Post-collision control strategies

In comparison to pre-collision control strategies, post-collision control strategies do not aim to prevent possible contact between humans and robots but rather as pointed out in [20], limit the contact force and the energy exchange between these two entities to a safe limit. In other words, post-collision control strategies refer to control strategies that respond to real-time changes in the manipulator's environment. These schemes are designed to enable the manipulator to adapt to unexpected events or changes in the task it is currently performing, where the majority of such control schemes for serial manipulators categorized to *direct-force control approaches*, *admittance control schemes* or *impedance Control schemes*. Where impedance control schemes involve the measurement of displacement or motion resulting from interactions and generate a reactive force to counter this displacement, with a Cartesian impedance control strategy, the manipulator can handle forces introduced by the human-

robot operator due to its compliant nature. Examples of this type of controller can be found in [21, 22]. Admittance control schemes manipulate the virtual model dynamics of a system in response to measured forces arising from interactions with a human operator or its environment. Examples of this type of controller can be found in [23, 24]. Direct-force control approaches regulate the manipulator's force along a constraint and its motion along unconstrained paths by measuring the force. A notable subcategory of Direct-force control approaches is hybrid force impedance control. Examples of this type of controller can be found in [25].

2.2.2 Communication

In order to facilitate a close and immersive interaction between both entities within the shared workspace, communication is another key element within human-robot collaboration. During a collaboration over a shared task, humans indicate their intentions through a variety of verbal and non–verbal cues either in real or virtual work environments [26]. These ways of communication will, for the remainder of this work, be grouped in the categories; (i) *verbal* (e.g., speech recognition and voice control) (ii) *non-verbal* (e.g., human pose tracking, intention recognition and gaze detection), (iii) as well as communication interfaces in *virtual, augmented and mixed realities*.

Verbal Communication

Verbal human-robot communication refers to the use of spoken language as a means of exchanging information and coordinating actions between humans and robots. This enables the human/operator to vocally asks for support from the robot or give the robot instructions. To facilitate effective verbal human-robot communication in a variety of settings, including manufacturing, it is essential that the robot is able to extract the necessary information and react/reply accordingly. In order to extract and communicate information from and to human work in recent years has utilized natural language processing (NLP) technologies [27, 28]. However, the effectiveness of verbal communication is depends on various factors such as the accuracy and reliability of the speech recognition, the quality of the artificial voice as well as the complexity of the conversation. When it comes to industrial environments where background noise can make the humans voice inaudible recording interpreting the humans command accuracy and reliability is a major challenge [29].

Non-verbal Communication

Non-verbal communication channels/interfaces between humans and robots not only enhance the communication between humans and robots but also replace verbal communication [30, 31]. One of these channels relies on visual systems in order to exchange information between humans and robots. Visual systems provide a convenient and intuitive way for humans and robots to communicate and interact with each other through gesture and pose recogni-

tion and eye and gaze tracking. The information exchanged through gestures and poses can be used to enhance the ergonomics of the human [32] and communicate each other's intentions more robustly [33]. In more recent research, even the human's cognitive load could be estimated through the combination of various visual and other non-verbal clues [34–36]. Another prominent non-verbal communication channel relies on *tactile and haptic* feedback. Communication relying on tactile and haptic feedback facilitates the exchange of information through touch and force. A prominent way of facilitating such communication through touch are skin-based interfaces such as hard skin or soft skin interface [37]. An example of a more force-centered approach was presented in [38], which enables the operator to guide the robot.

Virtual, Augmented, and Mixed-reality Communication

Over the past decade, communication between humans and robots in virtual, augmented, and mixed-reality workspaces has through technological advancements within the field of computer-generated simulations as well as in computational power, become more feasible.

They mainly differ in the level of immersion into the virtual environment these three methods support. Where virtual reality application such as [39,40] provides the user with a total immersion into a virtual environment, augmented reality applications as presented in [41,42], enhanced the real world experience with some virtual cues and details, and mixed reality techniques [43], enables the user to interact with objects both in the real and virtual world.

2.3 General Concept of Passivity

As mentioned earlier in chapter 1, since the introduction of collaborative-enabled robots, the number of robotic applications deployed in unstructured environments, where planned and unplanned contacts with the environment regularly occur, has increased in the past decade. In order to enable such applications, it is required that the modern robot controller is designed such that interactions with the robot are safe and the stability of the robotic system can be guaranteed. In the last few decades, the ability of robots to handle planned and unplanned interactions has improved immensely. For example, through variable impedance control, it is possible to instantaneously regulate the interaction with the environment. Nevertheless, one of the main challenges of such controllers consists in ensuring their stability [44]. A prominent energy-based method to ensure the system's stability is *passivity*. The formal definition of passivity was presented in [45] which states that a system Σ with a continuously differentiable positive semi-definite *Storage function* $S \in \mathbb{R}$ is strictly output passive w.r.t. its input-output pair ($\mathbf{u}$,$\mathbf{v}$) if

$$\mathbf{u}^\top \mathbf{v} \geq \dot{S} \quad \text{with} \quad \mathbf{u}, \mathbf{v} \in \mathbb{R}^m \tag{2.1}$$

holds true. Generally, such a robot system can be split into three main subsystems, i.e. controller, robot, and environment. A simple bond graph rep-

resentation of these subsystems is shown in Figure 2.1. The different subsys-

Figure 2.1: Simple bond graph representation of a robotic system, consisting of robot controller, kinematic structure, and environment. The energy flow between the controller and the robot is described by $\boldsymbol{\tau}_{\text{Ctrl}}\dot{\mathbf{q}}$. The energy flow between the robot and the environment is described by $\mathbf{w}_{\text{ext}}\dot{\mathbf{x}}$. A negative sign indicates the flow from the controller to the robot and from the environment to the robot, respectively. Adopted from [46].

tems are interconnected via power-preserving connections called *power-ports*, which describes an interface for exchanging energy between two interconnected subsystems [47]. As described by [47], a power-port can be mathematically defined as:

$$(f, e) \in \mathcal{P} := V \times V^* \tag{2.2}$$

where the pair e and f describe the *flow* and the *effort* which are respectively elements of the vector space V and its dual V^*. The power-port between the controller and the robot is referred to as *control-port* with the power variables $(\boldsymbol{\tau}_{\text{Ctrl}}, \dot{\mathbf{q}})$ and the port between the robot and environment as *interaction-port* with the power variables $(\mathbf{w}_{\text{ext}}, \dot{\mathbf{x}})$, where $\dot{\mathbf{q}} \in \mathbb{R}^n$ and $\boldsymbol{\tau}_{\text{Ctrl}}^\top \in \mathbb{R}^n$ are the joint velocities and the controlling joint torques respectively. For passive environments, a robotic system is passive w.r.t. the power port $(\mathbf{w}_{\text{ext}}, \dot{\mathbf{x}})$ if the robot and controller are passive [48], where $\mathbf{w}_{\text{ext}} \in se^*(3)$ and $\dot{\mathbf{x}} \in se(3)$ are the externally applied wrench and the twist. As stated in [48] the stored energy of a controlled robotic system Σ can be expressed in the form of the storage function

$$S = S_{\text{Ctrl}} + S_{\text{Rob}}, \tag{2.3}$$

where $S_{\text{Rob,Ctrl}} \in \mathbb{R}$ describe the storage functions of the robotic system (Σ_{Rob}), and the control system (Σ_{Ctrl}), respectively. Where the port between the controller and the robot is referred to as *control-port* with the power variables $(\boldsymbol{\tau}_{\text{Ctrl}}, \dot{\mathbf{q}})$ and the port between the robot and environment as *interaction-port* with the power variables $(\mathbf{w}_{\text{ext}}, \dot{\mathbf{x}})$. In other words the controlled robot system is passive if $S_{\text{Rob}} + S_{\text{Ctrl}} \leq \mathbf{w}_{\text{ext}}\dot{\mathbf{x}}$ holds true and the connection between $S_{\text{Rob,Ctrl}}$ is power continuous. For a robot system with rotational joints, it can be proven that it is a passive system by looking at the dynamics of a n-DOF rigid robot, which can be expressed as:

$$\mathbf{M}(\mathbf{q})\ddot{\mathbf{q}} + \bar{\mathbf{C}}(\mathbf{q}, \dot{\mathbf{q}})\dot{\mathbf{q}} + \bar{\mathbf{G}}(\mathbf{q}) = \boldsymbol{\tau}^\top, \tag{2.4}$$

with $\mathbf{q} \in \mathbb{R}^n$ being the generalized joint positions and $\mathbf{M}(\mathbf{q}) \in \mathbb{R}^{n \times n}$ being the positive-definite mass matrix. $\bar{\mathbf{C}}(\mathbf{q}, \dot{\mathbf{q}})\dot{\mathbf{q}} \in \mathbb{R}^n$ represents the centrifugal and Coriolis torques, $\bar{\mathbf{G}}(\mathbf{q}) \in \mathbb{R}^n$ the gravitational torques and $\boldsymbol{\tau}^\top \in \mathbb{R}^n$ the control torques, respectively. By choosing the definition of $\bar{\mathbf{C}}(\mathbf{q}, \dot{\mathbf{q}})$ as presented in [49], it can be shown that $\dot{\mathbf{M}}(\mathbf{q}) - 2\bar{\mathbf{C}}(\mathbf{q}, \dot{\mathbf{q}})$ has a skew-symmetry property hence it implies that a robot with only rotational joint, is a passive system as

its storage function $S_{\text{Rob}} = \frac{1}{2}\dot{\mathbf{q}}^\top \mathbf{M}(\mathbf{q})\dot{\mathbf{q}} + U_g(\mathbf{q})$ is physically bounded from below [21, 48, 50], with $U_g(\mathbf{q}) \in \mathbb{R}$ being the potential energy due to gravity. Therefore, as stated in [51], to prevent unstable/non-passive behavior, observing and controlling the energy flow from the controller to the manipulator through the control port is necessary. In other words, as S_{Rob} describes a passive system by itself, the controlled robot system described by S can only be passive w.r.t. the energy injected to the system from the environment through $(\mathbf{w}_{\text{ext}}, \dot{\mathbf{x}})$ if it is guaranteed that S_{Ctrl} is passive w.r.t. $(\boldsymbol{\tau}_{\text{Ctrl}}, \dot{\mathbf{q}})$. Hence, the following statement: $\dot{S}_{\text{Ctrl}} \leq -\boldsymbol{\tau}_{\text{Ctrl}}\dot{\mathbf{q}}$ must hold in order to ensure the passivity of the overall system.

CHAPTER 3

Human-robot collaboration in industrial environments: A literature review on non-destructive disassembly

This chapter consist of work from the following paper: Hjorth S, Chrysostomou D; Human–robot collaboration in industrial environments: A literature review on non-destructive disassembly (2021) *Robotics and Computer-Integrated Manufacturing*; DOI: 10.1016/j.rcim.2021.102208

3.1 Introduction

As previously mentioned in section 1.1, it must be financially viable to enable manufacturers to adopt a CEBM. However, due to the product design, which is currently optimized for past/current assembly processes, and the high variability in their conditions of EOLPs, highly/fully automated systems struggle to disassemble them efficiently. Resulting in the need for disassembly cells where humans and robots support each other. Over the last decade, technological advancement in then the field of human-robot collaboration (HRC) and disassembly strategies has enabled the development of a number of various HRCD solutions. Therefore, this chapter aims to provide the reader with an overview of the state of the art of HRCD, which is analyzed based on autonomous robotic disassembly systems as well as the various forms of HRC currently utilized. To achieve this goal, a comprehensive literature survey was conducted, which included more than 400 papers related to the field. The contribution presented in this chapter can be summarized as follows:

- It provides an analysis of how HRC is currently implemented in robotic disassembly applications as well as an insight in robotic disassembly process themselves.
- A framework is proposed to identify and classify future research focused on HRCD systems.

This chapter comprises the findings of paper [Paper A | [1]], so it is expected to encounter repeated information, such as context, wording, results, and figures, derived from that particular source.

3.2 Method

As mentioned previously, many automated disassembly systems utilize destructive disassembly operations for the extraction of sub-assemblies and components. This leads due to various reasons to a less efficient process.
In contrast, collaborative solutions that involve humans and robots collaborating together to disassemble EOLPs may be able to minimize or avoid the need for such destructive disassembly operations. With the aim to identify relevant literature, the search for relevant literature was carried out on the web-based databases Google Scholar, Scopus, and Web of Science, using search terms "human-robot collaboration" AND "disassembly," "robot-assisted disassembly," and "human-robot collaborative disassembly." These terms were selected based on their relevance to the disassembly process, which incorporates the role of human operators. The search was limited to the period from January 2009 to September 2020 since the first collaborative-enabled industrial manipulator was first made available in 2008, and new standards that enabled the implementation of HRC applications in the industry were first introduced in

2009. Additionally, the search terms related to economic evaluation, feasibility studies of disassembly lines, profitability scores, and literature discussing process optimization of disassembly line designs and tool design were excluded from the search.
Additionally, these publications are evaluated based on the current state-of-the-art within the two sub-field HRC and disassembly processes to identify publications that represent the current state-of-the-art.

3.3 Results

Since both the terms "human-robot collaboration" and "disassembly" as well as their s are general, the initial search based on the chosen keywords yielded 425 possible relevant publications. After eliminating duplicates across the web-based databases, the total number of relevant publications was reduced to 383. Further screening based on the exclusion criteria mentioned earlier resulted in a total of **9** publications that were deemed relevant.
A visual illustration of the selection process can be seen in Figure 3.1.

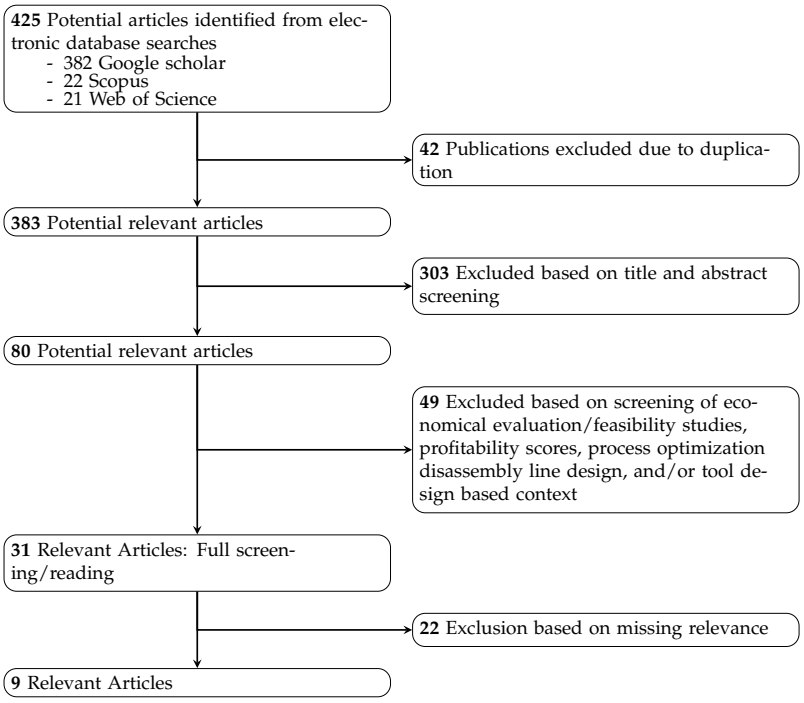

Figure 3.1: Illustrating the process of the literature selection related to HRCD.[Paper A | [1]]

The evaluation of the nine identified publications is based on the current state of the art within the subfields "human-robot collaboration" and "disassembly

processes". This evaluation has revealed a general trend towards incorporating human workers in the disassembly process, although ensuring safety remains a significant challenge in HRC within industrial environments, particularly for disassembly tasks. To ensure a safe interaction between humans and manipulators, the manipulator must be capable of adjusting its behavior safely based on the exchange of contact forces and energy. However, the absence of post-collision control schemes in the context of pHRI in HRCD applications raises concerns, as human workers may accidentally engage in a collaborative phase through unintended physical contact with the manipulator. Utilizing tools with human-aware design and energy-aware control schemes could potentially reduce the risk of severe hazards posed by the robot or attached tools. Furthermore, there are several areas within the field of HRCD where the current state-of-the-art can be improved. Ideally, human-robot collaboration should not differ from human-human collaboration. However, current solutions still fall short of human workers in terms of cognitive abilities, adaptation, and problem-solving skills. Developing skill acquisition interfaces that enable a more intuitive definition and teaching of tasks to robots can facilitate the transfer of human knowledge and cognitive abilities to robots. However, in the field of disassembly, such skill-acquisition interfaces are scars. Lastly, it is worth noting that various forms of HRI commonly used in other domains, such as social-aware and service robotics, are rarely implemented in HRCD systems. This could be attributed to the demanding challenges posed by the environmental conditions in industrial settings. However, addressing these challenges could lead to a more efficient and safer work environment.

3.4 Conclusion

The aim of this chapter was to present the reader with an overview and background knowledge about the current state-of-the-art in the field of HRCD. In summary, it can be concluded that due to the aforementioned uncertainties associated with the complexity and variability of mechatronic and mechanical EOLPs existing automated and HRCD systems can face numerous challenges. From the presented in-depth analysis, three general areas were identified where HRCD applications need to improve. These areas are: *Incorporation of safe pHRI*, *acquisition and learning (implementation) of skills* and *utilization of social, visual, and verbal HRI*. The main contributions of this work can be summarized as follows:

- A overview over the current state of the art with a extensive catalog of background knowledge was given,
- the current state of the art was analyzed based on the state of the art of the sub categories,
- and a framework was created which can be used for evaluating future work in the field of HRCD.

CHAPTER 4

An Energy-based Approach for the Integration of Collaborative Redundant Robots in Restricted Work Environments

This chapter consist of work from the following paper: Hjorth S, Lachner J, Stramigioli S, Madsen O, Chrysostomou D; An Energy-based Approach for the Integration of Collaborative Redundant Robots in Restricted Work Environments *IEEE International Conference on Intelligent Robots and Systems*; DOI: 10.1109/IROS45743.2020.9341561

4.1 Introduction

As aforementioned in chapter 3, during recent years, collaborative-enabled robots (e.g. KUKA LBR iiwa, ABB YuMi and FANUC CRX) are increasingly utilized in multiple work environments such as industrial and medical settings [52,53]. Therefore, collaborative-enabled robots have become key-enablers for the implementation of the HRCD cells, as they are no longer restricted to operating behind a fence as well as in static and well-defined environments. However, as stated previously in chapter 3, DeSantis et al. [19] states that the implementations of solutions relying on HRC face a number of challenges, amongst which are: (i) to guarantee safe physical human-robot interaction (pHRI), and (ii) the integration of such systems in areas with limited space. In areas where the physical workspace is limited, such as HRCD cells, pHRIs are unavoidable and often even desirable. It should, therefore, be possible for the human operators to affect the execution of the manipulator's task without compromising their safety. However, there is also a need for restrictions on the manipulator's workspace, as in those areas, an unintended collision could occur with other machinery or human operators that are not aware of the robot's task. Additionally, there are constraints such as singularities, self-collisions, and joint limits. In case one of these constraints is violated, the manipulator halts its motion which results and needs to be reinitialized. Therefore, in order to ensure efficient and safe pHRI scenarios, it is essential to avoid running into stability problems due to singularities and joint limit violations. Moreover, appropriately chosen joint limit avoidance strategies can reduce the risk of self-collisions in such scenarios. The presented formalism focuses on an energy-based control strategy in order to tackle the aforementioned challenges associated with safety and the robot's workspace by combining the concept of artificial potential fields introduced in [54] with the energy-aware control scheme presented in [55, 56]. The main contributions of the in [Paper B | [2]] presented work are:

(i) The introduction of Cartesian workspace restrictions and joint limit avoidance for all links/joints,

(ii) and presentation of an energy-based formulation of the control strategy ensuring safe robot behavior.

This chapter comprises the findings of paper [Paper B | [2]], so it is expected to encounter repeated information, such as context, wording, results, and figures, derived from that particular source.

4.2 Energy-aware Cartesian Impedance controller

In general impedance controller can be described as a mass-spring-damper system with adjustable parameters [57]. As stated by Hogan [58], an impedance

controller creates a dynamic relationship between the different state variables. Consequently, it is possible to describe any interaction with such a system as an energy exchange between the manipulator and its environment [Paper B | [2]].
Since an impedance controller can be described by an mass-spring-damper system; consequently, the general control torques of the impedance controller $\boldsymbol{\tau}_{\text{Imp}}^{\top} \in \mathbb{R}^n$ are constructed from the torques of the Cartesian springs $\boldsymbol{\tau}_{\text{Spring}}^{\top} \in \mathbb{R}^n$ the damping term $\boldsymbol{\tau}_{\text{Damp}}^{\top} \in \mathbb{R}^n$ as follows:

$$\boldsymbol{\tau}_{\text{Imp}}^{\top} = \boldsymbol{\tau}_{\text{Spring}}^{\top} - \boldsymbol{\tau}_{\text{Damp}}^{\top} \tag{4.1}$$

Where the joint torques $\boldsymbol{\tau}_{\text{Spring}}$ are generated through the elastic wrench at the manipulator's end-effector $\mathbf{w}_K^{\text{EE,EE}} \in se^*(3)$ that describe the motion generating Cartesian springs. These Cartesian springs are described on the basis of the infinitesimal body twist displacement $\Delta\boldsymbol{\eta} \in se(3)$ and the diagonal stiffness matrix elements $\mathbf{K}_{r,t} \in \mathbb{R}^{3\times3}$, that represent the stiffness values for the translation, rotational springs and $\mathbf{K}_c \in \mathbb{R}^{3\times3}$ which describes the decoupling between the rotational and translation terms.

$$\mathbf{w}_K^{\text{EE,EE}\,\top} = \begin{bmatrix} \mathbf{f}_K^{\text{EE,EE}\,\top} \\ \mathbf{m}_K^{\text{EE,EE}\,\top} \end{bmatrix} = \begin{bmatrix} \mathbf{K}_t & \mathbf{K}_c \\ \mathbf{K}_c^{\top} & \mathbf{K}_r \end{bmatrix} \Delta\boldsymbol{\eta}, \tag{4.2}$$

As presented in [56] it is possible to express the force $\mathbf{f}_K^{\text{EE,EE}} \in \mathbb{R}^{1\times3}$ and momentum $\mathbf{m}_K^{\text{EE,EE}} \in \mathbb{R}^{1\times3}$ on the basis of the end-effector's current transformation $\mathbf{H}_{\text{EE}}^0 \in SE(3)$ and the end-effector's desired goal transformation $\mathbf{H}_{\text{d}}^0 \in SE(3)$:

$$\begin{aligned} \widehat{\mathbf{f}}_K^{\text{EE,EE}} = &- \mathbf{R}_d^{\text{EE}} as\big(\mathbf{G}_t \widehat{\mathbf{p}}_{\text{EE}}^d\big)\mathbf{R}_{\text{EE}}^d - as\big(\mathbf{G}_t \mathbf{R}_d^{\text{EE}} \widehat{\mathbf{p}}_{\text{EE}}^d \mathbf{R}_{\text{EE}}^d\big) \\ &- 2as\big(\mathbf{G}_c \mathbf{R}_{\text{EE}}^d\big) \end{aligned} \tag{4.3}$$

and

$$\begin{aligned} \widehat{\mathbf{m}}_K^{\text{EE,EE}} = &- 2as\big(\mathbf{G}_r \mathbf{R}_{\text{EE}}^d\big) - as\big(\mathbf{G}_t \mathbf{R}_d^{\text{EE}} \widehat{\mathbf{p}}_{\text{EE}}^d \widehat{\mathbf{p}}_{\text{EE}}^d \mathbf{R}_{\text{EE}}^d\big) \\ &- 2as\big(\mathbf{G}_c \widehat{\mathbf{p}}_{\text{EE}}^d \mathbf{R}_{\text{EE}}^d\big). \end{aligned} \tag{4.4}$$

Where $as()$ returns the anti-symmetric part of a square matrix and $\widehat{\mathbf{f}}_K^{\text{EE,EE}}$ is the skew-symmetric matrix representation of $\mathbf{f}_K^{\text{EE,EE}}$. $\mathbf{G}_{r,t,c}$ represent the co-stiffnesses for the translational spring, the rotational spring and the coupling terms, respectively. The conversion between stiffnesses and co-stiffnesses are as follows

$$\mathbf{G}_{r,t,c} = \frac{1}{2} tr\big(\mathbf{K}_{r,t,c}\big)\mathbf{I}_3 - \mathbf{K}_{r,t,c}. \tag{4.5}$$

However, before the above presented $\mathbf{w}_K^{\text{EE,EE}}$ can be mapped into torques in joint space, it must first be mapped from the end-effector frame to the inertial reference frame with the help of the adjoint coordinate transformation

$Ad^{\top}_{\mathbf{H}^{\mathrm{EE}}_0} \in \mathbb{R}^{6\times 6}$, $\mathbf{w}^{0,\mathrm{EE}\top}_K = Ad^{\top}_{\mathbf{H}^{\mathrm{EE}}_0}\mathbf{w}^{\mathrm{EE},\mathrm{EE}\top}_K$. Now it is possible to calculate the joint torques $\boldsymbol{\tau}_{\mathrm{Spring}}$ by mapping the wrench $\mathbf{w}^{0,\mathrm{EE}}_K$ with the transposed of the spatial geometric Jacobian $\mathbf{J}_{\mathrm{EE}}(\mathbf{q}) \in \mathbb{R}^{6\times n}$ into joint space. The dissipative joint torques $\boldsymbol{\tau}_{\mathrm{Damp}}$ are set together of the damping matrix in joint space $\mathbf{B} \in \mathbb{R}^{n\times n}$ and the joint velocities $\dot{\mathbf{q}}$ in the follwoing way:

$$\boldsymbol{\tau}^{\top}_{\mathrm{Damp}} = \mathbf{B}\dot{\mathbf{q}}. \tag{4.6}$$

Now after having introduced the general derivation of a Cartesian impedance controller, the focus can be set on introducing the energy-based safety metrics. One of such safety metrics is associated with limiting the total energy of the system $E_{\mathrm{total}} \in \mathbb{R}$. This total energy is defined as follows $E_{\mathrm{total}} = T_{\mathrm{total}} + U_{\mathrm{total}}$, with $T_{\mathrm{total}} \in \mathbb{R}$ being the kinetic energy and $U_{\mathrm{total}} \in \mathbb{R}$ being the potential due to spatial springs [59]. In order to ensure that the total energy stored in the system does not violate the chosen maximum energy $\overline{E}_{\mathrm{total}}\mathbb{R}$ that is allowed to be stored by the system, a scaling parameter $\lambda \in \mathbb{R}$ is computed:

$$\lambda = \begin{cases} 1 & \text{if } E_{\mathrm{total}} \leqslant \overline{E}_{\mathrm{total}} \\ \frac{\overline{E}_{\mathrm{total}} - T}{U_{\mathrm{total}}} & \text{otherwise.} \end{cases} \tag{4.7}$$

where is defined as,

$$\begin{aligned} U_{\mathrm{total}} = -tr(\mathbf{G}_r\mathbf{R}^d_7) + \Big(-\frac{1}{4}tr(\widehat{\mathbf{p}}^d_7\mathbf{G}_t\widehat{\mathbf{p}}^d_7) \\ -\frac{1}{4}tr(\widehat{\mathbf{p}}^d_7\mathbf{R}^d_7\mathbf{G}_r\mathbf{R}^7_d\widehat{\mathbf{p}}^d_7)\Big) + tr(\mathbf{G}_c\mathbf{R}^7_d\widehat{\mathbf{p}}^d_7) \end{aligned}. \tag{4.8}$$

This formalism shows that the potential energy stored in the spatial springs U_{total} is proportional to the Co-stiffness $\mathbf{G}_{r,t,c}$ [51], and therefore it is sufficient to scale $\mathbf{G}_{r,t,c}$ by λ:

$$\mathbf{G}_{r,t,c} \leftarrow \lambda\mathbf{G}_{r,t,c}. \tag{4.9}$$

Next to the energy of the robot, the robot's power must also be monitored and, if necessary, limited, as the power describes the instantaneous energy transferred when the manipulator comes in contact with its environment. Therefore, the *damping injection* method is utilized to monitor and limit the power resulting from the manipulator's motion $P_{\mathrm{motion}} \in \mathbb{R}$:

$$P_{\mathrm{motion}} = \left(\mathbf{J}_{\mathrm{EE}}(\mathbf{q})^{\top}\mathbf{w}^{0,\mathrm{EE}\top}_K - \mathbf{B}_{\mathrm{init}}\dot{\mathbf{q}}\right)^{\top}\dot{\mathbf{q}}, \tag{4.10}$$

Whenever the manipulator moves toward a desired transformation $\mathbf{H}^0_d$, P_{motion} is monitored, and in case it exceeds a predefined power limit $\overline{P}_{\mathrm{motion}} \in \mathbb{R}$, the scaling parameter $\beta \in \mathbb{R}$ is calculated as:

$$\beta = \begin{cases} 1 & \text{if } P_{\mathrm{motion}} \leqslant \overline{P}_{\mathrm{motion}} \\ \frac{\left(\mathbf{J}_{\mathrm{EE}}(\mathbf{q})^{\top}\mathbf{w}^{0,\mathrm{EE}\top}_K\right)^{\top}\dot{\mathbf{q}} - \overline{P}_{\mathrm{motion}}}{\dot{\mathbf{q}}^{\top}\mathbf{B}_{\mathrm{init}}\dot{\mathbf{q}}} & \text{otherwise,} \end{cases} \tag{4.11}$$

multiplying β with the previously defined initial damping matrix $\mathbf{B}_{\text{Init}}$, the new damping term can be written as:

$$\boldsymbol{\tau}_{\text{Damp}}^{\top} = \underbrace{\beta \mathbf{B}_{\text{init}}}_{\mathbf{B}} \dot{\mathbf{q}}; \quad \mathbf{B}_{\text{init}} \in \mathbb{R}^{n \times n}. \tag{4.12}$$

4.3 Workspace restrictions

As aforementioned, this work presents a modified version of an artificial repulsive potential field with the aim of enforcing workspace constraints. It is noteworthy that this approach does not interfere with the path planning; but focuses on the restriction of the manipulator's Cartesian workspace. Hence, the focus is limited to repulsive artificial potential fields. In order to keep the manipulator's links i within some predefined Cartesian workspace constructed by a set of virtual walls C_j, a repulsive force $\mathbf{w}_{C_j,i}^{i,i} \in se^*(3)$ generated by the artificial repulsive potential field for each restricted link i is introduced.

$$\mathbf{w}_{C_j,i}^{i,i\ \top} = \begin{bmatrix} \mathbf{f}_{C_j,i}^{i,i\ \top} \\ \mathbf{m}_{C_j,i}^{i,i\ \top} \end{bmatrix}. \tag{4.13}$$

Its derivation is based on same concept as presented in [56] and its components $\mathbf{f}_{C_j,i}^{i,i} \in \mathbb{R}^{1\times 3}$ and $\mathbf{m}_{C_j,i}^{i,i} \in \mathbb{R}^{1\times 3}$ can be expressed in their skew-symmetric form. It is to note, that only the translational motion of the links that violates a workspace restriction has to be restricted. Therefore, it is only necessary to express $\mathbf{f}_{C_j,i}^{i,i}$ and $\mathbf{m}_{C_j,i}^{i,i}$ on the basis of the translational Co-stiffness $\mathbf{Q}_{C_j,i}$ as follows:

$$\widehat{\mathbf{f}}_{C_j,i}^{i,i} = -as\big(\mathbf{Q}_{C_j,i}\mathbf{R}_{C_j}^{i}\widehat{\mathbf{p}}_i^{C_j}\mathbf{R}_i^{C_j}\big) - \mathbf{R}_{C_j}^{i}as\big(\mathbf{Q}_{C_j,i}\widehat{\mathbf{p}}_i^{C_j}\big)\mathbf{R}_i^{C_j} \tag{4.14}$$

and

$$\widehat{\mathbf{m}}_{C_j,i}^{i,i} = -as\big(\mathbf{Q}_{C_j,i}\mathbf{R}_{C_j}^{i}\widehat{\mathbf{p}}_i^{C_j}\widehat{\mathbf{p}}_i^{C_j}\mathbf{R}_i^{C_j}\big). \tag{4.15}$$

Consequently, the co-stiffness $\mathbf{Q}_{C_j,i}$ are computed with the help of the spring stiffness $\mathbf{L}_{C_j,i} \in \mathbb{R}^{3\times 3}$ through $\mathbf{Q}_{C_j,i} = \frac{1}{2}tr(\mathbf{L}_{C_j,i})\mathbf{I}_3 - \mathbf{L}_{C_j,i}$. The generated repelling wrench is directly dependent on a repulsive potential field that is defined as a non-negative smooth surface for any given joint configuration $\mathbf{q}$ and is the transition function between unrestricted and restricted motion [Paper B | [2]]. More specifically, it is defined through the following potential function $\sigma_{C_j,i}$ that is constructed based on the shortest Euclidean distance $d_{i,C_j}(\mathbf{q}) \in \mathbb{R}$ between the Cartesian position of the link $\mathbf{p}_i^0 \in \mathbb{R}^3$ and its projec-

tion onto the virtual wall $\mathbf{p}^0_{i,C_j} \in \mathbb{R}^3$ in the following way.

$$\sigma_{C_j,i} = \begin{cases} \frac{1}{\gamma}\left(\frac{1}{d_{i,C_j}(\mathbf{q})} - \frac{1}{x_j}\right)^{\gamma} & \text{if } d_{i,C_j}(\mathbf{q}) \leq x_j \\ 0 & \text{otherwise,} \end{cases} \tag{4.16}$$

where the activation distance at which the potential given by $\gamma > 0$ for a virtual wall is applied to the link is denoted as $x_j \in \mathbb{R}$. As the constraint link passes the activation distance ($d_{i,C_j}(\mathbf{q}) < x_j$) the link specific potential of the virtual wall C_j ($\sigma_{C_j,i}$) increases towards infinity the closer $d_{i,C_j}(\mathbf{q})$ comes to the C_j. The potential $\sigma_{C_j,i}$ is then used to scale the translational co-stiffnesses $\mathbf{Q}_{C_j,i}$.

$$\mathbf{Q}_{C_j,i} \leftarrow \sigma_{C_j,i}\mathbf{Q}_{C_j,i} \tag{4.17}$$

However, as the repelling wrench ${\mathbf{w}^{i,i}_{C_j,i}}^{\top}$ generated by the constraint C_j acting on the i^{th} link is expressed in the body-frame of the respective link. Hence, it has to be mapped into the inertial reference 0-frame through the links respective adjoint coordinate transformation $Ad^{\top}_{\mathbf{H}^i_0}$, ${\mathbf{w}^{0,i}_{C_j,i}}^{\top} = Ad^{\top}_{\mathbf{H}^i_0}{\mathbf{w}^{i,i}_{C_j,i}}^{\top}$. Now, it is possible to map the link i and virtual wall C_j specific wrenches to their equivalent joint torque representation through the following convention

$$\boldsymbol{\tau}^{\top}_{\mathrm{C}} = \Big(\sum_i \big(\sum_j {\mathbf{J}_i}^{\top}(\mathbf{q}){\mathbf{w}^{0,i}_{C_j,i}}^{\top}\big)\Big), \tag{4.18}$$

where $\mathbf{J}_i(\mathbf{q})$ describe the spatial geometric Jacobian for the i^{th} link. The risk of the manipulator reaching one of its joint limits increases drastically when subjected to an external disturbance as it does not follow any pre-planned trajectory. In order to avoid that the manipulator reaches these joint limits, the concept of joint limit avoidance is applied. Similarly to the concept of Cartesian constraints, the concept of joint limit avoidance generates a repelling torque once a joint comes into a critical area. Thereby forcing the respective joint to stay within predefined limits. The implemented joint limit avoidance through artificial potential fields used in this work is described in detail by Khatib [54].

4.4 Results

The experimental validation of the presented control strategy was conducted stimulative and on the real robot KUKA LBR iiwa 7 R800 (seen in Figure 4.1). The validation of the presented control formalism is split into the following two different experimental use-cases:

(i) Use-case 1: Focuses on the manipulator's behavior when encountering Cartesian workspace restrictions (see subsection 4.4.1).

(ii) Use-case 2: Focuses on the manipulator's behavior of joint limit avoidance algorithm whilst the manipulator is in a compliant state (see subsection 4.4.2).

Figure 4.1: The experimental setup for the "Multiple link restriction" test, where links 4, 6 and 7 forced towards the constraint C_3 visualized as a grey plane Visualizing the experimental setup of the "Multiple link restriction" experiment, in which links 4, 6, and 7 are pushed into the virtual wall C_3.[Paper B | [2]]©2020 IEEE

4.4.1 Use-case 1: Validation of the enforcement of Cartesian workspace restrictions

Two separate experiments validated the concept of enforcing Cartesian workspace restrictions. The first experiment was conducted by forcing the manipulator's end-effector to violate two constraints simultaneously. In the second experiment, multiple manipulator links were simultaneously forced into a single workspace restriction.

Multiple Cartesian workspace restrictions acting on one link

The test was conducted by moving the manipulator's end-effector along a predefined trajectory. This movement forced the manipulator to violate the two virtual walls C_1 and C_2 that were respectively positioned along the z-axis and x-axis of the robot's inertial reference frame.
The resulting Cartesian motion of the manipulator's end-effector can be seen in Figure 4.2a. There it can be observed that as the end-effector crossed the activation distance of the respective Cartesian workspace restrictions, its motion deviated from the desired path for the entire period where it was subjected to the Cartesian workspace restrictions. Additionally, it can be observed in 4.2b that the energy scaling method ensures that E_{total} never exceeds the threshold

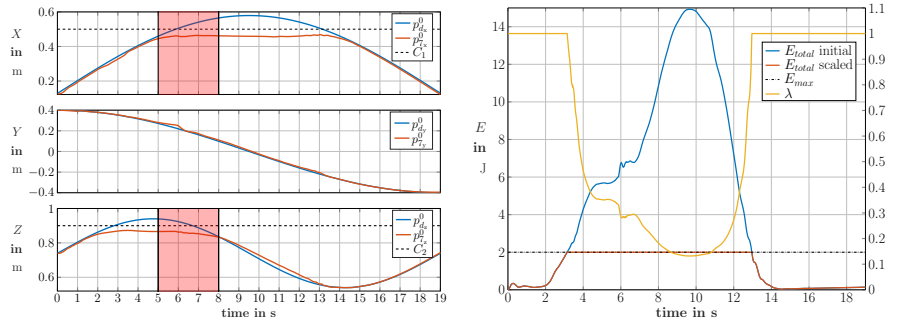

(a) (b)

Figure 4.2: In (a), the correlation between the trajectory and end-effector position is depicted for both the simulation and real-world tests. It is shown how the Cartesian workspace constraints C_1 and C_2 limit the movement of the end-effector along the x-axis and z-axis axes (seen from the base-frame) while the y-axis remains unrestricted. In (b), the graph illustrates the total energy E_{total} during the Multi-Cartesian workspace restriction test conducted in the real-world scenario. It demonstrates how the parameter λ, restricting E_{total} to E_{max}.[Paper B | [2]] © 2020 IEEE.

E_{max}, regardless if the manipulator's end-effector was subjected to a single or multiple Cartesian workspace restrictions. The implemented controller displays an additional benefit, which is evident when the energy threshold E_{max} is exceeded due to an interaction with the robot. In such cases, the stiffness of the spatial spring is decreased, allowing the robot to be manipulated freely. After the robot was released, it automatically returned to the desired trajectory while ensuring adherence to the designated threshold.

One Cartesian workspace restriction acting on multiple links

This experiment aimed to validate the behavior of the manipulator when multiple links are simultaneously subjected to a single Cartesian workspace restriction. For this experiment, a virtual wall C_3 was positioned such that it was within the reachable workspace of the manipulator's links 4, 6 and 7.
As shown in Figure 4.3, even when multiple links got manually pushed against the virtual wall C_3 (as indicated by the red zone in Figure 4.3a), none of the previously mentioned links violated the virtual wall. In the time instance where each link exceeds their respective activation distance, it can be observed in Figure 4.3a the corresponding spring scaling factor increases through which a repulsive force is generated. Note that in order to reach C_3 with all the links, the manipulator's end-effector had to be forced away from its desired configuration resulting in the reduction of the stiffness of the spatial spring through the energy scaling method of the Cartesian impedance controller, and the robot could be manipulated freely.

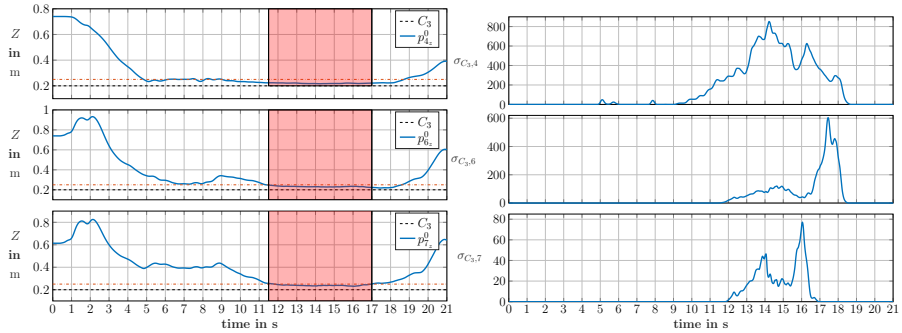

Figure 4.3: In (a), the Cartesian positions along the z-axis (seen from the base frame) are depicted for links 4, 6, and 7, while (b) illustrates the corresponding repulsive potential. The virtual wall C_3 imposes restrictions solely on the movement of the links along the z-axis of the base frame, while the x-axis and y-axis remain unrestricted. The red dashed-dotted line in (a) represents the threshold distance at which the constraint is activated or deactivated.[Paper B | [2]]© 2020 IEEE.

4.4.2 Use-case 2: Validation of joint limit avoidance

The concept of enforcing constraints in joint space was experimentally validated. Firstly, interaction with the manipulator caused the maximal specified energy to exceed its threshold, bringing the manipulator into a compliant state. Thereafter, multiple joints (i.e., joints 2, 4 and 6) were forced into their respective joint limit manually. As seen in Figure 4.4 none of these joints violated their limit, even when all axes were manually pushed into their respective limit simultaneously (highlighted in red). In the event that a joint passed into one of its respective activation regions by crossing their the upper or lower activation limit $\underline{q}_{i,J}$ or $\bar{q}_{i,J}$, a joint torque in the opposite direction was generated. As illustrated in Figure 4.4 the joint torque for link 2,4 and 6 $\tau_{\text{JLA}_{2/4/6}} \in \mathbb{R}$ increased as the distance to the constraint $\underline{qi}/\bar{q}i$ decreased and vice versa. As seen in the area highlighted in red, none of these joints exhibits an oscillatory behavior during this phase of the experiment. As shown, the restricted joints stays within their predefined bounds, throughout the experiment.

4.5 Conclusion

In the pursuance of enabling pHRIs within restricted work environments, such as HRCD cells, this chapter presented an energy-based control formalism for enforcing workspace restrictions for collaborative-enabled robots.

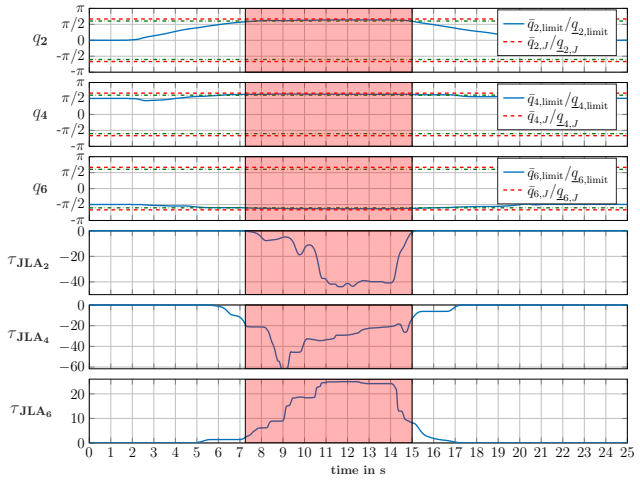

Figure 4.4: The visualization showcases the joint positions of joints 2, 4, and 6, along with the resulting torques from the joint limit avoidance strategy. The red-marked area highlights the time interval when all joints simultaneously reach their respective limits.[Paper B | [2]]© 2020 IEEE.

Additionally, to the limited space available for the manipulator to operate during human-robot collaborative application, it is possible that incidental contact between the robot and the human operator can occur. These challenges impose constraints on the robotic system in terms of the workspace and the manipulator itself.

To address these challenges, the presented formalism builds on the concept of artificial potential fields by combining it with an energy-aware Cartesian impedance control scheme. The energy-aware Cartesian impedance control scheme ensures that the manipulator is capable of adapting to pHRI within predefined energy thresholds and the modified artificial potential field approach ensures that the robot stays within its predefined workspace when disturbed through a pHRI. As demonstrated by the experimental validation of the presented control strategy, the control strategy is capable of handling external disturbances introduced by the human operator and staying within a predefined Cartesian workspace even when subjected to multiple constraints simultaneously as well as within its joint limits.

Two benefits that can be observed from the control framework are: the robot adheres to all Cartesian workspace restrictions while complying with the designated energy and power thresholds for the interaction. Additionally, as a result of the energy scaling, there are no oscillations during movement within the boundaries of the constraints as well as during the transition phase (cf. red zone in Figure 4.2) between C_1 and C_2.

4.5.1 Limitations and Future work

During the experimental validation, it was discovered that if the manipulator's end-effector was displaced such that it reached configuration, which is a local minimum, the robot got stuck and had to be guided manually out of this minimum. Therefore, future work could focus on implementing a safe recovery motion planner for handling such minima. Furthermore, future work could extend the current implementation of the Cartesian workspace restrictions to more complexly shaped surfaces (i.e., curved). However, the main limitation of the presented control strategy is the lack of a control mechanism that ensures the system's passivity. More specifically, control actions associated with the energy scaling functions and the repulsive forces from the workspace restrictions as they can cause the system to become non-passive, leading to unstable control actions. Additionally, it must be investigated if an energy-aware Cartesian impedance control scheme is suitable for HRCD tasks and how it performs compared to control schemes currently deployed in HRCD tasks.

CHAPTER 5

Design of an Energy-Aware Cartesian Impedance Controller for Collaborative Disassembly

This chapter consist of work from the following paper: Hjorth S, Lamon E, Chrysostomou D, Ajoudani; Design of an Energy-Aware Cartesian Impedance Controller for Collaborative Disassembly *IEEE International Conference on Robotics and Automation*; DOI: 10.1109/ICRA48891.2023.10160993

5.1 Introduction

As stated in [Paper A | [1]], to face the challenges associated with the variability and uncertainties of the products' state [12], solutions that keep the human part of the process such as (HRCD) cells, which can facilitate safe pHRI are needed. Safety is of great importance in HRCD, as the variability and uncertainties of the products state increase the risk of unpredictable events occurring associated with it. In the previous chapter 4, a control scheme was presented, which enables safe pHRI in restricted workspaces. However, the chapter did not cover the notion of the passivity of the system or the application of such a control strategy on a disassembly task. This chapter will focus on both of these aspects by introducing an energy-aware control strategy in combination with an augmented energy tank approach for the disassembly task. To summarize, the main contributions of the in [Paper C | [3]] presented work are:

(i) Design of an energy-aware Cartesian impedance controller which utilizes a global energy tank with power limitation for the insurance of the passivity of the system.

(ii) An experimental validation of the proposed energy-aware Cartesian impedance controller for a faulty unscrewing task with a stripped screw head.

(iii) An experimental comparison with the hybrid force-impedance controller [25], and a standard Cartesian impedance controller [44].

This chapter comprises the findings of paper [Paper C | [3]], so it is expected to encounter repeated information, such as context, wording, results, and figures, derived from that particular source.

5.2 Method

A heavily used control solution to ensure the passivity of the system is through the *energy tank* and *energy routing concept*, originally proposed in [60]. Energy tanks enforce the passivity of the system by bounding the total amount of energy that can be transferred between the controller and the robot [51]. Hence, in the event of disturbances or non-passive actions, only a limited amount of energy can be injected into the system in order to prevent unstable robot behaviors. When the tank is drained, the passivity violating control action is cut. A bond graph representation of this concept can be seen in Figure 5.1.
However, as recent works have highlighted, it is not only necessary to bound the total tank energy but also to limit the rate of energy exchange between the controller and the robot [22, 25, 61–63]. Otherwise, an unstable behavior can occur even though the energy is bounded [25]. While, previously, the only

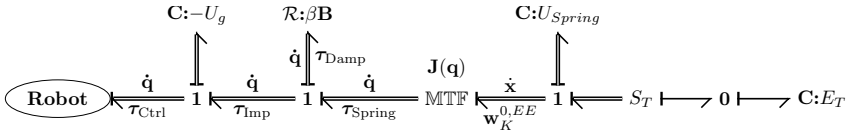

Figure 5.1: A bond-graph representation of the presented control system.

design criterion for energy tanks was the finite amount of energy that a tank can store [51], such approaches [22, 25] focus on modulating the energy flow from the tank to the robot, e.g., based on the energy needed for a given robotic task.

According to [25], the energy flow of the bounded energy storage functions of the system S_{Ctrl} and the possible power demand of the passivity-violating ports can be expressed as:

$$P_{\text{Ctrl}} + P_{\text{Diss}} + P_{\text{Spring}} = 0, \tag{5.1}$$

where the energy flow of the overall controller at $(\boldsymbol{\tau}_{\text{Ctrl}}, \dot{\mathbf{q}})$ is denoted as $P_{\text{Ctrl}} \in \mathbb{R}$ and the energy flow associated with the spring and dissipation is denoted as $P_{\text{Spring}} \in \mathbb{R}$ and $P_{\text{Diss}} \in \mathbb{R}^{\geq 0}$,respectively. The P_{Diss} can be defined on basis of a Rayleigh dissipation function such as $\mathcal{R}(\dot{\mathbf{q}}) = \frac{1}{2}\dot{\mathbf{q}}^\top \mathbf{B}\dot{\mathbf{q}}$ where damping matrix $\mathbf{B}$ is positive definite, which contributes to the passivity of the system [64]. As aforementioned, in order to ensure the passivity of the overall system, one can augment the storage function S with an energy tank E_{T} which is bounded by an upper $\overline{E}_T \in \mathbb{R}^+$ and a lower bound $\underline{E}_T \in \mathbb{R}^{\geq 0}$. The new storage function's energy flow can then be expressed as the following:

$$P_{\text{Ctrl}} + \dot{E}_T \leq 0, \tag{5.2}$$

where

$$\dot{E}_T = -P_{\text{Spring}}. \tag{5.3}$$

However, as aforementioned in case a rapid increase of the system energy occurs, the system can reach an unstable state even when E_{T} is bounded. Therefore, the authors in [25] propose the following formalism:

$$\dot{E}_T = \begin{cases} \gamma k \dot{E}_T & \text{if } \dot{E}_T \leq 0 \\ j\dot{E}_T & \text{otherwise,} \end{cases} \tag{5.4}$$

which restricts the positive energy flow in the system, where k and j ensure that the upper and lower bounds of E_{T} are not violated. The variables k and j are defined so that in case E_{T} reaches its upper or lower bound, the controller

can respectively neither inject or take out energy from the tank.

$$k = \begin{cases} 0 & \text{if } \dot{E}_T \leq 0 \wedge E_\mathrm{T} \leq \underline{E}_T \\ 1 & \text{otherwise} \end{cases}$$
$$j = \begin{cases} 0 & \text{if } \dot{E}_T \geq 0 \wedge E_\mathrm{T} \geq \overline{E}_T \\ 1 & \text{otherwise} \end{cases} \tag{5.5}$$

In addition to enforcing the respective bounds of the energy tank, the rate at which the controller is able to extract energy from E_T and inject into the system is limited by γ.

$$\gamma = \begin{cases} \frac{\dot{\underline{E}}_T}{\dot{E}_T} & \text{if } \dot{E}_T < \dot{\underline{E}}_T \leq 0 \\ 1 & \text{otherwise,} \end{cases} \tag{5.6}$$

is expressed as a ratio between a pre-defined maximal allowed energy flow $\dot{\underline{E}}_T \in \mathbb{R}$ out of the tank nd the originally calculated power demand of the task $\dot{E}_T$. In order to integrate the above described energy tank dynamic into the energy-aware Cartesian impedance controller that was presented previously in Chapter 4, the energy scaling variable λ (4.7) has to be reformulated as

$$\lambda = \begin{cases} 1 & \text{if } E_\mathrm{total} \leqslant \overline{E}_\mathrm{total} \wedge k \neq 0 \\ \lambda(t-1) & \text{if } k = 0 \wedge \dot{E}_T \leq 0 \\ \frac{\overline{E}_\mathrm{total} - T}{U_\mathrm{total}} & \text{otherwise.} \end{cases} \tag{5.7}$$

This ensures that if the energy tank reaches its lower limit ($k = 0$), the scaling factor λ is hindered from increasing any further, which would occur after an interaction that violated the safety metric $\overline{E}_\mathrm{total}$. The stiffness $\mathbf{G}_{r,t,c}$ are kept constant, reducing the controllers' performance.
However, the capability of λ to be scaled down further in order to comply with the safety metric $E_\mathrm{total} \leq \overline{E}_\mathrm{total}$ is not restricted. As aforementioned, it is necessary to ensure that the energy flow from the controller to the manipulator is restricted; therefore, it is necessary to ensure that λ does not rise too fast. Hence, by applying the previously introduced ratio γ (5.6) and rewrite $\boldsymbol{\tau}_\mathrm{Spring}^\top$ as

$$\boldsymbol{\tau}_\mathrm{Spring}^\top = \gamma \mathbf{J}_\mathrm{EE}{}^\top(\mathbf{q}) \mathbf{w}_K^{0,\mathrm{EE}\top}, \tag{5.8}$$

the energy flowing from the tank to the system is restricted. In addition to having an effect on the energy scaling variable λ, γ influences the damping injection term introduced in (4.11) and has, therefore, to be rewritten as:

$$P_\mathrm{motion} = \left(\gamma \left(\mathbf{J}_\mathrm{EE}{}^\top(\mathbf{q}) \mathbf{w}_K^{0,\mathrm{EE}\top} \right) - \mathbf{B}_\mathrm{init} \dot{\mathbf{q}} \right)^\top \dot{\mathbf{q}} \tag{5.9}$$

$$\beta = \begin{cases} 1 & \text{if } P_{\text{motion}} \leqslant \overline{P}_{\text{motion}} \\ \dfrac{\left(\gamma\left(\mathbf{J}_{\text{EE}}{}^{\top}(\mathbf{q})\mathbf{w}_K^{0,\text{EE}^{\top}}\right)\right)^{\top}\dot{\mathbf{q}} - \overline{P}_{\text{motion}}}{\dot{\mathbf{q}}^{\top}\mathbf{B}_{\text{init}}\dot{\mathbf{q}}} & \text{otherwise.} \end{cases} \tag{5.10}$$

The introduction of the energy flow limiting mechanism results in the following control law:

$$\tau_{\text{Imp}}^{\top} = \gamma\mathbf{J}_{\text{EE}}{}^{\top}(\mathbf{q})\mathbf{w}_K^{0,\text{EE}^{\top}} - \beta\mathbf{B}_{\text{init}}\dot{\mathbf{q}}. \tag{5.11}$$

5.3 Experimental Validation

As previously stated, the sample application for the experimental assessment is a disassembly task, more precisely, an unscrewing action. As mentioned in chapter 3, screws are a commonly used fastening method and do not require destructive disassembly. However, as highlighted in [65], when products have reached their respective EOL, the screw condition might have a considerable impact on the disassembly process. The worst-case situation during an unfastening operation is a structural component or screw breaking during the process. This might result in a loss of contact between the manipulator and the EOLP, resulting in damaged components and tools or potentially injuring the human operator. The aforementioned comparison of the presented control formalism and the performance of state-of-the-art techniques is thus carried out on an unscrewing task with a stripped screw on the setup depicted in Figure 5.2. To emphasize the strengths and shortcomings of the three control techniques, the experiment was divided into two phases:

(i) unscrewing phase, and

(ii) interaction with a human phase.

The task begins with the tool already being in contact with the screw, as it is assumed that the position of the screw is known a priori. The manipulator starts to exert a force onto the screw.
The unscrewing phase starts by increasing the force along the z-axis of the TCP until an engagement force of 20 N is reached such that slippage of the screw-bit during the unscrewing is prevented. To systematically and reliably generate the contact loss during the unscrewing, a broken shaft of the screw is simulated by using a screw that is 10 mm shorter than expected by the motion planner. Thus, the controller will still exert approximately 20 N onto the screw whilst the screw shaft is coming out from its fixture. Thereby leading to a contact loss between the screw and the drill bit. This results in the robot's end-effector moving along the z-direction and towards the table due to the motion generation wrench. As aforementioned, the controller's capability to operate in human-populated environments was evaluated as well. This was accomplished by disturbing the robot with a pHRI following the unscrewing phase when the end-effector came to rest on the workbench.

5.3.1 Results

As stated previously, experimental validation comprises of comparison between the presented control formalism and state-of-art approaches, namely a standard Cartesian impedance controller [44] and a Cartesian hybrid force-impedance controller with power limitation [25]. The remainder of this section is structured in the following way:

(i) Experiment 1: Focuses on the response of the standard Cartesian impedance controller.

(ii) Experiment 2: Focuses on the response of the Cartesian hybrid force-impedance controller.

(iii) Experiment 3: Focuses on the repsonse of the presented control energy-aware Cartesian impedance controller

In addition, a video showing the experimental results can found through the following link https://www.youtube-nocookie.com/embed/SgYFHMlEl0k.

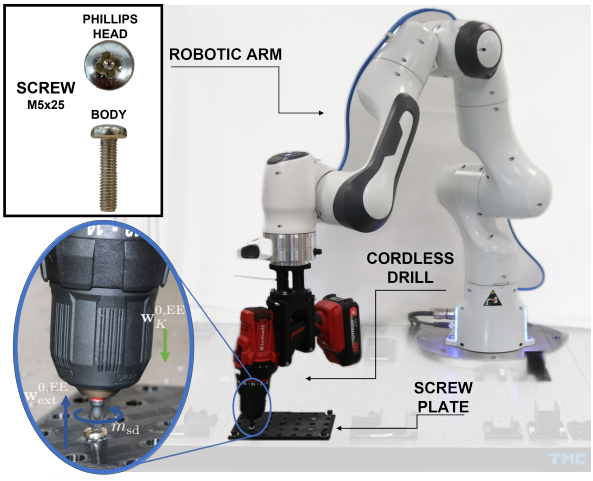

Figure 5.2: Illustrates the experimental setup consiting out of a manipulator that is equipped with a cordless drill used to loosen screws on a screw plate.[Paper C | [3]]©IEEE 2023

Experiment 1: Standard Cartesian Impedance Controller

The force required to perform the unscrewing process is generated by moving $\mathbf{p}^{0}_{\mathrm{d},z}$ incrementally below the screw-head until the z-componet of the force exerted by the controller $\mathbf{w}^{0,\mathrm{EE}}_{\mathrm{K},z}$ reaches the desired force as seen in Figure 5.3.

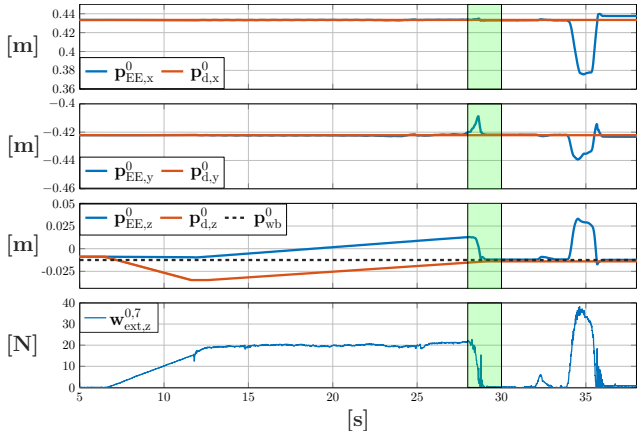

Figure 5.3: Visualizes the observable variables of the Cartesian impedance controller. It shows the discrepancy between the current position $\mathbf{p}^0_{\mathrm{EE}}$ and the desired position $\mathbf{p}^0_{\mathrm{d}}$ of the TCP, as well as the position of the workbench $\mathbf{p}^0_{\mathrm{wb}}$ as well as the linear z-component of the external force exerted on the TCP ($\mathbf{w}^{0,EE}_{\mathrm{ext,z}}$).[Paper C | [3]]© 2023 IEEE.

Followed by the unscrewing phase, here, the incremental change along the z-axis is in the opposite direction of before such that $\mathbf{w}^{0,\mathrm{EE}}_{\mathrm{ext,z}}$ stays within an acceptable working range. When focusing on the externally applied force, one can observe how the force suddenly decreases as the tool bit losses contact with the screw, which leads to the manipulator being driven into the workbench and hitting it with an impact force of 15 N (highlighted with a green area). During the interaction phase, which starts after the robot has come to rest on the workbench, the manipulator's end-effector is displaced by pHRI. Due to Hook's law, the spatial spring generates a force of 37 N that acts in the opposite direction. After reaching its maximum displacement, the end-effector is released, prompting the robot to return to its desired configuration and make contact again with the workbench for a second time with a force of 18 N

Experiment 2: Hybrid Force-Impedance Controller

The hybrid controller generates the necessary force which enables the unscrewing of the screw by the force control part. Hence, it is not necessary to manipulate the desired pose $\mathbf{H}^0_{\mathrm{d}}$. As seen in Figure 5.4, like the standard Cartesian impedance controller, as soon the desired force of 20 N is reached, the unscrewing phase is initiated. After the contact loss due to the failed unscrewing process has occurred, the force controller tries to maintain the desired force, thereby accelerating the manipulator's end-effector. This phenomenon still occurs, despite the power limit imposed on the implemented energy tank,

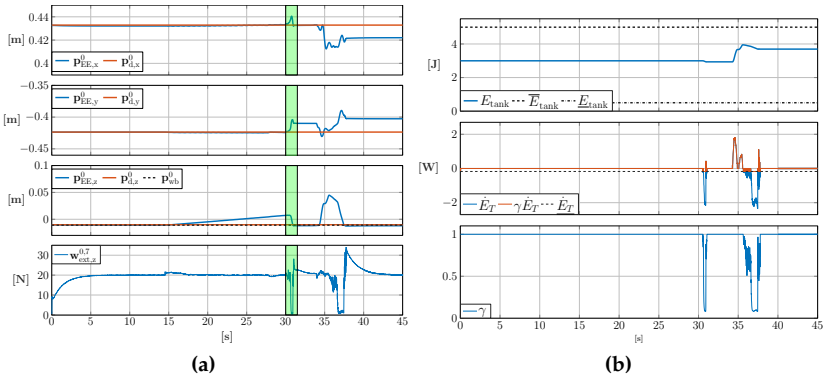

Figure 5.4: Illustrates the observable quanties of the hybrid force impedance controller, including the discrepancy between the current position $\mathbf{p}^0_{\text{EE}}$ and the desired position $\mathbf{p}^0_{\text{d}}$, the position of the workbench $\mathbf{p}^0_{\text{wb}}$, the linear z-component of the external force applied to the TCP ($\mathbf{w}^{0,\text{EE}}_{\text{ext,z}}$), the energy tank E_{T}, and its power flow P_T.[Paper C | [3]]© 2023 IEEE

which restricts the rate at which the controller can inject energy into the system. (see Figure 5.4). This results in a still significant force at an impact of approximately 26 N. During the interaction phase, which starts at 24.5 s, the manipulator's end-effector is again displaced by a pHRI. During the displacement of the robot, it can be seen how the force-control loop tries to adapt to this behavior. As soon as the end effector is released, the power limiting in the tank takes effect, thereby reducing the response of the force-loop; however, the impact force of the robots when making contact with the work surface is still significant with a force of approximately 34 N.

Experiment 3: Energy-Aware Impedance Controller

The unscrewing task presented here followed the identical procedure to that of the standard Cartesian impedance controller in Experiment 1 (subsubsection 5.3.1), where the desired pose was incrementally translated along the longitudinal axis of the screw. After approximately 10 seconds (Figure 5.5), the desired force was achieved, and the unscrewing phase started, during which the equilibrium pose was translated upward. At $\sim$ 26 s, the contact loss occurs, and the end effector moves toward its equilibrium pose, which resulted in a collision with the workbench at 29 s, without a significant impact force ($\sim$ 1.2 N). A similar behavior was observed during the interaction phase, where the end-effector contacts the workbench after the disturbance ends, which resulted in a negligible impact force (approximately 2.6 N). This behavior can be attributed to the energy scaling of the spring and the regulation of the energy flow of the energy tank E_T based on the power limit $\underline{\dot{E}}_T$. When

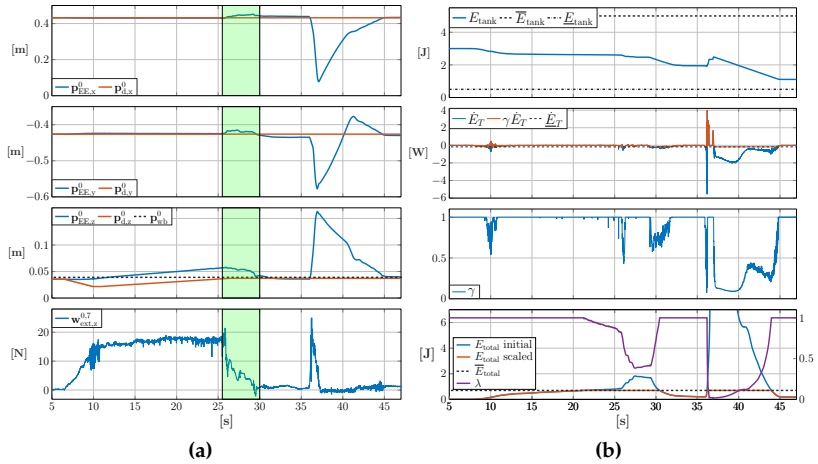

Figure 5.5: Shows the observable variables of the energy-aware impedance controller, which include the difference between the current position $\mathbf{p}^0_{\text{EE}}$ and the desired position $\mathbf{p}^0_{\text{d}}$, the position of the workbench $\mathbf{p}^0_{\text{wb}}$, the linear z-component of the external force applied to the TCP ($\mathbf{w}^{0,\text{EE}}_{\text{ext},z}$), the energy tank E_{T} along with its energy flow $\dot{E}_T$, and the energy scaling of the total energy E_{total}.[Paper C | [3]] © 2023 IEEE

the parameter λ decreases, the spring stiffness also decreases, reducing the energy stored in the system and storing it in E_T. However, when λ increases again, energy is injected back into the system. If this injection of energy is not controlled, it can lead to unstable and non-passive behavior. Therefore, the rate at which energy can be injected must be monitored and limited. Comparing the response of λ and γ, it can be observed that whenever λ increases, γ decreases. Equation (5.8) shows that γ directly affects the rate at which energy can be injected into the system, regulating how quickly λ can increase at each time step. Additionally, the energy tank ensures that λ can only increase if there is sufficient energy in the tank ($E_T > \underline{E}_T$). If the energy tank is depleted, λ remains constant.

5.4 Conclusion

The work in this chapter presented an energy-based control approach with an augmented energy tank to ensure system passivity during a disassembly task. This approach has not been used in such a task before. The formalism's ability to handle contact loss and pHRI is evaluated in an unscrewing task and compared to a standard Cartesian impedance controller and a hybrid force-impedance controller. The force-impedance controller outperforms the other controllers in maintaining a constant force on the screw, but generates the highest impact force in the event of contact loss. The Cartesian impedance

controller generates a significant impact force due to task requirements, while the presented energy-aware formalism introduces a scaling mechanism and a energy flow regulated energy tank to ensure passivity and allow the manipulator to react compliantly. During pHRI, a larger displacement can be achieved with reduced impact force compared to the Cartesian impedance controller. In the event of contact loss, the impact force is reduced by up to 91% and 95% for the Cartesian impedance and hybrid force-impedance controllers, respectively.

5.4.1 Limitations & Future work

A well known problem when it comes to the design of energy tanks for ensuring the passivity of a system is the question on what should the size of the tank be as well as what should the initial energy level be. These questions are not covered in this work. Additionally, a future research direction could investigate other design criteria such as the maximal allowed energy flow from the tank, to make the maximal allowed energy flow formulation depended on the remaining energy in the tank. Finally, another research direction could focus on investigating the implementation of similar concepts for ensuring the passivity of the system when encountering virtual workspace restriction for the method presented in [Paper B | [2]].

CHAPTER 6

Enabling passivity for Cartesian workspace restrictions

This chapter consist of work from the following paper: Hjorth S, Lachner J, Ajoundani A, Chrysostomou D; Enabling passivity for Cartesian workspace restrictions (2023) *Preprint*

6.1 Introduction

As previously mentioned, the previous chapter 4 presented a control scheme which enables safe pHRI in restricted workspaces. However, the passivity of the system or the application of such a control strategy on a disassembly task was not considered as part of the proposed solution. Hence, in the previous chapter 5, an augmented global energy tank was introduced to ensure the passivity of the energy-aware Cartesian impedance controller. Additionally, the adapted control scheme was compared to two other control approaches on a faulty unscrewing task, which are currently used in state of the art unscrewing applications. However, the proposed controller still did not ensured the passivity of the control action of the virtual workspace restrictions. This chapter, will present a state-of-the-art methodology, which will ensure the passivity of the system when subjected to virtual workspace restrictions (as defined in chapter 4) by proposing two different approaches in combination with an energy-aware control strategy presented in chapter 5.
To summarize the main contributions of the presented work are:

(i) Design of two approaches to ensure the the passivity of the system when an energy-aware Cartesian impedance controller is subjected to Cartesian workspace restrictions.

(ii) An experimental validation of the two proposed approaches on a proof of concept faulty extraction task.

This chapter comprises the findings of paper [Paper D | [4]], so it is expected to encounter repeated information, such as context, wording, results, and figures, derived from that particular source.

6.2 Methods

As previously mentioned, this work utilizes an energy-aware Cartesian impedance controller (presented in chapter 5), and as discussed in section 2.3, it is possible to express the energy stored in an impedance-controlled robot the storage function $S = S_{\text{Ctrl}} + S_{\text{Rob}}$; where it was shown that S is only passive if S_{Ctrl} is passive.
Consequently, as seen in the bond graph representation in Figure 6.1, P_{Ctrl} is constructed out of energy flow of the ports of the impedance controller $(\boldsymbol{\tau}_{\text{Imp}}, \dot{\mathbf{q}})$ and the virtual walls $(\boldsymbol{\tau}_C, \dot{\mathbf{q}})$, which are denoted as $P_{\text{Imp}} \in \mathbb{R}$ and $P_{\text{C}} \in \mathbb{R}$, respectively.

$$P_{\text{Ctrl}} = P_{\text{Imp}} + P_{\text{C}} \tag{6.1}$$

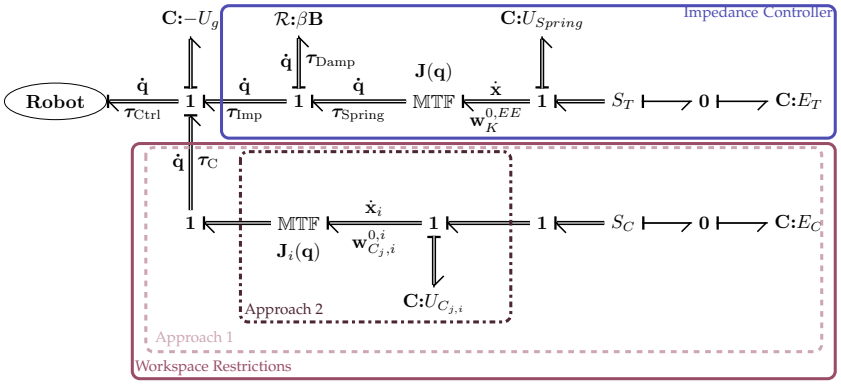

Figure 6.1: The bond graph representation of the presented controller, with the impedance controller highlighted in blue and the workspace restrictions in purple. Adopted from [Paper D | [4]]

.

This equation can be expanded further by expanding P_{Imp} into its sub-components P_{Spring} and P_{Diss}.

$$P_{\text{Ctrl}} + \underbrace{\underbrace{P_{\text{Diss}}}_{\boldsymbol{\tau}_{\text{Damp}}\dot{\mathbf{q}}} + \underbrace{P_{\text{Spring}}}_{\boldsymbol{\tau}_{\text{Spring}}\dot{\mathbf{q}}}}_{\boldsymbol{\tau}_{\text{Imp}}\dot{\mathbf{q}}} + \underbrace{P_{\text{C}}}_{\boldsymbol{\tau}_{\text{C}}\dot{\mathbf{q}}} = 0. \tag{6.2}$$

As previously discussed, the control action of the energy-aware impedance controller is passive. Hence, possible non-passive behavior originates from the injected energy by the control action of the virtual walls at $(\boldsymbol{\tau}_C, \dot{\mathbf{q}})$. In the event of an external disturbance affecting the robot's link(s) i, which results in it moving towards the virtual Cartesian workspace restriction C_j and its activation distance x_j. At the moment where the link enters the activation distance ($d_{i,C_j}(\mathbf{q}) \leq x_j$), the virtual Cartesian workspace restriction starts to introduce the repelling wrench $\mathbf{w}_{C_j,i}^{0,i}$ (4.13) on the respective link.

This repelling wrench increases exponentially due to the in Equation 4.16 defined potential as the link gets closer to the workspace restriction, slowing the motion of the link down and thereby virtually dissipating the kinetic energy of the link.

In the time instance where the link's motion towards the virtual workspace restriction stops, no energy flows between the workspace restriction and the robot's link as the link's velocity is zero. However, in the event that the robot's link is accelerated in the opposite direction of the virtual wall through $\mathbf{w}_{C_j,i}^{0,i}$, energy is injected into the system. Consequently, it can be seen that the system becomes non-passive in the event $P_C + P_{\text{Spring}}$ becomes greater than the dissipated power P_{Diss}, potentially resulting in the instability of the system.

6.2.1 Approaches

Due to the nature of the above presented response related to the restricting control action of the virtual walls, two approaches to preserve the overall passivity of the system are presented and investigated:

(i) Approach 1: This approach utilizes splits the overall energy budget for the virtual walls and the impedance controller across two separate augmented energy tanks.

(ii) Approach 2: This approach observes the resulting overall energy flow of the controller as well as of the virtual walls and decouples if necessary non-passive control actions from the constraint individually.

Approach 1: Separate Energy Tank

This approach adopted the design philosophy of adding an additional energy tank E_C for bounding the energy associated with the virtual workspace next to the energy tank E_T for the implemented impedance controller introduced in chapter 5. Besides enabling the separation between the demand on the overall allocated energy budget of the impedance controller and the workspace constraints across these two energy tanks, it is possible to regulate their individual flow of energy without restricting each other.
This becomes particularly crucial when links without influence on the primary task are subjected to a workspace constraint. As such a scenario could result, in the case of a single energy tank, either in the depletion of the tank, through which the main task gets unnecessarily penalized due to lack of energy in E_T or E_T gets constantly refilled through a link that is in contact with the workspace constraint which would result in the primary task always having energy available.
The concept described above enables us to split the energy flow P_{Ctrl} of the storage function of the controller S_{Ctrl} as defined in (6.1) across the two tanks, E_T and E_C, which have their individual energy flows $\dot{E}_C$ and $\dot{E}_T$ and are bounded by their respective upper and lower bounds, $\overline{E}_T/\underline{E}_T$ and $\overline{E}_C/\underline{E}_C$. Based on the previous definition of P_Diss in (6.1), it can be seen that any increase in energy of S_{Ctrl} is a result of the negative flow direction of the power P_Spring and P_C.

$$-\left(P_\mathrm{Spring} + P_C\right) \geq P_\mathrm{Ctrl} \tag{6.3}$$

Where the energy flow resulting from the virtual walls (P_C), defined as the sum of the individual energy flow for the by C_j restricted link i

$$P_C = \sum_j \sum_i P_{\mathrm{C}_j,i}. \tag{6.4}$$

Hence, through the incorporation of the aforementioned virtual energy tanks E_T and E_C, it is possible to bound the energy that can be injected into S by

S_{Ctrl}. Consequently, the inclusion of E_T and E_C modifies the energy flow of the system, resulting in the following way:

$$P_{\text{Ctrl}} + \dot{E}_T + \dot{E}_C \leq 0 \tag{6.5}$$

where $\dot{E}_T$ and $\dot{E}_C$ as seen in Figure 6.1 are defined as

$$\dot{E}_T = -P_{\text{Spring}} \quad \text{and} \quad \dot{E}_{\text{C}} = -P_{\text{C}}. \tag{6.6}$$

The in chapter 5 presented energy-aware control strategy has been demonstrated to be passive due to its augmented energy tank E_T. Subsequently, the remainder of this section will focus on the tank dynamics associated with virtual walls presented in chapter 4. The design of E_C adheres to the same philosophy as presented in both [Paper C | [3]] and [25]. Firstly, one has to ensure that the energy tank remains within its upper and lower limits, denoted as $\overline{E}_C$ and $\underline{E}_C$. This was achieved by the utilization of the binary variable $h \in \mathbb{R}$ for enforcing $\overline{E}_C$ and $l \in \mathbb{R}$ to hinder any violation of $\underline{E}_C$ in the following way:

$$\begin{aligned} h &= \begin{cases} 0 & \text{if } \dot{E}_C \geq 0 \wedge E_C \geq \overline{E}_C \\ 1 & \text{otherwise} \end{cases} \\ l &= \begin{cases} 0 & \text{if } \dot{E}_C \leq 0 \wedge E_C \leq \underline{E}_C \\ 1 & \text{otherwise} \end{cases} \end{aligned} \tag{6.7}$$

Identically to the impedance controller (described in chapter 5) the energy flow $\dot{E}_C$ at E_C is restricted in the negative direction to a set constraint $\underline{\dot{E}}_C$ which is enforced through the scaling factor $\alpha \in \mathbb{R}$ whilst $\underline{E}_C$ is not violated ($l = 1$),

$$\alpha = \begin{cases} \frac{\underline{\dot{E}}_C}{\dot{E}_C} & \text{if } \dot{E}_C < \underline{\dot{E}}_C \leq 0 \wedge l = 1 \\ 1 & \text{otherwise.} \end{cases} \tag{6.8}$$

Based on the augmentation through the binary variables h and l as well as the scaling factor α, the energy flow at E_C ($\dot{E}_C$) can be reformulated as

$$\dot{E}_C = \begin{cases} \alpha l \dot{E}_C & \text{if } \dot{E}_C \leq 0 \\ h \dot{E}_C & \text{otherwise.} \end{cases} \tag{6.9}$$

In order to transfer this limitation on the energy flow $\dot{E}_C$ that depletes E_C, the scaling factor α as well as the binary variable l have to be included in the calculation of $\boldsymbol{\tau}_{\text{C}}$ in order to ensure that not only a limited amount of energy can be injected through $(\boldsymbol{\tau}_C, \dot{\mathbf{q}})$ at each timestep but also that no energy flows when E_C is empty ($E_C \leq \underline{E}_C$). Consequently, the resulting torques $\boldsymbol{\tau}_C$ as defined in (4.18) are reformulated to:

$$\boldsymbol{\tau}_{\text{C}}^{\top} = \alpha l \sum_i \sum_j \mathbf{J}_i{}^{\top}(\mathbf{q}) \mathbf{w}_{C_j,i}^{0,\text{i}}{}^{\top} \tag{6.10}$$

Approach 2: Flow Monitoring

As aforementioned, to guarantee the passivity of the control actions associated with the enforcement of the virtual walls, this method utilizes a single energy tank, in contrast to Approach 1. Instead, this approach employs a strategy that combines an energy flow regulation technique and a power-based decoupling mechanism to handle non-passive behavior induced by virtual walls. The method presented in Approach 1 allowed for the regulation of the rate of energy of the control actions from the virtual walls, which, as mentioned above, is also a feature in this approach. However, as depicted in Figure 6.1, the regulation of energy flow for virtual walls is now occurring at the port $(\boldsymbol{\tau}_C, \dot{\mathbf{q}})$ instead of at E_C.

As mentioned earlier in this section, in addition to restricting the energy injected by control actions of the virtual walls in the non-passive direction ($P_C > 0$), the individual energy flow of P_C can be decoupled on the basis of the overall energy flow at the power port $(\boldsymbol{\tau}_{\text{Ctrl}}, \dot{\mathbf{q}})$ (P_{Ctrl}). This is necessary due to the absence of the in Approach 1 proposed augmented energy tank E_C in the control architecture; it is no longer possible to utilize the previously virtually dissipated energy stored in the energy tank.

Therefore, it is necessary to observe and restrict the energy flow P_C in a positive direction as well as decouple individual energy flows of P_C that contribute to the flow in this direction. This is achieved by first calculating the initial energy flow from the virtual walls P_C (6.4). In order to limit the flow $P_C > 0$ on basis of a upper limit $\overline{P}_C$ the energy flow restriction variable $\kappa \in \mathbb{R}$ is introduced:

$$\kappa = \begin{cases} \frac{\overline{P}_C}{P_C} & \text{if } P_C > \overline{P}_C > 0 \\ 1 & \text{otherwise,} \end{cases} \tag{6.11}$$

which as already shown in Approach 1 influence the resulting torques $\boldsymbol{\tau}_C^\top$ (4.18) in the following way:

$$\boldsymbol{\tau}_{C,\kappa}^\top = \kappa \sum_i \sum_j \mathbf{J}_i{}^\top(\mathbf{q}) \mathbf{w}_{C_{j,i}}^{0,i}{}^\top. \tag{6.12}$$

Consequently, the resulting energy flow can be expressed as $P_C^\dagger = \kappa \sum_j \sum_i P_{C_{j,i}} \in \mathbb{R}$. However, as mentioned previously, due to the lack of an energy tank, the energy that can be injected into the system, even though it is restricted through κ, can still possibly result in the violation of the system's passivity. Therefore, it is necessary to observe the energy flow P_{Ctrl} at the power port $(\boldsymbol{\tau}_{\text{Ctrl}}, \dot{\mathbf{q}})$, which is defined as

$$P_{\text{Ctrl}} = (\boldsymbol{\tau}_{\text{Imp}}^\top + \boldsymbol{\tau}_{C,\kappa}^\top)\dot{\mathbf{q}} \tag{6.13}$$

Using P_{Ctrl}, one can assess whether the system becomes non-passive ($P_{\text{Ctrl}} > 0$) through the scaled control action of the virtual walls ($\boldsymbol{\tau}_{C,\kappa}$). If $P_{\text{Ctrl}} > 0$ holds true, the individual energy flows of P_C (i.e.,$P_{C_{j,i}}$) are examined to identify their contributions to the system's non-passivity ($P_{C_{j,i}} > 0$) and energy

flows are then decoupled using the binary variable $\phi_{j,i}$:

$$\phi_{j,i} = \begin{cases} 0 & \text{if } P_{\text{Ctrl}} > 0 \wedge P_{C_{j,i}} > 0 \\ 1 & \text{otherwise.} \end{cases} \tag{6.14}$$

Consequently, the energy flow at the port $(\boldsymbol{\tau}_{\text{Ctrl}}, \dot{\mathbf{q}})$ can be rewritten to:

$$P_{\text{Ctrl}} + P_{Imp} + \underbrace{\kappa \sum_i \sum_j \phi_{j,i} P_{C_{j,i}}}_{P_C^{\dagger}} = 0. \tag{6.15}$$

In order to transfer this limitation on the energy flow at $(\boldsymbol{\tau}_C, \dot{\mathbf{q}})$ that contributes to the non-passivity of the system, the scaling factor α as well as the individual decoupling variables $\phi_{j,i}$ have to be included in the calculation of $\boldsymbol{\tau}_C$ in order to ensure that no passivity violating energy can be injected through $(\boldsymbol{\tau}_C, \dot{\mathbf{q}})$ Consequently, the equation for $\boldsymbol{\tau}_C$ (4.18) has to be is reformulated to:

$$\boldsymbol{\tau}_C^{\top} = \kappa \sum_i \sum_j \phi_{j,i} \mathbf{J}_i{}^{\top}(\mathbf{q}) \mathbf{w}_{C_{j,i}}^{0,i\ \top} \tag{6.16}$$

6.3 Experimental Validation

As previously stated, the sample application for the experimental validation of the presented approaches is a disassembly task, i.e., a proof-of-concept component extraction/separation task. The concept of the experimental setup is to simulate an accidental contact loss during a separation process of two components while a human operator is in close proximity to the robot. This scenario aims to showcase the possibility of enabling close collaboration during HRCD tasks. In order to showcase the strength and shortcomings of the two presented approaches, the experiment was divided into two different phases:

(i) accidental phase , and

(ii) pHRI phase.

The task begins with the gripper already being in contact with the fixture that should be extracted. Hence, the accidental phase, highlighted in the plots in green, starts with increasing the force along TCP z-axis, pulling on the fixture until it reaches a value of 62 N is reached. In order to get a reliable and repeatable simulation of the failure of the part through an instantaneous contact loss during the extraction, the gripper is opened, through an external trigger, simulating a failure of the part. This results in the robot's end-effector being accelerated in an upwards direction until 6^{th}-link encounters the virtual wall C_1, which is set to avoid collisions with the human co-worker in case of a failure.

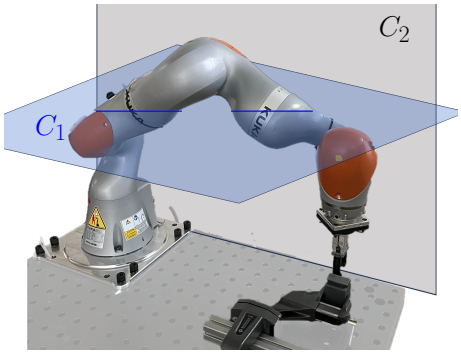

Figure 6.2: Experimental setup for component extraction: a robot gripper extracts a component, simulated by a 3D-printed fixture, while being subject to virtual walls C_1 and C_2.

As aforementioned, the use case is in a HRC setting. Hence, during the pHRI phase, highlighted in the plots in red, links 6 and 4 of the robot were manually pushed with excessive force into the virtual walls C_1 and C_2, respectively, to be able to validate that the robot does not become unstable through the additional energy that is injected to the system through the virtual walls.

6.3.1 Results

As stated previously, experimental validation comprises of comparison between a separated energy tank (Approach 1) and a purely energy flow observation based (Approach 2) approach. The remainder of this section is structured in the following way:

(i) Experiment A: Focuses on the response of the separate tank approach presented in Approach 1.

(ii) Experiment B: Focuses on the response of the flow monitoring approach presented in Approach 2.

Additionally, a video showcasing the experimental results can found through the following link https://youtu.be/wzOtvGffonY.

Experiment A: Separate Energy Tank Approach

The accidental phase started by translating robot's desired pose $\mathbf{H}_{\mathrm{d}}^{0}$ along the TCPs z-axis until $\mathbf{w}_{\mathrm{ext},z}^{0,\mathrm{EE}}$ reached $\mathbf{f}_{\mathrm{pull},z} = 62$ N (Figure 6.3, $4 - 12$ s). After which the gripper got triggered to release the fixture, resulting in abrupt acceleration of the end effector towards $\mathbf{H}_{\mathrm{d}}^{0}$ due to the release of the potential energy U_{Spring}. This caused the end-effector to pass $\mathbf{H}_{\mathrm{d}}^{0}$, which resulted in link 6 passing into the activation area of C_1 (indicated by d_{6,C_1} crossing the dashed line). This resulted in being applied $\mathbf{w}_{C_1,6}^{0,6}$, which virtually dissipated

the link's kinetic energy through which the level in E_C increased due to a positive energy flow $\dot{E}_C$ (Figure 6.3 magnified in purple) at the port of the energy tank E_C. As link 6 got pushed out by $\mathbf{w}_{C_1,6}^{0,6}$ it can be seen that the energy flow $\dot{E}_C$ changes direction ($\dot{E}_C < 0$).

However, as seen in the purple magnification window, $\dot{E}_C$ did not exceed the

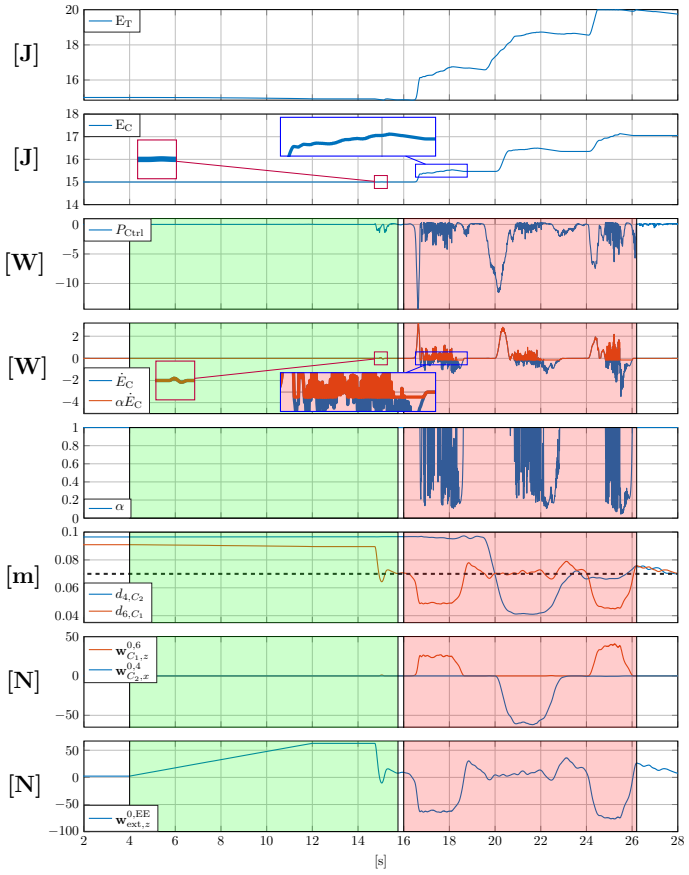

Figure 6.3: Visualizes the observable quantities of Approach 1. The two energy tanks E_T, and E_C; the difference between the unrestricted and through α and restricted energy flow $\dot{E}_C$ due to the repelling wrenches $\mathbf{w}_{C_1,z}^{0,6}$ and $\mathbf{w}_{C_2,x}^{0,4}$ of virtual walls C_1 and C_2 along their repelling direction as well as the external wrench acting along the TCP's z-axis $\mathbf{w}_{\text{ext},z}^{0,\text{EE}}$.

limit $\underline{\dot{E}}_C$ and the injected energy was close to equal as the virtual dissipated one. Hence, the energy injected due to $\mathbf{w}_{C_1,6}^{0,6}$ during the accidental phase did not violate the passivity of the system.

The pHRI-phase started by the robot's 6^{th}-link being manually pushed into the virtual wall C_1 ($16.2 - 18$ s and $23 - 26.2$ s). The identical procedure was

applied to link 4 with respect to C_2 ($\sim 20 - 22$ s).
The observed behavior is similar to the accidental phase one, with the amount of energy stored in E_C being increased until link 4 or 6 reached its equilibrium point within the activation distance based on their respective externally applied wrenches and decreased as the links exited the virtual wall. When either of the two links approached a virtual wall and was held within the activation distance virtual wall with a significant force, $\dot{E}_C$ changed direction high frequent manner, this behavior occurred due to high forces acting on the links and the fluctuation of the force applied by the human operator in the direction of the virtual wall (max. $\mathbf{w}^{0,6}_{\text{ext},z} = -40$ N, max.$\mathbf{w}^{0,4}_{\text{ext},x} = 60$ N). This behavior, as explained in section 6.2 could, if the energy flow is left unchecked, result in instability of the system even though E_C is bounded.
However, as seen in the magnification in blue, the initial energy flow of $\dot{E}_C$ got limited to $\underline{\dot{E}}_C$ through α, resulting in that a fraction of the virtually dissipated energy stored E_C got injected back into the system.
Consequently, the level in E_C rose at a high rate then it was drained, showcasing that the system stays passive. Additionally, it can be observed that despite forcefully pushing the link into the virtual walls, the links did not violate their respective distances from the walls.

Experiment B: Flow Monitoring Approach

Identically to the experiment conducted in Experiment A is highlighted in green, and started by translating $\mathbf{H}^0_{\text{d}}$ until force $\mathbf{w}^{0,\text{EE}}_{\text{ext},z} = \mathbf{f}_{\text{pull},z}$ at 14.5 s (see Figure 6.4). At this point, the gripper released the fixture, resulting in a similar behavior as during Experiment A. Where the repelling wrench $\mathbf{w}^{0,6}C_1, 6$ was applied to link 6, leading to a negative energy flow P_C at the power port $(\boldsymbol{\tau}_C, \dot{\mathbf{q}})$ and during the exiting of the activation distance (dotted line), the energy was produced ($P_C > 0$). However, as seen in the purple magnified view in Figure 6.4 the energy injected by control action of C_1 did, similar to the experiment described in Experiment A, not result in P_C reaching the set limit on the overall energy flow at port $(\boldsymbol{\tau}_C, \dot{\mathbf{q}})$ $(\overline{P}_C)$.
Hence, no scaling of P_C through κ occurred. As explained earlier during the pHRI phase (highlighted in red), link 6 and link 4 were manually pushed into their respective virtual walls C_1 and C_2, with link 6 between in contact with C_1 at $15.7 - 17.2$ s and $22 - 24.5$ s and link 4 with C_2 at $\sim 19 - 21$ s).
As already observed in Experiment A, when the links were pushed into the virtual walls, the kinetic energy of the link was virtually dissipated through the wrenches $\mathbf{w}^{0,6}_{C_1,4}/\mathbf{w}^{0,4}_{C_2,4}$, which resulted in a negative energy flow at the port $(\boldsymbol{\tau}_C, \dot{\mathbf{q}})$ ($P_C < 0$). Once $\mathbf{w}^{0,6}_{C_1,6}/\mathbf{w}^{0,4}_{C_2,4}$ reached their respective equilibrium point based on the externally applied wrenches onto the links, the energy flow P_C changed direction with high frequency due to fluctuations in the externally applied wrench by the operator. Resulting in a behavior similar to that described in Experiment A.

As already stated earlier, these fluctuations in the energy flow could lead, if

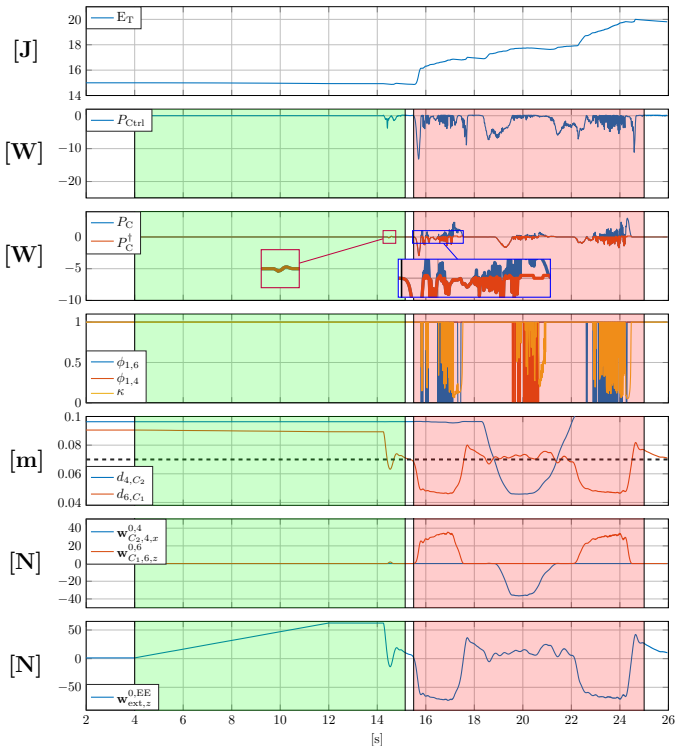

Figure 6.4: Visualizes the observable quantities of Approach 2. The energy tank E_T, the energy flow P_{Ctrl}, the difference between the unrestricted and through κ and $\phi_6, 1/\phi_{4,1}$ restricted energy flow P_C due to the repelling wrenches $\mathbf{w}^{0,6}_{C_1,6_z}$ and $\mathbf{w}^{0,4}_{C_2,4_x}$ of virtual walls C_1 and C_2 along their repelling direction as well as the external wrench acting on the TCP's along its z-axis $\mathbf{w}^{0,EE}_{ext,z}$.

left unaddressed, to a non-passive behavior as well as to the potential instability of the system. In order to ensure that the system stays passive, the energy flow P_C is restricted through the scaling factor κ (equation (6.11)) and the individual decoupling terms $\phi_{6,1}$ and $\phi_{4,1}$ (equation (6.14)).
Then looking at $P_C^\dagger$ when link 6 is subjected to C_1 (blue magnified view in Figure 6.4), one can observe how $P_C^\dagger$ changed value between the predefined limit on the energy flow at $(\boldsymbol{\tau}_C, \dot{\mathbf{q}})$, $\overline{P}_C$ and 0. This behavior is directly related to the decoupling term introduced in (6.14), with $\phi_{6,1}$ decoupling $P_{C_{6,1}}$ from the energy flow at the power port $(\boldsymbol{\tau}_C, \dot{\mathbf{q}})$ on the basis that the through κ limited energy flow is in a positive direction ($\kappa P_C > 0$). This resulted in $P_{\text{Ctrl}} \leq 0$ held true, and therefore the overall system was kept passive.

6.4 Conclusion

The work presented in this chapter proposed and compared two approaches (Approach 1 and Approach 2) to ensure the passivity of a kinematically redundant robot when subjected to Cartesian workspace restrictions. The proposed control extended the energy-aware Cartesian Impedance control strategy presented in [Paper C | [3]] with an energy-based approach for enforcing virtual walls presented in [Paper B | [2]]. Both approaches were evaluated on a faulty disassembly, and demonstrating their effectiveness in maintaining passivity, when the links of the robot are subjected to a virtual wall due to a sudden loss in contact between the robots end-effector and the fixture, as well as even when subjected to virtual walls under significant forces through a pHRI. In Approach 1, a separate augmented energy tank dedicated to the control action of the virtual wall was utilized to separate the two energy demands of the system from each other. Approach 2 focuses on observing and limiting the overall energy flow of the control action coming from the workspace restrictions and decouples individual energy flow resulting from the different virtual walls based on the controller's overall energy flow. The experimental validation of both approaches showed that they were able to ensure the passivity of the system while securing that the robots did not violate any of the virtual even subjected to them through an externally applied force.

6.4.1 Limitations & Future Work

The general limitation of the presented control architecture, regardless of the presented passivity-based approaches one chooses, is that it does not include any prioritization between the task or the virtual wall nor prioritize between the active restrictions themselves. Additionally, both of the presented approaches have some limitations which were not covered in this work. In Approach 1, it is a necessity to select suitable upper and lower bounds of the energy tank; however, this is non-trivial due to the randomness involved in the potential interactions between the robot and a virtual wall in terms of their amount, severity, and timing.
Regardless of the chosen approach to ensure passivity, the overall design of the control structure has a drawback: it does not prioritize either the task or the virtual wall nor does it prioritize the restrictions imposed by the virtual walls themselves. One could argue that in situations where an event could potentially result in harm or damage, the control action becomes secondary to enforcing the task. Therefore, in future research, it would be worthwhile to explore how to incorporate such conflicts between tasks and compare controllers that saturate the robots' nullspace.
In the case of approach 2, the main limitation lies in the increasing complexity that is encountered while observing and decoupling the individual energy flows associated with the links and virtual walls, as with an increasing num-

ber of virtual walls and restricted links associated with these walls. Hence, future research could focus on implementing a prioritization between the restrictions.

CHAPTER 7

General Conclusion

This thesis provides an investigation into the current state of the art in non-destructive HRCD applications as well as the utilization of an energy-aware control approach for kinematically redundant robots for such tasks. Furthermore, a reformulated artificial potential field approach was proposed to enable the robot to stay within predefined workspaces during physical human-robot interaction.

The key contributions presented in this thesis can be summarized the as follows:

- An in-depth analysis of the current state-of-the-art in the field of human-robot collaborative disassembly on bases on the current state-of-the-art in HRC and disassembly as well as a framework to evaluate future contributions.
- An energy-based approach to enforce workspace restrictions for kinematically redundant and torque controller manipulators.
- An extension for an energy-aware Cartesian impedance controller with an augmented energy tank as well as an experimental comparison with control schemes currently applied in human-robot collaborative disassembly unscrewing task.
- An extension of an energy-based approach to enforce virtual Cartesian workspace restrictions through to different passivity based methods with an experimental comparison between the two presented approaches on a proof-of-concept human-robot collaborative disassembly task.

The in chapter 1 presented research questions where answered in the following way:

Q1: What are the main technological hurdles HRCD applications face?

In the work discussed in chapter 3, it was found that the main focus within the field still lies on how to tackle the disassembly processes on the robotic

side and that technological enablers for HRI, such as visual and verbal interface are generally rare and only to a limited extend implemented. This holds especially true for pHRIs, as there is a notable absence of post-collision control schemes that are able to limit the energy exchange between the robot and its environment, which is essential for a safe, closer, and more engaging HRC.

Q2: How can the workspaces of kinematically redundant manipulators be restricted while ensuring safe pHRI?

In the work discussed in chapter 4, an energy-based approach was also been presented to enforce the virtual work space for kinematically redundant manipulators during pHRI. This approach enables the human to interact physically with the manipulator whilst ensuring that the manipulator stays within its virtually restricted workspace. The method combined an energy-aware Cartesian Impedance control scheme that ensures that the manipulator is capable of adapting to pHRIs based on energy thresholds specified on the ISO standards with a modified artificial potential field approach.

Q3: How does an energy-aware Cartesian Impedance control strategy perform on Disassembly tasks?

The work discussed in chapter 5 investigated the utilization of an energy-aware Cartesian impedance controller for a disassembly task, more specifically, a faulty unscrewing task. In this work, an energy-aware Cartesian impedance controller approach was adapted with an augment energy tank to ensure the passivity of the system and compared to currently utilized control schemes in the field of HRCD. It was shown that the presented formalism outperformed the other control schemes when it came to handling contact loss and pHRI during and after the completion of the unscrewing task.

Q4:How can virtual workspace restrictions be enforced without violating the system's passivity?

The work discussed in chapter 6 extended on the previously proposed works that were described in chapter 4 and chapter 5 by investigating the effect the enforcing control action of the workspace restrictions has on the passivity of the system. Based on this investigation, two different approaches were proposed that focused on observing and limiting the energy flow of the workspace restriction and compared to each other on a faulty extraction/separation task. It was shown that both the presented approaches were able to keep the system passive and the restricted links within their predefined workspaces when subjected to significant force.

This work postulates that in order to successfully integrate an HRCD cell, the collaboration between the robots and the human must allow not just for verbal or visual HRI but also enable pHRIs during the disassembly process of EOLP. However, as pointed out chapter 3, there is currently a lack of the integration of control strategies that can facilitate pHRI or handle sudden contact loss between the robot and the workpiece. Hence, this work proposed and show-cased control approaches in chapter 5 and chapter 6 that are capable of handling such scenarios by observing and limiting the flow of energy as well as the energy stored in the system. However, this work did not investigate how such control strategies could be utilized efficiently in a human-robot collaborative disassembly setting. Therefore, future work can investigate how the different control parameters specifically to such energy-aware approaches could be adapted during the task to maximize the efficiency and safety of the system. Additionally, the presented work did not cover the notion of solving task conflicts between the different control actions of the control strategy.

Bibliography

[1] S. Hjorth and D. Chrysostomou, "Human–robot collaboration in industrial environments: A literature review on non-destructive disassembly," *Robotics and Computer-Integrated Manufacturing*, vol. 73, p. 102208, 2022. [Online]. Available: https://www.sciencedirect.com/science/article/pii/S0736584521000910

[2] S. Hjorth, J. Lachner, S. Stramigioli, O. Madsen, and D. Chrysostomou, "An energy-based approach for the integration of collaborative redundant robots in restricted work environments," *2020 IEEE/RSJ International Conference on Intelligent Robots and Systems*, 2020.

[3] S. Hjorth, E. Lamon, D. Chrysostomou, and A. Ajoudani, "Design of an energy-aware cartesian impedance controller for collaborative disassembly," *2023 IEEE/RSJ International Conference on Robotics and Automation*, 2023.

[4] S. Hjorth, J. Lachner, A. Ajoudani, and D. Chrysostomou, "Enabling passivity for cartesian workspace restrictions," *PrePrint*, 2023.

[5] European Parliament, "No E-waste in the EU: facts and figures (infographic)," 2023. [Online]. Available: https://www.europarl.europa.eu/news/en/headlines/society/20201208STO93325/e-waste-in-the-eu-facts-and-figures-infographic

[6] F. Ardente, L. Talens Peiró, F. Mathieux, and D. Polverini, "Accounting for the environmental benefits of remanufactured products: Method and application," *Journal of Cleaner Production*, vol. 198, pp. 1545–1558, 2018.

[7] Ellen MacArthur Foundation, "Intelligent Assets: Unlocking the Circular Economy Potential," *Ellen MacArthur Found.*, pp. 1–25, 2016. [Online]. Available: https://bit.ly/39WkeXb

[8] E. Commission, D.-G. for Research, and Innovation, *Waste as a resource : EU research*. Publications Office, 2012.

[9] P. Drazan, "The impact of robots on manufacturing processes and society at large," in *The Management Implications of New Information Technology*. Routledge, 2018, pp. 48–55.

[10] W. Figueiredo, "A High-speed Robotic Disassembly System for the Recycling and Reuse of Cellphones," Master Thesis, Massachusetts Institute of Technology, 2018.

[11] Y. Zhang, H. Lu, D. T. Pham, Y. Wang, M. Qu, J. Lim, and S. Su, "Peg–hole disassembly using active compliance," *Royal Society Open Science*, vol. 6, no. 8, 2019.

[12] K. Elo and E. Sundin, "Automatic dismantling challenges in the structural design of LCD TVs," *Procedia CIRP*, vol. 15, pp. 251–256, 2014.

[13] T. Tolio, A. Bernard, M. Colledani, S. Kara, G. Seliger, J. Duflou, O. Battaia, and S. Takata, "Design, management and control of demanufacturing and remanufacturing systems," *CIRP Ann. - Manuf. Technol.*, vol. 66, no. 2, pp. 585–609, 2017.

[14] ISO, "Robots and robotic devices — Vocabulary (ISO 8373:2016)," 2016.

[15] ——, "Robots and robotic devices - Safety requirements for industrial robots - Part 1: Robots (ISO 10218-1:2012)," 2012.

[16] ——, "Robots and robotic devices – Safety requirements for industrial robots – Part 2: Robot systems and integration (ISO 10218-2:2012)," 2012.

[17] ——, "Robots and robotic devices — Collaborative robots (ISO-15066:2016)," 2016.

[18] S. Haddadin, A. De Luca, and A. Albu-Schaffer, "Robot Collisions: A Survey on Detection, Isolation, and Identification," *IEEE Transactions on Robotics*, vol. 33, no. 6, pp. 1292–1312, dec 2017.

[19] A. De Santis, B. Siciliano, A. De Luca, and A. Bicchi, "An atlas of physical human-robot interaction," *Mech. Mach. Theory*, vol. 43, no. 3, pp. 253–270, 2008.

[20] P. Aivaliotis, S. Aivaliotis, C. Gkournelos, K. Kokkalis, G. Michalos, and S. Makris, "Power and force limiting on industrial robots for human-robot collaboration," *Robotics and Computer-Integrated Manufacturing*, vol. 59, pp. 346–360, 2019.

[21] J. Lachner, F. Allmendinger, S. Stramigioli, and N. Hogan, "Shaping impedances to comply with constrained task dynamics," *IEEE Transactions on Robotics*, 2022.

[22] Y. Michel, C. Ott, and D. Lee, "Safety-aware hierarchical passivity-based variable compliance control for redundant manipulators," *IEEE Transactions on Robotics*, 2022.

[23] A. Q. Keemink, H. van der Kooij, and A. H. Stienen, "Admittance control for physical human–robot interaction," *Int. J. Rob. Res.*, vol. 37, no. 11, pp. 1421–1444, sep 2018.

[24] I. Ranatunga, S. Cremer, D. O. Popa, and F. L. Lewis, "Intent aware adaptive admittance control for physical Human-Robot Interaction," in *IEEE Int. Conf. Robot. Autom.*, vol. 2015-June. Seattle: IEEE, 2015, pp. 5635–5640.

[25] E. Shahriari, L. Johannsmeier, E. Jensen, and S. Haddadin, "Power flow regulation, adaptation, and learning for intrinsically robust virtual energy tanks," *IEEE Robotics and Automation Letters*, vol. 5, no. 1, pp. 211–218, 2019.

[26] A. Ajoudani, A. M. Zanchettin, S. Ivaldi, A. Albu-Schäffer, K. Kosuge, and O. Khatib, "Progress and prospects of the human–robot collaboration," *Autonomous Robots*, vol. 42, no. 5, pp. 957–975, 2018.

[27] R. Scalise, S. Li, H. Admoni, S. Rosenthal, and S. S. Srinivasa, "Natural language instructions for human–robot collaborative manipulation," *The International Journal of Robotics Research*, vol. 37, no. 6, pp. 558–565, 2018.

[28] W. Wang, R. Li, Y. Chen, Z. M. Diekel, and Y. Jia, "Facilitating human–robot collaborative tasks by teaching-learning-collaboration from human demonstrations," *IEEE Transactions on Automation Science and Engineering*, vol. 16, no. 2, pp. 640–653, 2019.

[29] L. Wang, R. Gao, J. Váncza, J. Krüger, X. V. Wang, S. Makris, and G. Chryssolouris, "Symbiotic human-robot collaborative assembly," *CIRP annals*, vol. 68, no. 2, pp. 701–726, 2019.

[30] S. Robla-Gomez, V. M. Becerra, J. R. Llata, E. Gonzalez-Sarabia, C. Torre-Ferrero, and J. Perez-Oria, "Working Together: A Review on Safe Human-Robot Collaboration in Industrial Environments," *IEEE Access*, vol. 5, pp. 26 754–26 773, 2017.

[31] C. Jost, B. Le Pévédic, T. Belpaeme, C. Bethel, D. Chrysostomou, N. Crook, M. Grandgeorge, and N. Mirnig, *Human-Robot Interaction: Evaluation Methods and Their Standardization*. Springer Nature, 2020, vol. 12.

[32] W. Kim, L. Peternel, M. Lorenzini, J. Babič, and A. Ajoudani, "A human-robot collaboration framework for improving ergonomics during dexterous operation of power tools," *Robotics and Computer-Integrated Manufacturing*, vol. 68, p. 102084, 2021. [Online]. Available: https://www.sciencedirect.com/science/article/pii/S0736584520302945

[33] S. Sheikholeslami, A. Moon, and E. A. Croft, "Cooperative gestures for industry: Exploring the efficacy of robot hand configurations in expression of instructional gestures for human–robot interaction," *The International Journal of Robotics Research*, vol. 36, no. 5-7, pp. 699–720, 2017.

[34] M. Lagomarsino, M. Lorenzini, E. De Momi, and A. Ajoudani, "An online framework for cognitive load assessment in industrial tasks," *Robotics and Computer-Integrated Manufacturing*, vol. 78, p. 102380, 2022. [Online]. Available: https://www.sciencedirect.com/science/article/pii/S0736584522000679

[35] M. Lagomarsino, M. Lorenzini, P. Balatti, E. D. Momi, and A. Ajoudani, "Pick the right co-worker: Online assessment of cognitive ergonomics in human-robot collaborative assembly," *IEEE Transactions on Cognitive and Developmental Systems*, pp. 1–1, 2022.

[36] M. Lagomarsino, M. Lorenzini, E. De Momi, and A. Ajoudani, "Robot trajectory adaptation to optimise the trade-off between human cognitive ergonomics and workplace productivity in collaborative tasks," in *2022 IEEE/RSJ International Conference on Intelligent Robots and Systems (IROS)*, 2022, pp. 663–669.

[37] B. D. Argall and A. G. Billard, "A survey of tactile human–robot interactions," *Robotics and Autonomous Systems*, vol. 58, no. 10, pp. 1159–1176, 2010. [Online]. Available: https://www.sciencedirect.com/science/article/pii/S0921889010001375

[38] J. M. Gandarias, P. Balatti, E. Lamon, M. Lorenzini, and A. Ajoudani, "Enhancing flexibility and adaptability in conjoined human-robot industrial tasks with a minimalist physical interface," in *2022 International Conference on Robotics and Automation (ICRA)*, 2022, pp. 8061–8067.

[39] M. Koppenborg, P. Nickel, B. Naber, A. Lungfiel, and M. Huelke, "Effects of movement speed and predictability in human–robot collaboration," *Human Factors and Ergonomics in Manufacturing & Service Industries*, vol. 27, no. 4, pp. 197–209, 2017.

[40] E. Matsas, G.-C. Vosniakos, and D. Batras, "Prototyping proactive and adaptive techniques for human-robot collaboration in manufacturing using virtual reality," *Robotics and Computer-Integrated Manufacturing*, vol. 50, pp. 168–180, 2018.

[41] R. S. Andersen, O. Madsen, T. B. Moeslund, and H. B. Amor, "Projecting robot intentions into human environments," in *2016 25th IEEE International Symposium on Robot and Human Interactive Communication (RO-MAN)*. IEEE, 2016, pp. 294–301.

[42] H. Liu and L. Wang, "An ar-based worker support system for human-robot collaboration," *Procedia Manufacturing*, vol. 11, pp. 22–30, 2017.

[43] M. Ostanin, S. Mikhel, A. Evlampiev, V. Skvortsova, and A. Klimchik, "Human-robot interaction for robotic manipulator programming in mixed reality," in *2020 IEEE International Conference on Robotics and Automation (ICRA)*. IEEE, 2020, pp. 2805–2811.

[44] C. Ott, *Cartesian Impedance Control of Redundant and Flexible-Joint Robots*. Springer, Berlin, Heidelberg, 2008.

[45] H. Khalil, *Nonlinear Systems*, ser. Pearson Education. Prentice Hall, 2002. [Online]. Available: https://books.google.dk/books?id=t_d1QgAACAAJ

[46] J. Lachner, "A geometric approach to robotic manipulation in physical human-robot interaction," Ph.D. dissertation, University of Twente, Netherlands, Jul. 2022.

[47] S. Stramigioli, E. Fasse, and J. C. Willems, "A rigorous framework for interactive robot control," *International Journal of Control*, vol. 75, no. 18, pp. 1486–1503, 2002.

[48] S. Stramigioli, "Energy-aware robotics," in *Mathematical Control Theory I*, M. K. Camlibel, A. A. Julius, R. Pasumarthy, and J. M. Scherpen, Eds. Cham: Springer International Publishing, 2015, pp. 37–50.

[49] S. S. S. Richard M. Murray, Zexiang Li, *A Mathematical Introduction to Robotic Manipulation*. CRC Press, 1994.

[50] A. van der Schaft, *Dissipative systems theory*. Springer Berlin Heidelberg, 1996, pp. 32–52. [Online]. Available: https://doi.org/10.1007/3-540-76074-1_10

[51] S. Stramigioli, *Modeling and IPC Control of Interactive Mechanical Systems - A Coordinate-Free Approach*. Springer, 2001.

[52] A. M. Zanchettin, E. Croft, H. Ding, and M. Li, "Collaborative Robots in the Workplace," *IEEE Robot. Autom. Mag.*, vol. 25, no. 2, pp. 16–17, 2018.

[53] A. Ajoudani, A. M. Zanchettin, S. Ivaldi, A. Albu-Schäffer, K. Kosuge, and O. Khatib, "Progress and prospects of the human–robot collaboration," *Autonomous Robots*, vol. 42, no. 5, pp. 957–975, 2018.

[54] O. Khatib, "Real-time obstacle avoidance for manipulators and mobile robots," in *Proc. - IEEE Int. Conf. Robot. Autom.*, vol. 2, 1985, pp. 500–505.

[55] S. Stramigioli, "From differential manifolds to interactive robot control," Ph.D. dissertation, University of Twente, 12 1998.

[56] G. Raiola, C. A. Cardenas, T. S. Tadele, T. De Vries, and S. Stramigioli, "Development of a Safety- and Energy-Aware Impedance Controller for Collaborative Robots," *IEEE RA-L*, vol. 3, no. 2, pp. 1237–1244, 2018.

[57] B. Siciliano and O. Khatib, Eds., *Springer Handbook of Robotics*. Cham: Springer International Publishing, 2016, vol. 2.

[58] N. Hogan, "Impedance control: An approach to manipulation. part i, ii, iii," *Journal of Dynamic Systems, Measurement, and Control*, vol. 107, pp. 304 – 313, 07 1984.

[59] T. Tadele, "Human-friendly robotic manipulators: safety and performance issues in controller design," Ph.D. dissertation, University of Twente, 11 2014.

[60] V. Duindam and S. S., "Port-based asymptotic curve tracking for mechanical systems," *European Journal of Control*, 2004.

[61] N. Ramuzat, S. Boria, and O. Stasse, "Passive inverse dynamics control using a global energy tank for torque-controlled humanoid robots in multi-contact," *IEEE Robotics and Automation Letters*, vol. 7, no. 2, pp. 2787–2794, 2022.

[62] B. Gerlagh, F. Califano, S. Stramigioli, and W. Roozing, "Energy-aware adaptive impedance control using offline task-based optimization," in *2021 20th International Conference on Advanced Robotics (ICAR)*. IEEE, 2021, pp. 187–194.

[63] F. Califano, D. van Dijk, and W. Roozing, "A task-based post-impact safety protocol based on energy tanks," *IEEE Robotics and Automation Letters*, vol. 7, no. 4, pp. 8791–8798, 2022.

[64] A. van der Schaft, *L2-Gain and Passivity Techniques in Nonlinear Control*, ser. Communications and control engineering. Netherlands: Springer Nature, 2016.

[65] S. Vongbunyong and W. H. Chen, "Disassembly Automation," in *Disassembly Automation*, C. Herrmann and S. Kara, Eds. Springer, 2015, pp. 25–54.

PAPER A

Human–Robot Collaboration in Industrial Environments: A Literature Review on Non-destructive Disassembly

written by
Sebastian Hjorth, Dimitrios Chrysostomou

The paper has been published in: *Robotics and Computer-Integrated Manufacturing*

Robotics and Computer–Integrated Manufacturing 73 (2022) 102208

Contents lists available at ScienceDirect

Robotics and Computer-Integrated Manufacturing

journal homepage: www.elsevier.com/locate/rcm

Review

Human–robot collaboration in industrial environments: A literature review on non-destructive disassembly ☆

Sebastian Hjorth *, Dimitrios Chrysostomou

Department of Materials and Production, Aalborg University, 9220 Aalborg East, Denmark

ARTICLE INFO

Keywords:
Human–robot collaboration
Circular economy
Human–robot collaborative disassembly
Sustainable manufacturing
Industrial manipulators

ABSTRACT

Nowadays, numerous companies and industries introduce recycling processes in their production, aiming to increase the sustainable use of the planet's natural resources. Nevertheless, these processes remain inefficient due to the high degree of complexity and variation in the products. In order to remedy this, industry stakeholders adopt the circular economy business model and introduce take-back programmes and remanufacturing processes for their End of Life products in their own supply chains. Take-back programmes enable the re-sourcing of sub-assemblies and components of previously manufactured products while remanufacturing processes encourage non-destructive disassembly. Due to the uncertain conditions of the re-sourced products, fully automated cells cannot cope with the demanding disassembly processes. Therefore, there is a need to establish hybrid disassembly robot cells where humans and robots work closely together in a process known as human–robot collaborative disassembly (HRCD). This paper examines the landscape of HRCD and reviews the progress in the field during the period 2009–2020. The analysis investigates principles and elements of human–robot collaboration in industrial environments such as safety standards and collaborative operation modes, HRI communication interfaces, and the design characteristics of a disassembly process. Additionally, the various technical challenges of HRCD are explored, and a review of existing systems supporting HRCD is presented. This review aims to support the robotics community in the future development of HRCD systems, discuss identified literature gaps, and suggest future research directions in this area.

1. Introduction

The rapid progression in technology over the last decades has changed the world's consumptive behaviour significantly. However, with the current business model, this trend is not environmentally and economically sustainable [1]. A significant number of manufacturers have initiated a paradigm shift by applying various recycling processes in the production lines. For example, they attempt to reduce the number of raw materials that have to be extracted from Earth, by sending the excess amount directly back to their vendors; an action that has already shown environmental and economical benefits [2].

However, this remains insufficient; therefore, policy providers have discussed and promoted the so-called circular economy business models (CEBMs) in UN- and EU-summits [1,3,4] and significant industrial stakeholders, such as Bosch [5], Grundfos [6] and Apple Inc. [7] have already started to adopt this model. Fig. 1 illustrates the central concept behind circular economy, which is to reuse/remanufacture parts and components of products, that have reached their End-Of-Life (EOL) stage and as a result extend the life of sub-assemblies and single components.

Fig. 1 illustrates the central concept behind circular economy, where the aim is to extend the life of sub-assemblies and single components of products, by reuse-/remanufacturing parts and components of products, which have reached their End-Of-Life (EOL) stage.

Traditional manufacturing practices that require, e.g. shredding and reproduction of raw materials, can be less environmentally friendly compared to the remanufacturing/requalification reproduction process for the following reasons: (i) contains non-environmentally friendly chemicals, (ii) is energy consuming, (iii) the new component still has to be produced, (iv) the requalification of used parts is economically more viable than their recycling [8]. In addition, a report from Ellen MacArthur Foundation [9] outlines the fact that the CEBM brings the following benefits for manufacturing companies:

(i) Substantial net material savings

☆ This paper is supported by the European Union's SMART EUREKA programme under grant agreement S0218-chARmER and H2020-WIDESPREAD project no. 857061 "Networking for Research and Development of Human Interactive and Sensitive Robotics Taking Advantage of Additive Manufacturing – R2P2".

* Correspondence to: Fibigerstraede 16, 9220 Aalborg East, Denmark.
E-mail address: sshj@mp.aau.dk (S. Hjorth).

https://doi.org/10.1016/j.rcim.2021.102208
Received 11 December 2020; Received in revised form 10 May 2021; Accepted 16 June 2021
Available online 4 August 2021

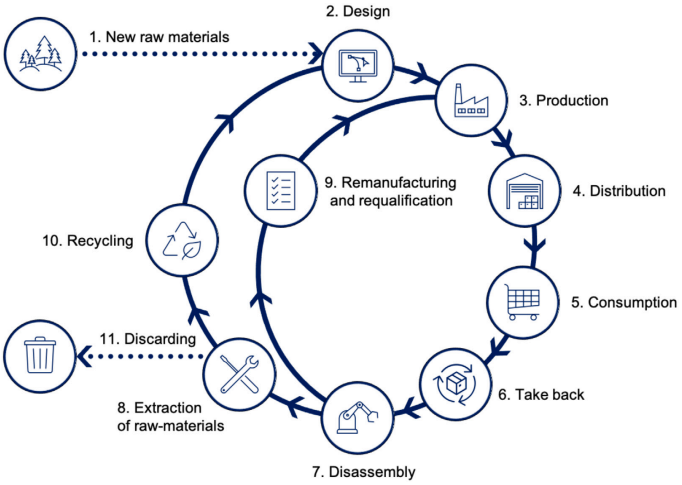

Fig. 1. Abstract visualization of the resource life cycle according to the circular economy business model. 01: New raw materials enter the production; 02: Design & manufacturing of sub-components; 03: Production of final product; 04: Distribution of the product to customers; 05: Consumption of the product; 06: Take back of the EOL product (EOLP); 07: Disassembly of the EOLP; 08: Extraction of raw materials; 09: Remanufacturing and requalification of extracted sub-components; 10: Recycling of raw materials; 11: Discarding non-recyclable raw materials.

(ii) Reduced exposure to price volatility
(iii) Increased economic development
(iv) Increased innovation and job creation potential
(v) Increased resilience in living systems and the economy

These findings are further backed by Li et al. [10], where in a case study for the analysis of a disassembly process where robots are used for the recovery of strategically important materials from electric vehicles, concluded that an average 95% of the materials and their associated recovery values could be extracted. It also states that it is crucial to take the design for disassembly (DfD) of products into account as a pre-treatment process for future EOL vehicles as it has a direct and positive influence on the efficiency of disassembly processes. Consequently, this leads to a reduction in material lost during the recycling process. According to Graedel et al. [11], this can be traced back to the increased complexity of multi-material products. Therefore, companies that adopt this business model still face major challenges in the following three fields:

Logistics/ Take-back programme: Take-back programmes serve the purpose of souring EOL products from customers and end-consumers to extract reusable sub-assemblies and components. Establishing and maintaining a take-back programme profitable remains a major challenge for most companies.
Disassembly Process: The disassembly process itself focuses on the extraction of sub-assemblies and individual components of EOLPs in such a way that they can be re-used/-manufactured. Non-destructive disassembly of final products remains a process highly dependable on the original design and assembly of the product.
Requalification Process: The requalification process is another essential area for the realization of the circular economy. Here, the disassembled sub-assembly or components are tested to evaluate if they are suited to be introduced back into the manufacturing process and integrated into a new product. The design of such evaluation process to identify all potential defects and predict the future life span of said sub-assembly/component remains a major challenge.

Table 1
Technological challenges for de-/remanufacturing system. [12].

Challenges
• High variability in the conditions of post-use parts
• Poor information about return products
• Increasing product complexity
• Short life-cycle of products and high product variety
• Increasing quality requirements on recovered materials and component
• Pressure on costs and efficiency

The main challenges between these three areas lay in the technological challenges, as stated in [12]: "The role of advanced de- and remanufacturing technologies and systems is fundamental to achieve the required quality and efficiency of the regeneration process". Additionally, some major challenges that were pointed out are presented in Table 1. As recently pointed out in [13], the economic viability of the take-back programme is affected by its high proportion of manual labour. There was concluded that the cycle time for the disassembly of a product takes three minutes, compared to a cycle time of 20 s for a conventional recycling setup (i.e., shredding).

In order to make CEBM viable for any manufacturer, it is necessary to automate the disassembly process. One of the main technological enablers that facilitate the automation of the vast majority of manufacturing processes and consequently disassembly is industrial manipulators [14].

However, as stated previously and also concluded in an analysis of the structural design of LCD TVs for automatic disassembly by Elo et al. [15], the major challenge for a disassembly system is the variability and uncertainties concerning the state of the product, e.g., in-homogeneous materials, the mixture of materials, component location and the variation of the structural rigidity of the components.

This variability and uncertainty can make it impossible for a fully automated system to complete the process in an economically viable time or even complete it at all.

Therefore, it is necessary to keep the human-in-the-loop and create a hybrid automated disassembly cell in which humans and robots support each other to complete a given disassembly task. Such implementation introduces a new set of challenges to the disassembly process with regards to the collaboration between humans and robots, i.e., task sharing/allocation/programming and safety in human–robot interaction/collaboration.

This paper aims to clarify these challenges and provide the reader with an overview of the progress during the past decade in the field of human–robot collaborative disassembly (HRCD). The contributions of the paper are:

(i) An analysis of the way that human–robot collaboration (HRC) is currently interpreted and implemented within the field of robotic disassembly in industrial settings.
(ii) An insight on the main components of a robotic disassembly process.
(iii) A framework for identification and classification of research papers focused on human–robot collaborative disassembly systems

The paper continues with a description of the methodology to identify and select relevant papers in Section 2. In Sections 3 and 4, the necessary background knowledge for the analysis of the current state of the art in the field of HRCD is provided. Section 3 presents the definition of HRC, an overview of standards and methods ensuring robot safety, and a summary of communication methods that enable HRC in industrial settings. Section 4 explores the various areas composing disassembly processes i.e., Task Definition, Task Planning and Task Implementation. Section 5, highlights the literature which explicitly covers the topic of HRCD. Lastly, Sections 6 and 7, evaluate the most relevant papers and conclude with a summary of the gained knowledge, several discussion and reflection points and a list of identified research gaps in the research area.

2. Search methodology

In order to solve the challenges associated with the disassembly of EOLPs (see Table 1), multiple robotic technologies and concepts have been developed since the 1990s. Although numerous surveys and reviews on HRC in industrial settings have been proposed, to the best of the authors' knowledge, only one extensive literature review exists on the topic of robotic solutions for disassembly tasks and was conducted by Poschmann et al. [16].

That particular work highlights that the current research trend within this field moves towards completely autonomous robotic disassembly cells and the improvement of HRC process implementations. The importance of HRC in disassembly is also solidified by acknowledging its investment value for companies in terms of complexity and adaptability compared to fully automated solutions. However, [16] mainly focuses on robotic disassembly in a contextual sense. It does not provide an analysis of the research outside of the field of disassembly that might be beneficial for this field.

On the contrary, the objective of this review is to provide an overview and an analysis of autonomous robotic disassembly systems as well as robotic solutions used for industrial disassembly tasks while incorporating various forms of HRC. For this aim, a broad literature survey was executed, and the contents of more than 400 papers in related areas were researched and reviewed. A summary of the chosen search criteria can be found in Table 2. Furthermore, a visualization of the selection process of related literature is illustrated in Fig. 2. Initially, an extensive search on web-based databases (i.e., Google Scholar, Scopus, WebofScience) for the related works in the area of HRC within disassembly for the period from 2009 to 2020 was conducted. Several search terms related to the application context were used, such as: "Human-Robot Collaboration" AND "Disassembly", "robot assisted disassembly", and "Human-Robot Collaborative Disassembly". The selection of these terms was based on the argumentation that they must include a relation to the process (i.e. disassembly), a robotic mechanism as well as indicate a supportive/role by either one or multiple of the autonomous quantities (i.e. human operators and robots) involved in the process.

At the same time, search terms relevant to the general area of industrial disassembly but were not suitable for the scope of this review had to be excluded. For example, since HRC encapsulates any form of HRI in industrial processes, the authors decided to exclude HRI as a search term in this review. Moreover, papers with a contextual background of economic evaluation/feasibility studies of a disassembly line and profitability scores are excluded. Most companies focus on the economic feasibility and profitability of the disassembly line itself rather than the choice of a robot or a specific enabler of the technology. Therefore, most of these studies focused on cycle time and regained/preserved value of the components rather than on the technology enabling the disassembly of a product.

Besides, literature discussing the process optimization of disassembly line designs is excluded from the paper selection. The authors believe that such studies do not add significant value to analysing how and what technology/approach is currently used to realize a human–robot collaborative disassembly system. Lastly, literature presenting the design of tools is excluded because the general practice of designing a tool that can be safety-certified for an HRC application is identical regardless of the task.

The period for this search was selected to cover from January 2009 until September 2020. The beginning of this period was chosen because the first collaborative enabled industrial manipulator was made available for purchase in 2008 [17]. Furthermore, new standards were put in place in 2009, allowing the incorporation to of HRC on shop-floors.

Taking all these parameters into consideration, the initial search resulted in 425 possible relevant publications, while after eliminating the duplicates, they resulted in 383 publications. A later screening of the papers based on title and abstract information and the search/review criteria of Table 2, resulted in **9** publications that are relevant in the field of *human–robot collaboration in disassembly*.

3. Principles of Human–Robot Collaboration

The topic of HRC has been discussed before the first collaborative enabled industrial manipulator (i.e., KUKA LWR 4) was made available in 2008 [17]. However, there is an ongoing debate about the definition and interpretation of the non-normative terms HRC and human–robot interaction within academia and industry. This debate was summarized by Vicentini, where an overview was presented over the different interpretations across the community and also highlighted the risks and consequences of enforcing the labels in the real-world by using the term "collaboration" for branding purposes [18].

Some of the different viewpoints in this debate were explored in [19,20], where definitions and various levels/subcategories of HRI and HRC were presented. According to Hentout et al. [19], HRI can be categorized into the following categories: (i) human–robot coexistence, (ii) human–robot cooperation, (iii) human–robot collaboration, where human–robot collaboration can be split into *physical collaborations* and *contact-less collaborations*.

At the same time, other viewpoints regarding which category embodies the most immersive/direct interaction between humans and robots exist within the research community. On the one hand, Haddadin et al. [21] supported the categorization based on physical proximity between a human and a robot. This interpretation classifies cooperative robot interactions as being in closer proximity than collaborative robot interactions. As a result, human–robot cooperation (HRCoop) occurs when a robot and a human are at the closest possible distance and human–robot coexistence (HRCox) when they are farthest

Table 2
Overview of the various review criteria applied during the search process for relevant literature.

Search Criteria	Description
Search terms	"Human-Robot Collaboration" AND "Disassembly", "robot assisted disassembly", "Human-Robot Collaborative Disassembly"
Time period	January 2009–September 2020
Publication type	peer-reviewed academic conference paper, journal articles and books
Exclusion criteria	**Description**
Language	non-English
Contextual	economical evaluation/feasibility studies, profitability scores, process optimization disassembly line design, tool design

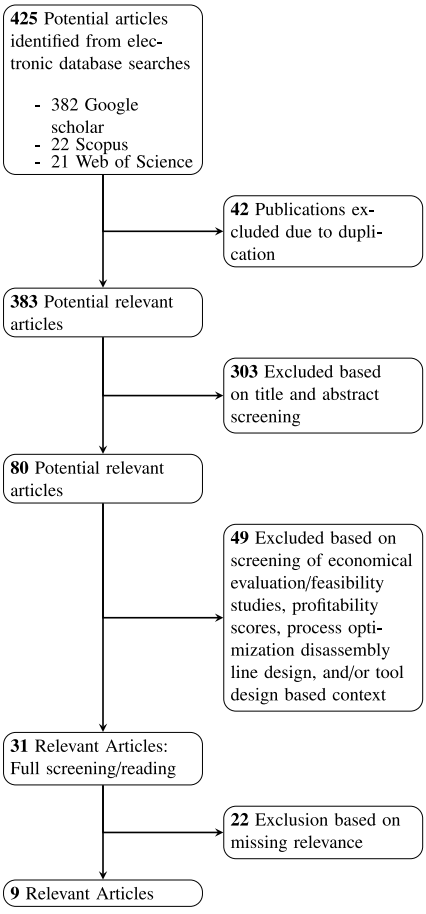

Fig. 2. Visualization of the literature selection process for identified literature related to human–robot collaborative disassembly.

apart. On the other hand, Kolbeinsson et al. [22] mentioned that HRC is based on how humans and robots share their workspace and tasks. Therefore, they interpret HRC as more immersive as human–robot cooperation (see Fig. 3).

In the meantime, most industry stakeholders have a different interpretation of HRC where they assume that any robot that can operate without a fence is collaborative. Different elements of HRC in industrial environments are examined by Villani et al. [23] who have reviewed the topic and identified the main challenges as: (i) safety issues, (ii) HRI communication interfaces, (iii) HRI process design methods.

In our paper we tackle the element of safety by covering the *safety standards* and *collaborative operation modes*; the HRI communication interfaces by covering *programming approaches*, *input modes*, and *reality enhancement*, and lastly we cover the design characteristics of a disassembly process by discussing *task definition*, *task sequence planning* and *automated disassembly applications*.

3.1. Robot Safety

The current trends in the industry according to [24] go towards robotic setups, which are fenceless and intrinsically safe by considering the static force and speed of the robot as well as the human's reflex actions. An extensive survey that summarizes the field of HRC and HRI was conducted by Vicentini in [25]. The research found that physical interactions between robots and humans can, in general, be categorized into *desired* and *undesired contacts*. In this context, undesired contact is being classified as collisions. Haddadin et al. have made an extensive investigation into the different forms/kinds of collisions and their corresponding critical contact force values in [26,27]. There Haddadin et al. differentiated between the following forms of impacts: (i) unconstrained impacts, (ii) clamping in the robot structure, (iii) constrained impacts (iii) partially constrained impacts, (iv) resulting in secondary impacts. This investigation was expanded in [28] to cover different severity levels for various types of injuries depending on the collision types. Based on these investigations, Haddadin et al. progressed with analysing extensively model-based algorithms designed for real-time collision detection, isolation, and identification of pHRIs [29] and Golz et al. classified contact types to intended and unintended ones to highlight the importance of detecting and interpreting contacts for safe pHRI [30].

3.1.1. ISO standards

In an attempt to classify HRC in a general and robot safety context, several ISO standards were put in place and are regularly updated. The introduction of these standards aims to categorize the different forms of collaboration and interaction based on their kind (e.g. verbal, non-verbal), severity, and control modes.

ISO 8373

The ISO 8373 standard [31] specifies the vocabulary used within the area of HRC, in the context of robots, the interaction between humans and robot (HRI), and other relevant terms related to robots and control system/strategies.

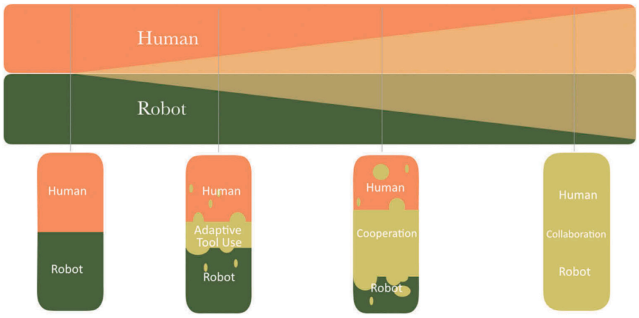

Fig. 3. A visualization of the various levels of interaction, according to Kolbeinsson et al. [22]. The outer left of the graph represents the absence of interaction between human and robot. The most right part of the graph represents a level of interaction between human and robot which classifies as collaborative.

ISO 10218

The ISO 10218-1/2 standard, in general, describes the concepts of collaborative enabled robots, workspaces and operations. ISO 10218 is comprised the following two parts: (i) ISO 10218-1 [32] concerns the specification of the requirement and limitations of the robot's behaviour when interacting with an operator in collaborative operation. (ii) *ISO 10218-2* [33] defines the requirements for the robot systems concerning the safety when applied in an HRC setting.

ISO 15066

ISO 15066 [34] attempts to further specify HRC by supplementing the requirements and guidelines established in ISO 10218. More precisely, this standard defines the appropriate procedure for the limitation of speed values, which keeps force and pressure values within the defined pain sensitivity threshold for humans in collision scenarios with robots. It defines twelve specific areas for testing on the human body as well as the maximum permissible pressure and force values, specific formulas to obtain the maximal permissible energy transfer for each body of the defined areas on the human body, and lastly the speed limit values for transient contact between a human body and a part of a robot system. Derived from these specifications, the following four-level (see Fig. 4) of control modes are defined:

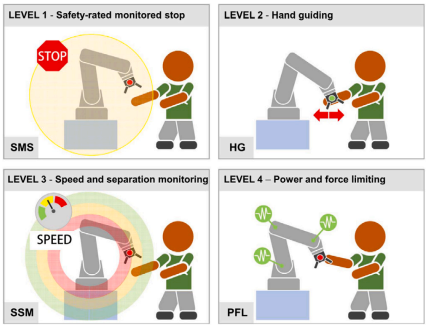

Fig. 4. Visualization of the four different control levels. [23].

Safety-rated Monitored Speed (SMS) enables humans and manipulators to have a shared workspace, but they cannot work in this workspace at the same time. As soon as the human operator enters the shared workspace, the robot stops immediately until the operator leaves the shard workspace again.

Hand-Guidance (HG), methods are designed for the manual guidance of robot systems. Control methods falling into this category have no defined upper limit in terms of speed with regards to the robot or forces acting on the human body but the generation of the motion input. It requires but not limited to that the risks of: (i) unintentional commands given by the human and (ii) mismatched commanded and executed motion

Speed and Separation Monitoring (SSM) control schemes enable human operators to share the same workspace with the manipulator while being in motion. However, the robot motion is like SMS proximate on the distance between the operator and the robot. The difference is that the SSM can adapt the velocity of the manipulator based on the proximity-based zones between human and manipulator. This ensures that the protective distance at which the robot has to stop can be made smaller compared to SMS.

Power and force limitation (PFL) reduces the effects of unintended contact between human and robot. This can be achieved by implementing control schemes which control the motion of the robot in such a way that the forces and momentum upon impact with the operator are within the set limits to avoid injury.

3.2. Enablers of Human–Robot Collaboration

Previously in this work, the debate regarding the definition of the HRC was discussed, followed by an overview of the various safety standards related to robots. However, regardless of the chosen definition of HRC and which of the safety standards must be followed to enable a safe implementation, they all require the same thing; the so-called *Enablers*, which are control strategies and human–robot communication techniques equally necessary so the human worker can interact safely as well as intuitively with the robot.

3.2.1. Control

One of the main concerns in the implementation of industrial HRC is the classification of physical contact, an area in which De Santis et al. examined thoroughly and analysed the different aspects and requirements for safe pHRI [35]. One conclusion of that work is that control

methods cannot compensate for a poor mechanical design on their own; however, they remain an essential aspect when it comes to performance, reduction of the sensitivity to uncertainties, and improvement of reliability.

Control schemes, in general, can be divided into the following two types:

(i) Pre-collision
(ii) Post-collision

3.2.2. Pre-collision strategies

Pre-collision control strategies focus on preventing harmful contact between the robot and its environment with so-called collision avoidance. These strategies use sensory input (e.g., camera, laser sensors) to adjust the velocity or the motion of the manipulator based on the distance to autonomous quantities and their behaviour in the manipulator's work environment.

Along with these ideas, Safeea et al. used various sensors (i.e., cameras, lasers, IMUs) to capture the human operator's position and motion to adapt the manipulator's pre-defined/planned path based on a framework incorporating artificial potential fields [36]. In parallel, Chen et al. explored a collision-free motion path planner for a 6-DoF serial manipulator [37]. The presented method tracks dynamic obstacles in the manipulator's workspace by utilizing depth images captured by multiple KinectV2 cameras. Based on the estimated position and velocity of the obstacle, an artificial potential field is adapted, such that the manipulator's nullspace can avoid the obstacle while preserving the original end-effector's trajectory.

For the generation of a collision-free path in an HRC setting, Landi et al. proposed an optimization-based method that utilizes safety barriers positioned around the robot links [38]. It also minimizes the differential between the nominal input and commanded acceleration such that the manipulator can adapt its motion accordingly to obstacles detected by depth visual sensors. Another method for addressing the challenge of avoiding joint limits and Cartesian obstacles was presented by Scheurer et al. in [39]. This approach used a closed-loop-inverse-kinematic control approach on velocity level and was evaluated on a 12-DoF mobile manipulator.

Liu et al. presented a dynamic modified SSM method to enable HRC while maintaining a certain productivity level [40]. The setup consists of a vision-based detection system based on which the risk assessment and response strategy for industrial HRC can be dynamically adapted. Another effective online collision avoidance was proposed by Mohammad et al. where they utilize an augmented environment containing a three-dimensional virtual model of the manipulator and real images of human operators captured by depth cameras [41]. The manipulator adapts its behaviour based on four strategies, either alerting the operator, halting the manipulator in its motion, moving it into a safe position, or modifying its trajectory.

Even though the examples for pre-collision control schemes mentioned above enable the robot to avoid collisions, they cannot guarantee that it will not come to harmful contact between human and robot. As pointed out by Haddadin et al. this happened because the relative motions between robot and human can be hard to predict as the use of exteroceptive sensors monitoring the workspace and adapting the robot's movement may not be sufficient for the prevention of collisions [42]. This observation is also highlighted by De Santis et al. who mention that to ensure a safe robot motion, pure motion control is inadequate, as it might generate undesirable contact forces in case of collisions [35]. Thus, it is necessary to implement a post-collision control strategy capable of limiting the contact forces between humans and robots to a desirable level.

3.2.3. Post-collision strategies

Contrary to pre-collision control strategies, post-collision control strategies do not prevent possible contact between humans and robots but instead limit the contact force and the energy exchange between the two entities to a safe limited [43]. Such post-collision control strategies are also known as "interaction control strategies", where the two most prominent sub-categories are direct and indirect control strategies. The former includes so-called hybrid control strategies, whereas the latter includes Admittance and Impedance control schemes.

Direct-force control approaches control the manipulator's force along the constrain as well as the motion along with the directions of the unconstrained path by measuring the force.[44]. As aforementioned, a prominent subcategory of Direct-force control approaches is the so-called hybrid force/motion control.

Yip and Camarillo [45] propose a hybrid position/force control approach capable of manipulating the manipulator's end-effector position and force in the presence of unknown body constraints. This method enables manipulators with complex joint mechanics to navigate when subject to unknown environmental constraint. Leite et al. [46] presents a hybrid control scheme that combines adaptive visual servoing and direct force control enabling non-redundant robotic manipulators to perform interaction tasks on smooth surfaces. The presented method enables the manipulator to exert a predefined contact force with its end-effector with a smooth surface for visually tracking the desired path. Another adaptive position and force control approach for a robotic manipulator in interaction with a flexible environment is presented by Gierlak and Szuster in [47]. It utilizes a manipulator–environment system model that takes various parameters such as motion resistance and environment elasticity into account, intending to define the position and force control task.

Compared to direct-force control, indirect force control schemes achieve force control via motion control, instead of closing the force feedback loop resulting in nonlinear and coupled impedance or admittance [44].

Admittance control schemes manipulate the virtual model dynamics of a system by creating an adequate response to the measured forces caused by interactions with a human operator. Keemink et al. provided a comprehensive overview and analysis of admittance control applied in pHRIs in terms of framework, the influence of feed-forward control, force signal filtering, post-sensor inertia compensation, internal robot flexibility, the effect of virtual damping on the systems stability, passivity and other performance-critical criteria [48].

An approach for this kind of control strategy was put forward by Dimeas et al. where a variable admittance control approach for human–robot cooperation tasks is presented [49]. It combines a Fuzzy Inference System designed to adjust the damping of the manipulator's admittance based on force introduced by the human operator and its measured velocity. A Fuzzy Model Reference Learning Controller adjusted the Fuzzy Inference Systems response based on the minimum jerk trajectory model.

Additionally, Ranatunga et al. proposed an adaptive admittance controller capable of adapting to human intent and variations of the manipulator's dynamics [50]. The control strategies consist of an outer and inner control loop with the outer-loop using an adaptive inverse control technique and the inner-loop linearizing the robot dynamics via a neuro-adaptive controller. This control strategy enables an efficient online adaptation of the manipulator's admittance model for different operators and a smooth human–robot interaction due to the reduction of jerks.

For improving the performance of HRC tasks, Bea et al. combined a variable admittance control strategy with virtual stiffness guidance [51]. The approach prevents unnecessary adjustments of the damping parameters based on the classification of the operator's intentions and additionally aiding the operator via virtual spring supporting the task, which the operator can adjust.

Impedance Control schemes measure the displacement/motion caused by the interaction and create a reactive force to compensate for this displacement. In an experimental study on human–robot co-manipulation for kinematically redundant manipulators conducted by Ficuciello et al. it was investigated that the manipulator's performance during pHRIs, can be enhanced by the combination of Cartesian impedance modulation and redundancy resolution [52]. A Cartesian impedance control strategy enables the manipulator to handle the forces introduced by the human–robot operator due to its compliant nature. The study established that variable impedance strategies with a suitable modulation strategy outperform non-variable impedance control strategies when it comes to the perceived comfort by human operators during manual interaction like guidance.

Additionally, Ficuciello et al. presented another Impedance control paradigm, focused on the control of redundant robot manipulators in the task space [53]. Its null-space impedance control approach allows for the safe reaction of the manipulator during intentional and unintentional/accidental physical interaction with its environment. Laffrance et al. proposed an energy-based control strategy for enabling manipulators to work closely with humans by bounding their behaviour in the first instance of an impact between the two entities [54]. This is achieved by limiting the energy stored into the system to a set maximum value of the position-based controller, which adapts the position trajectory reference in correlation with the set maximum energy value. Raiola et al. investigated the impedance control scheme, which enables safe human–robot interaction through energy and power limitation. In addition to the limited energy and power of the manipulator, the system's passivity is also ensured due to the implemented energy tanks [55]. Vanderborght et al. provided an extensive insight on the topic of Variable Impedance Actuators (VIA) by giving a structured overview [56]. This work classifies the VIA based on how the variable stiffness and damping were implemented. Ott et al. presented a hybrid reactive control strategy capable of continuously switching and interpolating between Impedance and Admittance Control [57]. Thereby merging robustness properties of Impedance Control and the accuracy in free motion associated with Admittance Control.

Regardless if a control strategy is designed to avoid collisions or minimize contact forces, they both face the challenge of possible restrictions in their workspace due to the location/placement of the manipulator in an environment with limited space (e.g., existing production lines and residential houses). However, manipulators controlled by an interaction control strategy are more exposed to this problem. This is due to the compliance introduced to the system by the control scheme; thereby, enabling the robotics system to adapt to unplanned interactions with its environment by deviating from its original planned trajectory.

3.2.4. Workspace restrictions

Therefore, workspace restrictions are necessary when implementing such control strategies, and to enforce these restrictions/constraints, various methods have been developed to restrict the manipulator's workspaces. To begin with, Kimmel et al. presented a method that enforces Cartesian constraint with an invariance control scheme approach in combination with a discrete-time Euler solver to reduce oscillations when encountering the constraints [58]. Similarly, Rauscher et al. imposed Cartesian workspace-restrictions for a redundant robot successfully by combining an impedance control strategy with control-barrier-functions and quadratic programming [59].

The work conducted by Dimeas et al. presented a method hindering the operator from forcing the manipulator into a configuration, which reduces its performance capabilities [60]. The methods consist of virtual constraints and a Cartesian admittance control scheme, which adapts based on the kinematic manipulability index.

Han et al. focused on an operational-space-control (OSC) framework capable of handling the encounter of joint limits and singularities [61]. The energy-aware control scheme from Raiola et al. [55], previously discussed in this work, was extended by Hjorth et al. [62] by implementing the concept of artificial potential fields, first introduced in [63], for the enforcement of workspace restriction for collaborative enabled robots while being in a compliant state (see Fig. 5).

Fig. 5. Visualization of the enforcement of virtual workspace constraints while the manipulator is in a compliant state [62].

A method proposed by Flacco et al. saturates the manipulator's Nullspace by combining the Stack-of-Tasks approach with quadratic programming [64]. This approach can be adapted to restrict the manipulator's workspace as it is designed to keep the manipulator within a set of hard constraints for its positions, velocities and accelerations within its configuration space. Muñoz Osorio et al. extended this method and transformed the algorithm to a torque-based approach [65],by combining the Operation Space Control formulation with the stack-of-task technique. The creation of high priority tasks in the task stack enables the restriction of the manipulator's motion within the Cartesian and configuration space, respectively.

3.2.5. Human–Robot Communication

There are several ways for an operator to interact with a robot on the production floor. As mentioned before, sharing the same workspace is a fundamental element in HRC. Humans tend to communicate their intentions during the collaboration over a shared task via a variety of verbal and non–verbal cues either in real or virtual work environments [66].

In this work, these ways of communication are grouped in two broad categories, i.e., *verbal* where voice control and speech recognition are the key elements and *non–verbal* where methods including gesture recognition, human pose and skeleton tracking, gaze detection, and intention recognition are considered. A short overview of how these enablers of human–robot communication in industrial HRC are applied in augmented, virtual and mixed realities is also presented. The main focus remains within industrial applications; however, approaches used in social robotics and present great potential to be introduced in manufacturing are also briefly discussed.

Verbal communication. Voice control and speech recognition are primarily used in manufacturing applications as interfaces for robot control [67]. Maksymova et al. presented a wide range of different models for the voice control of an industrial robot such as logical, semantic networks, frame model and Petri Nets in the context of an assembly task [68]. Bingol and Aydogmus investigated the performance of a natural speech recognition system based on deep neural networks for the classification of different commands during the interactive control of a KUKA KR Agilus robot arm in multiple industrial tasks [69].

Fig. 6. Example of a pointing gesture identification validation setup from [75].

Fig. 7. Two of the manipulation gestures used in [101].

González-Docasal et al. progressed a step further to integrate a semantic interpreter who, with the support of a knowledge manager, extracted semantic information from transcribed spoken content and enabled an industrial robot to understand the intention of the operator and execute a collaborative task accordingly [70].

However, most of the applications solely based on speech recognition may face performance issues due to background noise that usually exists in industrial environments [71]. Thus, speech recognition is often combined with other modalities such as gesture recognition [72], eye gaze detection [73] and haptic control [74] to enhance HRC and improve the accuracy of human action recognition. More specifically, Maurtua et al. examined a semantic approach for multimodal interaction between human workers and industrial robots to enhance the dependability and naturalness of the collaboration between them in real industrial settings [75]. The approach is based on the recognition of verbal commands and gestures which communicate requests for processing and execution of a disassembly task (involving screwing and unscrewing operations) and deburring of wax pieces (see Fig. 6).

Additionally, Markis et al. presented a multimodal framework for interaction with dual-arm robots. It is based on a hierarchical model that handles various inputs from gestures, voice commands, and intuitive graphical user interfaces to decompose the working tasks into different abstraction levels [76]. Neto et al. incorporated wearable sensors and inertial measurement units (IMUs) to capture the human upper body gestures, which afterwards act as inputs to an artificial neural network (ANN) for gesture classification. This multimodal approach in combination with a parameterized task manager based on speech and visual feedback enables the human operator to complete collaborative robot tasks such as handover and delivery of parts [77].

Hongyi et al. introduced a deep learning framework for multimodal control of an industrial robot where voice, hand motion and body posture recognition are combined based on Convolutional Neural Networks (CNNs) and a multilayer perceptron model (MLP) to dynamically affect the programming of the robot [78,79]. Gustavsson et al. presented a pilot study where speech recognition and haptic control are combined to control a UR3 robot. Naturally, inexperienced users discovered the challenges of operating a voice-controlled interface in a noisy environment. However, the robot's haptic control altered the overall impression of the participants who evaluated the concept as intuitive to use [80]. Mohammed and Wang explored the behaviour of the human brain using electroencephalography (EEG) to develop a brainwave-driven robotic application to assist the HRC during the assembly of a car engine manifold [81]. The major advantages of such a framework are its easy integration with voice, gestures and haptic commands and the ability to free up the mental and physical capacity of the operators to allow them to control the robot while performing a shared task.

Non-verbal communication. Human–robot interaction systems based on visual cues can often compliment the ones based on verbal communication and even replace them in cases where the communication is unreliable [82,83]. *Visual* systems based on recognizing gestures have been a cornerstone of a repertoire of HRI techniques used in many manufacturing scenarios. Berman and Stern explored the wide range of the sensors used in gesture recognition systems. They divided their taxonomy into three significant components, i.e., sensor stimuli, the context of use, and sensor platform [84]. There are a plethora of methods in the literature that use a mixture of these components for gesture-based control of robots in HRC scenarios.

To begin with, a crucial point in the vast majority of gesture recognition methods is the detection of the pose or skeleton outline of the operator [72]. There are numerous sensors used to produce robust detection and tracking of the pose of the operator mostly based on RGB-D cameras such as the Kinect v2 [85,86] and Intel Realsense [87,88] while other sensors such as Leap motion can be used for specialized tracking of the hand and fingers for robot control [89,90]. Similarly, accurate pose detections can be achieved by using IMU sensors [91], thermal cameras [92] and various wearable sensors [93], however, their restrictive mobility, low resolution and time-consuming setup render them less popular.

During the past decade, machine learning methods have been widely used in recognizing human actions and classifying them to respective commands for robot control in industrial HRC. Traditional machine learning methods such as Gaussian Mixture Models (GMM) [94], Hidden Markov Models (HMM) [95] and Support Vector Machines (SVM) [96] have been used for the detection of humans with high accuracy ranging from 80 to 90%. To achieve more accurate results, researchers have used Deep Learning techniques where 3D-CNNs perform close to 96% accuracy [97–99] and a combination of a novel 3D descriptor for detection of joints and MLP for classification can achieve close to 98% accuracy [100].

In parallel, there is intriguing research that examines the effect of gesture-based communication when the robots themselves produce the gestures. Sheikholeslami et al. explored the efficiency of gestures performed by various robot hand configurations in cooperative industrial tasks [101]. They concluded that the robot could communicate its intentions robustly and led to a higher acceptance rate from the operators. Gleeson et al. produced a lexicon of communicative terms and robot gestures to characterize the steps of commonly used industrial tasks such as part acquisition and fastening of screws [102]. The lexicon used in a representative HRC industrial task, i.e. vehicle door assembly, where it proved adequate for an intuitive and efficient human–robot communication (see Fig. 7).

Other than gesture and pose recognition methods, several methods have also been proposed in the literature to track the gaze and attention of the operators to improve the communication with robots in industrial HRC. Eye gaze tracking has been studied extensively as a human–computer interaction interface where multiple intrusive and non-intrusive techniques have been identified [103]. Palinko et al. used gaze tracking as means of human–robot communication and proved that eye tracking is superior to head tracking techniques in HRC with an iCub robot as the robot was able to exploit richer information from tracking the eye gaze of the operators than tracking the position of their head [104]. Similarly, in industrial settings, eye gaze tracking techniques have been used to improve robustness during robot manipulation tasks [105], to assess the comfort levels of the operators during an HRC task [106], and as an aspect of a shared attention interaction model that affected the timing of human–robot handover tasks [107] positively.

In addition to gaze tracking, researchers have used tactile and haptic feedback to ensure robust communication with industrial robots. Casalino et al. introduced tactile feedback directly at the fingers of the operators to track their operational awareness. A Bayesian recursive classifier was utilized to estimate the human intention, while a wearable vibrotactile ring provided feedback about the different stages of HRC [108]. Salvietti et al. explored a bilateral haptic interface where a soft gripper was used in combination with a wearable, remote ring interface to improve the effectiveness of the collaboration [109]. Bergner et al. used an innovative interface based on distributed cells acting as a large scale skin around robot manipulators which computes the joint torque in the contact points to enable more intuitive human–robot communication based solely on touch [110]. Similarly, Tang et al. developed a novel signalling system based on robot light skin that improved the reaction time of the users significantly and reduced the mental workload of the operators resulting in fewer errors during the execution of simple industrial tasks [111].

Human–Robot Communication in virtual, augmented and mixed realities. Furthermore, due to the technological advancements in computer-generated simulations and the increase of available computational power, human–robot communication in virtual, augmented, and mixed reality workspaces has become more feasible. The main differences in this virtuality continuum originate from the level of immersion into the virtual environment the methods support. In virtual reality, there is a total immersion in a virtual environment. In contrast, in augmented reality applications, the real world is enhanced with some virtual details, and in a mixed reality environment, the real and virtual world intertwines, enabling manipulation with physical and virtual objects.

In general, Augmented and Virtual reality (AR/VR) techniques have been used extensively in manufacturing settings [112,113] for worker training [114] and support [115], digital twin implementations [116], and optimization of industrial processes such as polishing [117], assembly [118–120], laser welding [121,122] and prefabrication of raw materials [123].

More specifically, AR techniques have been utilized in connection with HRC to understand robot intentions in shared workspaces, where Andersen et al. projected related task information on physical objects, e.g., car doors, inside the collaborative environment, to assist human co-workers [124]. Similarly, Liu and Lihui developed an AR-based instruction system that empowers the human worker to access assembly instructions of industrial components from the AR device [125] while Papanastasiou et al. used AR glasses in combination with feedback from smart watches to monitor industrial assembly processes and ensure a seamless human–robot collaboration [126].

Koppenborg et al. recreated robot's motions in VR to study the impact of the robot's speed and predictability of its trajectory in HRC cases. As expected, as the robot moved faster, it was more challenging to predict its desired position, resulting in feelings of uncertainty, more mental workload from the operators and a decreased sense of safety [127]. Moving a step further, Matsas et al. implemented proactive and adaptive techniques in highly interactive and immersive VR environments based on multiple cognitive aids to enhance the feeling of safety from the operators [128].

In cases where manipulating real objects in restricted environments is required, mixed reality (MR) interfaces offer sufficient solutions. Chen et al. developed an MR interface based on a stereo vision in combination with virtual fixtures to create a novel stereo vision-guided teleoperation control method for manipulating mobile manipulators and teaching them new tasks [129] (see Fig. 8). At the same time, MR interfaces offer flexible solutions for programming robot manipulators. Ostanin et al. showcased that programming of a UR10e and a KUKA iiwa for geometrical path planning and trajectory generation is possible with an interface based on Hololens glasses [130]. Munoz et al. used MR methods in the area of quality control to automatically detect defects on a car body with a high success rate [131].

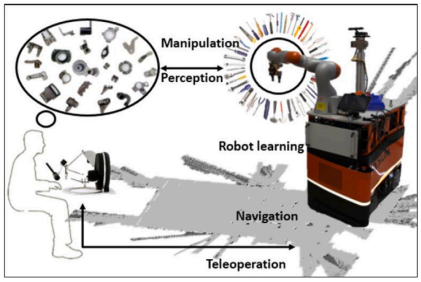

Fig. 8. Visualization of the conceptual representation of the work presented in [129].

4. Characteristics of a disassembly process

The disassembly process of an industrial component is not as trivial as just its reversed assembly process. This is partly due to the fact that the links joining sub-components of a product together are designed to make the assembly process more straightforward (e.g. Snap fittings, glueing, riveting). However, connecting sub-components in this way makes it hard and, most times impossible, to disassemble a product in a non-destructive way.

As mentioned earlier, de/remanufacturing systems face several technological challenges (see Table 1), most of which are related to the states of a product, as they can differ significantly between the observed, the actual and the original state. The added uncertainty makes the disassembly process a non-trivial operation, especially when considering that components or sub-assemblies are not allowed to be damaged to qualify for requalification. This section will cover the following three subtopics of a (disassembly) process: Task Definition, Task Planning, Automated Disassembly applications. As aforementioned, the focus of this paper is on the topic of disassembly; however, some parts of the process is either directly or closely related to assembly operation. Therefore, some of the presented publications in this section have their origin within assembly applications.

4.1. Task Definition

In general, a task is comprised of a set of skills as stated by [137]. For example, a typical pick and place operation consists of multiple sub-tasks such as a pick, move and place task, which all have different characteristics and parameters. The human analogy of these three elementary tasks is so-called skills. In other words, skills are a way of defining/quantifying various low-level operation/tasks to enable the operator to formulate tasks based on human terms. However, this definition is quite broad, as skills can be related to several areas, such as Socio-Cognitive Skills [138], Communication Skills [139] and more task-specific skills. The latter will be the focus in the remainder of this work, more specifically on the various frameworks for the definition of executable robotic skills such as screwing and pick and place operations.

> *CoSTAR* [140,141] is a cross-platform architecture for describing industrial robot task plans. As most skill-based programming approaches for industrial manipulators, it provides the capability of performing various tasks and enables non-expert users to programme the manipulators. Rather than relying on an extensive task library, CoSTAR relies on the end-user to specify a task based on a limited set of geometric states (i.e. InFrontOf, LeftOf). In addition to a Behaviour Tree-based graphical user interface, the user

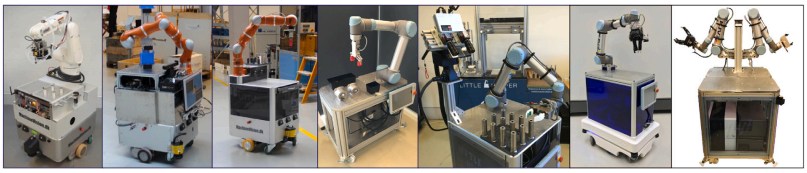

Fig. 9. Various Little helper setup utilizing SBS in the projects like TAPAS [132], CARLOS [133],ACAT [134], CARMEN [135], and [136].

can programme the robot through kinaesthetic teaching methods and predefined analogies to achieve high-level task specifications.

Skill-Based-System (SBS) is a framework, which was first presented by Schou et al. [142] in 2013. It provides a human–robot interface for the utilization of skills in industrial settings. The central point of SBS is the user interface designed accordingly to facilitate the intuitive configuration of complex tasks from non-expert users. SBS contains an extended library of skills and execution engines for managing the execution of parameterized skills and ensuring the sequential description of a task for proper execution. Since its development it has been used in multiple national and international research projects such as TAPAS [132], ACAT [134], CARMEN [135], CARLOS [133] (see Fig. 9) as well as in use-cases in advanced production lines [143] and shipyards [144].

Motion Primitives is a task definition which was utilized by Stenmark et al. in [145] as a user interface that assists the kinaesthetic teaching mode of a collaborative enabled industrial robot. This allows the capturing of semantic information while working with the robot. The programming can be done via the following two modalities: graphical point-and-click and natural language. Another utilization of motion primitives is presented by Canal et al. [146], which combined a high-level task-planner and the low-level motion primitives for enabling an adaptive HRI. The low-level actions are taught to the system beforehand via demonstration and can be adapted to variations in the current situation by tracking relevant entities.

Additional Skill-based methods are presented by:

(i) Saukkoriipi et al. [147] presented a tool for programming robot skills offline. The utilized skills are conceptually similar to SBS, specified by configuration parameters, and offer integrated tool support. The Skills are executable sequences specified as UML action diagrams enabling them to be executed as robot programmes on various robotic platforms and PLC platforms. However, compared to SBS, the specification of the parameters is done offline, and it heavily relies on the use of CAD models in a simulation environment to define a task successfully.

(ii) Wallhoff et al. [137] introduced a system that combines high-level skills to reach a predefined goal in a hybrid assembly station. This system consists of a human operator, industrial manipulator, and a multi-sensory perception system overseeing the shared workspace between humans and robots. The skills in this work consist of various basic blocks with actions, e.g., opening/closing the gripper, moving to position, and picking up operation. The controller then breaks these skills down into "atomic operations" such that the manipulator is capable of executing the associated motions.

(iii) Huckaby et al. [148] proposed a method utilizing model-based system engineering in combination with Systems Modelling Language (SysML), which is a modelling language for the creation of simplified and reusable software modules for the programming of the robotic system. The skill primitives utilized in this work are basic atomic action/operations each robot can be associated with a specific motion.

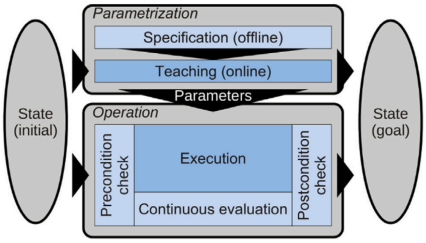

Fig. 10. A representation of the skill model including both operation and manual parameterization [149].

Skill acquisition methods focus on the specification of the above-mentioned skill definition. Most of these methods rely on Graphical User Interfaces (GUI) or a simple programming interface for this step, requiring a certain level of expert knowledge. Therefore, different methods have been proposed to acquire and teach these skills in a more intuitive way.

(i) Schou et al. extended the SBS to incorporate Programming by demonstration (PbD) in [149]. This extension enables novice operators to use a more hands-on and practical way of programming industrial tasks on the fly. A visualization of the adaption to the original skill Framework can be seen in Fig. 10.

(ii) The work of Vongbunyong et al. in [150] presented a platform for capturing disassembly skills/operations done by a skilled operator such that an intelligent agent can acquire these skills. The system utilizes an RGB-D camera as a capturing device and marker equipped tools. The markers on the tool serve the purpose of identifying and tracking the tool's position, orientation, and operation sequence of the disassembly process.

(iii) Another method for teaching skills was proposed by Abu-Dakka et al. in [151]. There a framework was developed to enable the teaching of variable impedance skills, such that the manipulator is capable of performing force-based tasks by adapting its variable stiffness. The framework computes the stiffness estimate based on human demonstrations and a probabilistic model of the skill enabling the manipulator to execute force-based tasks.

4.2. Task sequence planning

Task sequence planning is used to identify a sequence of sub-tasks to successfully solve an overall task (i.e., assembly, disassembly). In the case of assembly, the objective is to have a complete product constructed of multiple sub-assemblies/components. In order to get to that stage, the final product has to be assembled in a specific order. This is where the planning of the sequence of different steps come into place, which in most cases can be straight forward as products are designed for assembly. For the disassembly of products, this process is not as straight forward since most products are not designed for disassembly. Additionally, the state of the used products can vary based on, e.g., their work environment, workload and maintenance cycle. The planning of task sequences can, in general, can be divided into the following two steps:

(i) Disassembly/assembly task modelling (Sequence generation)
(ii) Task Sequence Optimization

During the disassembly/assembly task modelling phase, a sequence is generated based on the product's layout and state. This sequence can then be optimized based on various criteria and constraints, e.g., time, number tool-changes, and cost. The review by Zhou et al. [152] analysed the different characteristics of the main disassembly sequence planning methods in disassembly mode, disassembly modelling and planning process and highlights future trends and current gaps in the existing research.

It proposes that the generation of models for planning of disassembly sequences, is based on *Petri net-based*, *Model type-based*, *Graph-based* and *Matrix-based* methods with the last two being the most prominent ones in literature. Examples of research works using *Graph-based* and *Matrix-based* methods for disassembly sequence planning are listed in Table 3. The general conclusion drawn in this survey was that most of the research has focused on: (i) complete and sequential disassembly planning, (ii) offline planning approaches, and (iii) purely economic factors rather than investigating environmental factors. Additionally, they suggest that future research should focus on dynamic systems capable of handling uncertainties, exploring the dynamic economic and environmental factors affecting the disassembly of EOL products as well as the possibility of combining *Disassembly Sequence Planning* with integrated obstacle avoidance and path planning for robots.

This observation also aligns with a recent publication by Xu et al. which proposed a Disassembly sequence planner for human–robot collaboration based on a discrete Bees algorithm [159]. The approach firstly generates a feasible disassembly sequence based on a disassembly model. Secondly, the resulting disassembly tasks are classified based on their difficulty, followed by developing a disassembly sequence for HRC. Lastly, the generated sequence is evaluated and optimized to minimize the disassembly time, cost and difficulty.

A similar approach Liu et al. investigated using a so-called *enhanced discrete bee algorithm* algorithm to minimize the disassembly time in order to minimize the disassembly time [160]. However, the authors have found that the calculation of specific parameters can be time-consuming, especially for products with a high number of components.

In addition to finding the most time-efficient disassembly sequence on purely the order operation, Li et al. proposed a method that takes the strain during the human workforce associated with continuous manual labour. This method aims is to minimize the total disassembly time for HRCD [161].

Besides the planning algorithms for disassembly tasks, there have been various approaches within assembly planning, which show promising results and possible application within disassembly. One of these applications is a two-armed robotic autonomous assembly system for aluminium profiles designed by Rodriguez et al. [162], which could apply to disassembly as well. The system based on deducting semantic assembly constraints before matching critical features on the semantic level with the help of graph matching. Later, it is followed by applying pattern recognition and classification based on transferring the knowledge of constraints for the different sub-assemblies into the overall assembly of the part through the utilization of machine learning.

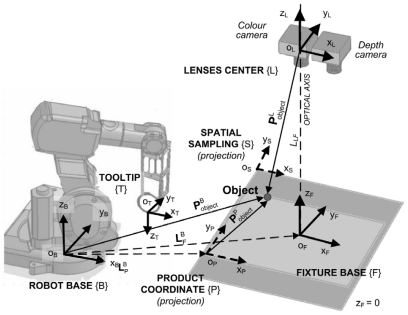

Fig. 11. An abstract representation of the robotic cell utilized by Vongbunyong et al. [167].

Moreover, Rodriguez et al. presented a method to iteratively refine feasibility checks for sequence planning in robotic assembly, which was experimentally validated for the assembly of aluminium profiles and could be further investigated for its use in disassembly [163].

4.3. Existing automated disassembly cells

During the last decade, numerous (semi-) automated robotic disassembly systems have been presented in the research community. Vongbunyong et al. investigated extensively the utilization of a cognitive robotics-based system for the (semi-)destructive disassembly, which is capable of reasoning, execution monitoring, learning and revision. It was also shown that the vision-based disassembly system (see Fig. 11) was capable of adjusting to any product model without prior information [155,164–167].

A system for the disassembly process of electric motors where they utilize an image processing algorithm for the autonomous detection and classification of screws was investigated by Bdiwi et al. [168]. The applied algorithm detects the screws based on their characteristics concerning their greyscale, depth and Hue, Saturation and Value (HSV) colour space values and does not need a database of templates for matching.

Schneider et al. explored using an algorithm to compute complex nonlinear disassembly paths for two objects that collide in their initial state and the disassembly path. This is done by incorporating the information about the flexible and rigid parts together with connected components of intersection volumes to a motion planner [169]. Whereas, Chen et al. [170] proposed an ontology and case-based reasoning (CBR) method which enables the computer to understand complex structures of various mechanical products and fully automates the disassembly decision-making process of products.

An extensive study on robotic disassembly for the recycling and reuse of cellphones was conducted by Figueiredo in [171]. The study shows an in-depth analysis of the different components within three phones from other manufacturers and what forces and tools are needed to extract the various parts. The developed system consists of a robotic manipulator, vision system, decision-making system and focuses on the prying operation. The developed decision-making system utilizes captured images of the vision system to detect the current state of the

Table 3
Examples for Graph and Matrix-based Disassembly sequence planning methods based on [152].

Authors	Summary
Graph-based	
Behdad et al. [153]	Presented an Immersive Computing Technology method to optimize disassembly sequences of a product by considering the cost involved in the process and estimation of possible damage during the process in a virtual disassembly simulation with Dynamic programming.
Alshibli et al. [154]	Presented a Tabu search algorithm for Disassembly Sequencing to minimize the travelled distance by the industrial manipulator, a number of disassembly method changes and eliminating unnecessary operations.
Vongbunyong et al. [155]	Proposed a cognitive robotic agent capable of learning by reasoning throughout the disassembly process.
Matrix-based	
Jin et al. [156]	Developed an approach for generating a disassembly solution space for LCD televisions. This approach generates an interference matrices based on a CAD model, which is used to represent the spatial relationship between components in a Cartesian workspace.
Wang et al. [157]	Designed a method to break apart assemblies containing interlocking components into sub-assemblies. This was achieved by generating feasible disassembly sequences by definitions and derivations of a contact and relation matrix.
Xia et al. [158]	Presented a simplified teaching-learning-based optimization algorithm for the planning of disassembly sequences of Waste Electrical and Electronic Equipment (WEEE).

cellphone and thereby enables the system to handle multiple types of uncertainties associated with the cellphone's state.

The challenges associated with the autonomous generation and execution of disassembly actions is tackled by Chen et al. [172], where the robotic system used in this work is equipped with three different tools (i.e., screwdriver, hole-saw and angle-grinder) and utilizes a method based on a geometrical estimation to asses and selects a corresponding disassembly action. The proposed method is tested and validated on various models of LCDs.

The extraction of cylindrical components from their fixtures can often result in the jamming or wedging of the component; thereby, applying unnecessary forces and strain on the extracted component, which can reduce the chance of passing the re-qualification process. In order to minimize and mitigate the occurrence of such scenarios, Zang et al. [173] used a theoretical derived method utilizing active compliance and key parameters such as the location of the compliance centre, initial compliance, degree of compliance. Also, Zang et al. concluded on the effect of the presented method based on experimental validation. Another proof-of-concept presented by Bulh et al. [136] integrated two UR5 robotic manipulators in a dual-arm disassembly cell to showcase the potential of disassembly of mockup mobile phones in a smart production facility.

Liu et al. investigated a framework for the use of a service platform for robotic disassembly planning in remanufacturing [174]. This investigation aimed to find the optimal solutions for both robotic disassembly sequence and line configuration. Finally, they verified their analysis of the service platform with a case study on an idler shaft.

5. HRC in the field of disassembly

HRC in Disassembly (HRCD) is a timely topic that has become the focus of industry stakeholders and researchers during the last decade. Due to its complexity, it requires several advancements both in HRC technologies and standardization policies in terms of take-back requirements, product interfaces and possible serviceability to become profitable and environmentally viable. As mentioned earlier, the collaboration between humans and robots for the disassembly of EOLPs has many advantages compared to fully automatic systems. In this section, the results of the literature survey on human–robot collaborative solutions for disassembly are presented.

Liu et al. introduced a systematic development framework towards human–robot collaborative disassembly based on perception, cognition, decision, execution and evolution [175]. The implementation for enabling HRCD is presented, where technologies such as cyber–physical production systems (CPPS) and artificial intelligence (AI) are combined. The framework's feasibility regarding perception, decision making, and control was explored and verified with a case study. The case study consists of a non-collaborative ABB manipulator while a discrete bees algorithm was used to optimize disassembly sequence planner by assessing the condition of various objects with quality indicators based on the stage of the disassembly process. Finally, a motion-driven control method utilized in combination with a safety assurance strategy.

The same research team worked on a deep learning system enabling a fluent and natural interaction between a human operator and an industrial manipulator for an industrial human–robot cooperative disassembly scenario [176]. The system utilized a CNN–LSTM network to predict the motion of the human operator purely on the inputs of a vision system without the need for wearable devices or tags. The approach was validated in a case study for the disassembly of personal computers, which tested the system capable of identifying and predicting the motions of the human operators based on the tools, parts or scenarios.

Huang et al. investigated the integration of HRC in disassembly processes for a case study of press-fitted components [177]. In the study, the press-fitted component originates from an automotive water pump. The setup consists of a manual operated press and three jigs for the fixation and handling of the components during the disassembly process and KUKA LBR iiwa 14 R800 equipped with a Robotiq 2-FINGER 140 gripper.

The separate steps of the disassembly process are as follows: Firstly, the operator actuates the press to separate the first sub-assembly of the pump, with the robot waiting with its gripper underneath the press to support the extraction process. In the other process, the robot places the extracted sub-assembly in the press and waits again underneath the press for the sub-components to be pressed out by the manual operated press (Fig. 12). The overall process time of this procedure is approximately five minutes and can be adapted to pumps that require the same basic operations for their disassembly.

The majority of industrial products contain a large number of screws that hold them together. Therefore, an essential aspect of a disassembly system is its ability to unscrew. In that context, Chen et al. proposed a hybrid disassembly station equipped with a compliant robot with a bit-changing mechanism for unscrewing battery screws from electric vehicles [178]. The control strategy uses a skill-based formulation based on a finite state machine approach meaning that the different states of the manipulator are described by a sequence of primitive motions, which a human operator can teach. This state machine allows the authors to programme the engagement and removal of a threaded fastener and an autonomous bit exchange. The authors also highlight that implementing an Impedance control scheme enables the manipulator to handle direct physical interaction between a robot and human, thereby allowing seamless integration of such a

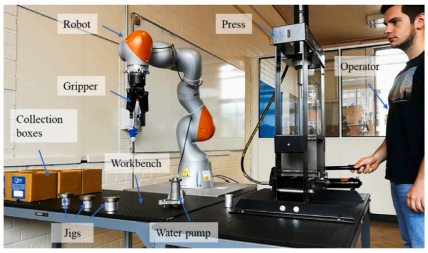

Fig. 12. The setup of the robotic cell for the extraction of press fit components used in [177].

robotic assistant for disassembly tasks, which would lead to an increase in the through-put in labour-intensive tasks. In order to address the challenge of unfastening hexagonal headed screws, Li et al. introduced an automated method [179]. It was accomplished by implementing an electric nutrunner spindle equipped with a geared offset adapter at the TCP of a collaborative enabled robot. The tool and location strategy of the screws were demonstrated in a disassembly case study of a turbocharger. The location strategy is implemented in the form of a novel spiral search technique based on force/torque feedback, which can detect if the tool is engaged with the screw.

The research works of Jungbluth et al. [180,181] aim to add the concept of HRC to a cognitive robotics based framework for the disassembly of EOLP as proposed in [165]. Initially, Jungbluth et al. aimed to enable a robotic system to act autonomously to execute disassembly task and improve the ergonomics of disassembly workstations with the utilization of knowledge and skills [180]. This was achieved by providing information on the product model to an intelligent agent to generate the disassembly sequence. This sequence is then utilized to create a series of disassembly actions for the robot assistant. At a later stage, this research focused on implementing a multi-agent control architecture [181]. This control architecture is based on product and process-based knowledge models and enables the workers to choose labour division between themselves and the robot for each disassembly task. According to the authors, this approach allows the system to assist the human co-worker in complex disassembly processes.

Axenopulos et al. described a framework for a hybrid human–robotic recycling plant for electrical and electronic equipment [182]. This framework aims to optimize the process of extracting valuable resource and reducing the risks involved for humans in this process by introducing HRC to this process. The authors of this work mention that a key aim of the framework is to enhance the disassembly process by introducing HRC cells comprising a single human operator that collaborates with several robots. In pursuance of achieving this goal, the proposed framework foundation consists out of the following pillars: (i) Factory-level modelling and orchestration (ii) Cell-level perception methods (iii) Robotic actions planning and control (iv) Principles of moral actions and ethics engine (v) HRC schemes.

Lastly, Ding et al. investigated the possibility of transferring the valuable knowledge of disassembling EOLPs from the human operators to an HRCD system [183]. This investigation utilized the combination of a video capturing system, a Natural Language Processing (NLP) algorithm and a graph-based knowledge representation. The collected knowledge was then used to improve the robot's capability to support the human during the HRCD task.

In order to summarize the key elements of the aforementioned works in HRCD, we present an overview in Table 4 while we discuss the important findings in Section 6.

6. Discussion

The article reviewed the literature and state-of-the-art methods in HRCD for the period 2009–2020 based on current technological advancements in relevant areas. Firstly, it was identified that the currently applied research related to industrial fully automated disassembly systems is focused on consumer electronics (i.e., TVs and smartphones). A potential explanation for this trend could be derived from the fact that the amount of WEEE produced every year is proportionally disadvantageous with the current available capacity for recycling and remanufacturing of such waste. Additionally, many of these systems tend to utilize destructive operations in their attempts to extract sub-assemblies and components for remanufacturing uses, resulting in inefficient processes.

Moreover, it can be derived that due to the increase in the complexity and variability of mechatronic and mechanical EOLPs, the existing automated disassembly systems cannot cope with the complexity of the disassembly task. Therefore, more solutions incorporating human workers in the process showed up during the past decade. As a result, ensuring safety remains one of the most challenging concepts of HRC in industrial environments, and specifically in disassembly tasks. Multiple methods incorporating safety have been identified and analysed. However, it is evident that regardless of the vast amount of standards and communication methods applied in HRC, the amount of task-sharing between a robot and a human defines the final implementation. Similarly to Vicentini's conclusions in [18], only a few research works of the identified literature promote physical interaction and focus mostly on cooperative and coexistent tasks rather than collaborative.

Regarding the current implementations of HRCD systems, there is a lack of post-collision control schemes in the context of pHRI. The absence of such post-collision control schemes concerns as, during HRC tasks in the disassembly domain, a human worker may interfere physically with the manipulator and engage in a collaboration phase accidentally. In order to keep the interaction safe, the manipulator must be able to adapt its behaviour safely based on the exchange of contact forces. Taking this into account, it is also essential to highlight that an HRCD system, like any other HRC system, enables symbiotic collaboration with humans only when an appropriate tool is used for the task at hand. Regardless of the robot and its task, the tool remains a potential risk of severe hazards. These safety aspects can be improved by introducing energy-aware control schemes and using tools with human-aware design.

In an ideal scenario, human–robot collaboration should feel the same as a human–human collaboration; however, there are several areas where the current state-of-the-art in the field can be improved. Human workers still surpass their robotic partners with their cognitive, adaptation and problem-solving abilities. When it comes to the field of disassembly, the main oversight of the explored HRC systems is the absence of skill acquisition interfaces (see Table 4). Such interfaces would enable a more intuitive definition and teaching of tasks to the robots and allow humans to transfer their domain knowledge and cognitive abilities to them.

At the same time, researchers have presented complete frameworks that can support HRCD without practical implementations at this current stage [182]. It will be interesting to witness the evaluation of the integration of a complete cell where a robot and a human worker would collaborate in a disassembly task based on that framework. Additionally, available research has been presented showcasing the application of robotic task-oriented knowledge graph in HRCD [183]. However, the lack of presentation of the key implementation details of the robot cell makes it difficult to conclude on the type of collaboration and related aspects explored in Table 4.

In addition, various kinds of HRI that are usually used in other domains, e.g., social and service robotics, are rarely implemented in HRCD systems. A potential explanation for this gap could be that several audiovisual and learning techniques can still face demanding

Table 4
Overview over the utilization/form of implementation of the different key-elements for (future) human–robot collaborative disassembly applications. SMS: Safety-rated Monitored Speed, HG: Hand-Guidance, SSM: Speed and Separation Monitoring, PFL: Power and force limitation. ✓, — indicate if the listed attributes are included in the work and ? indicates the absence of information from which a conclusion can be draw from.

Publications		Liu et al. [175]	Liu et al. [176]	Huang et al. [177]	Chen et al. [178]	Li et al.[179]	Jungbluth et al. [180]	Jungbluth et al. [181]	Axenopulos et al. [182]	Ding et al. [183]
Task		—	Computer	extraction of press fit components	unscrewing	unscrewing	Disassembly of mechatronic drive	Disassembly of mechatronic drive	Disassembly of WEEE	Disassembly of Roller chain
Robot		ABB IRB1200	ABB IRB1200	KUKA LBR iiwa 14 R820	KUKA LWR IV	KUKA LBR iiwa 14 R820	KUKA LBR iiwa 14 R820	KUKA LBR iiwa 14 R820	—	KUKA LBR iiwa 14 R820
Human–robot coexistence		—	—	—	—	—	—	—	—	?
Human–robot cooperation		—	✓	✓	—	—	✓	✓	—	?
Human–robot collaboration		✓	—	—	✓	—	—	—	✓	—
ISO 15066		SSM	SSM	SSM	—	—	—	HG	HG, SSM, PFL	?
pre-collision control scheme		✓	✓	✓	—	—	—	—	✓	—
post-collision control scheme		—	—	✓	✓	✓	—	—	✓	—
verbal HRI		✓	—	—	—	—	—	✓	✓	✓
visual HRI		✓	✓	—	—	—	—	in progress	✓	—
physical HRI		—	—	—	—	—	—	—	✓	—
Task Definition	Skills	—	—	—	✓	—	✓	✓	—	—
	Skill acquisition	—	—	—	—	—	—	—	—	—
Task sequence planning		✓	—	—	—	—	✓	✓	✓	?

challenges with the environmental conditions in industrial environments. The addressing of these challenges would result in a more efficient and safe work environment and enable people who are limited in their physical and mental capabilities to be included in HRCD systems.

7. Concluding remarks

Given the importance of production's environmental and economic sustainability, the CEBM has started to be adopted across various companies and industries. This adoption poses a number of challenges regarding the resourcing, the disassembly, and the remanufacturing/qualification of ELOPs. This paper started by investigating the principles of human–robot collaboration in industrial environments and the characteristics of a disassembly process. Later, it presents an investigation into the existing literature on HRCD covering hybrid disassembly robot cells to disassemble EOLPs.

In the last part of this survey paper, the gaps in the existing literature on HRCD systems are discussed, based on which it was suggested that future research could move towards the investigation and implementation of (i) Control strategies which not just focus on the avoidance of contact between the manipulator and the worker but enables safe pHRI (ii) Skill teaching approaches which intuitively enable workers to expand the skill set of the robotic system (iii) Interaction through a combination of verbal and non-verbal communication methods enables a more immersive interaction between robots and humans.

CRediT authorship contribution statement

Sebastian Hjorth: Conceptualization, Methodology, Writing – original draft, Writing – review & editing, Visualization. **Dimitrios Chrysostomou:** Conceptualization, Writing – review & editing, Supervision.

Declaration of competing interest

No author associated with this paper has disclosed any potential or pertinent conflicts which may be perceived to have impending conflict with this work. For full disclosure statements refer to https://doi.org/10.1016/j.rcim.2021.102208.

References

[1] E. Commission, Circular Economy Action Plan, Tech. Rep., European Commission, 2015.
[2] European Environment Agency, Recycling industry can boost the European economy, (November) 2020, p. 2020, URL https://www.eea.europa.eu/highlights/recycling-industry-can-boost-the.
[3] U. von der Leyen, A Union That Strives for More, Tech. Rep., European Commission, 2019, p. 24, URL https://ec.europa.eu/commission/sites/beta-political/files/political-guidelines-next-commission{_}en.pdf.
[4] U. Nations, Transforming our world: The 2030 agenda for sustainable development, in: A New Era Glob. Heal., Springer Publishing Company, New York, NY, 2018, pp. 529–567, http://dx.doi.org/10.1891/9780826190123.ap02.
[5] Robert Bosch GmbH, Sustainability innovations for resource and energy efficiency, 2020, URL https://www.bosch.com/research/fields-of-innovation/sustainability-innovations-for-resource-and-energy-efficiency/.
[6] Grundfos, Environmental initiatives, 2020, pp. 1–3, URL https://www.grundfos.com/about-us/sustainability-responsibility/green-at-heart/environmental-initiatives.html.
[7] Apple Inc., Making without taking sounds impossible. But it's our goal, 2019, pp. 1–11, URL https://www.apple.com/environment/our-approach/.
[8] F. Ardente, L. Talens Peiró, F. Mathieux, D. Polverini, Accounting for the environmental benefits of remanufactured products: Method and application, J. Cleaner Prod. 198 (2018) 1545–1558, http://dx.doi.org/10.1016/j.jclepro.2018.07.012.
[9] Ellen MacArthur Foundation, Intelligent assets: Unlocking the circular economy potential, Ellen MacArthur Found. (2016) 1–25, URL https://bit.ly/39WkeXb.
[10] J. Li, M. Barwood, S. Rahimifard, Robotic disassembly for increased recovery of strategically important materials from electrical vehicles, Robot. Comput. Integr. Manuf. 50 (September 2017) (2018) 203–212, http://dx.doi.org/10.1016/j.rcim.2017.09.013.

[11] T.E. Graedel, J. Allwood, J.-P. Birat, B.K. Reck, S.F. Sibley, G. Sonnemann, M. Buchert, C. Hagelüken, UNEP (2011) recycling rates of metals – A status report, A report of the working group on the global metal flows to the international resource panel, in: Ned. Tijdschr. Geneeskd., International Resource Panel, 2011, p. 44.

[12] T. Tolio, A. Bernard, M. Colledani, S. Kara, G. Seliger, J. Duflou, O. Battaia, S. Takata, Design, management and control of demanufacturing and remanufacturing systems, CIRP Ann. - Manuf. Technol. 66 (2) (2017) 585–609, http://dx.doi.org/10.1016/j.cirp.2017.05.001.

[13] M.T. Bockholt, J. Hemdrup Kristensen, M. Colli, P. Meulengracht Jensen, B. Vejrum Whrens, Exploring factors affecting the financial performance of end-of-life take-back program in a discrete manufacturing context, J. Cleaner Prod. 258 (2020) 120916, http://dx.doi.org/10.1016/j.jclepro.2020.120916.

[14] P. Drazan, The impact of robots on manufacturing processes and society at large, in: The Management Implications of New Information Technology, Routledge, 2018, pp. 48–55.

[15] K. Elo, E. Sundin, Automatic dismantling challenges in the structural design of LCD TVs, Procedia CIRP 15 (2014) 251–256, http://dx.doi.org/10.1016/j.procir.2014.06.058.

[16] H. Poschmann, H. Brüggemann, D. Goldmann, Disassembly 4.0: A review on using robotics in disassembly tasks as a way of automation, Chem. Ing. Tech. 92 (4) (2020) 341–359, http://dx.doi.org/10.1002/cite.201900107.

[17] German Aerospace Center (DLR), History of the DLR LWR, 2020, pp. 20–21, URL https://www.dlr.de/rm/en/desktopdefault.aspx/tabid-12464/21732{_}read-44586/.

[18] F. Vicentini, Terminology in safety of collaborative robotics, Robot. Comput.-Integr. Manuf. 63 (November 2019) (2020) 101921, http://dx.doi.org/10.1016/j.rcim.2019.101921.

[19] A. Hentout, M. Aouache, A. Maoudj, I. Akli, Human–robot interaction in industrial collaborative robotics: a literature review of the decade 2008–2017, Adv. Robot. 33 (15–16) (2019) 764–799, http://dx.doi.org/10.1080/01691864.2019.1636714.

[20] S. El Zaatari, M. Marei, W. Li, Z. Usman, Cobot programming for collaborative industrial tasks: An overview, Robot. Auton. Syst. 116 (2019) 162–180, http://dx.doi.org/10.1016/j.robot.2019.03.003.

[21] S. Haddadin, E. Croft, Springer Handbook of Robotics, Springer International Publishing, Cham, 2016, pp. 1835–1875, Ch. Physical human–robot interaction, Vol. 2 of Siciliano and Khatib [184], https://doi.org/10.1007/978-3-319-32552-1.

[22] A. Kolbeinsson, E. Lagerstedt, J. Lindblom, Foundation for a classification of collaboration levels for human-robot cooperation in manufacturing, Prod. Manuf. Res. 7 (1) (2019) 448–471, http://dx.doi.org/10.1080/21693277.2019.1645628.

[23] V. Villani, F. Pini, F. Leali, C. Secchi, Survey on human–robot collaboration in industrial settings: Safety, intuitive interfaces and applications, Mechatronics 55 (2018) 248–266, http://dx.doi.org/10.1016/j.mechatronics.2018.02.009.

[24] G. Michalos, S. Makris, J. Spiliotopoulos, I. Misios, P. Tsarouchi, G. Chryssolouris, ROBO-PARTNER: Seamless human-robot cooperation for intelligent, flexible and safe operations in the assembly factories of the future, in: 5th CATS 2014 - CIRP Conference on Assembly Technologies and Systems, Procedia CIRP 23 (2014) 71–76, http://dx.doi.org/10.1016/j.procir.2014.10.079.

[25] F. Vicentini, Collaborative robotics: a survey, J. Mech. Des. (2020) 1–29, http://dx.doi.org/10.1115/1.4046238.

[26] S. Haddadin, A. Albu-Schäffer, M. Frommberger, J. Rossmann, G. Hirzinger, The "DLR crash report": Towards a standard crash-testing protocol for robot safety - Part I: Results, in: Proc. - IEEE Int. Conf. Robot. Autom., 2009, pp. 272–279.

[27] S. Haddadin, A. Albu-Schaffer, M. Frommberger, J. Rossmann, G. Hirzinger, The DLR crash report: Towards a standard crash-testing protocol for robot safety - part II: Discussions, in: 2009 IEEE Int. Conf. Robot. Autom., IEEE, 2009, pp. 280–287, http://dx.doi.org/10.1109/ROBOT.2009.5152711.

[28] S. Haddadin, A. Albu-SchäCurrency Signffer, G. Hirzinger, Requirements for safe robots: Measurements, analysis and new insights, Int. J. Robot. Res. 28 (11–12) (2009) 1507–1527, http://dx.doi.org/10.1177/0278364909343970.

[29] S. Haddadin, S. Haddadin, A. Khoury, T. Rokahr, S. Parusel, R. Burgkart, A. Bicchi, A. Albu-Schäffer, On making robots understand safety: Embedding injury knowledge into control, Int. J. Robot. Res. 31 (13) (2012) 1578–1602, http://dx.doi.org/10.1177/0278364912462256.

[30] S. Golz, C. Osendorfer, S. Haddadin, Using tactile sensation for learning contact knowledge: Discriminate collision from physical interaction, in: Proceedings - IEEE International Conference on Robotics and Automation, vol. 2015-June, no. june, 2015, pp. 3788–3794, http://dx.doi.org/10.1109/ICRA.2015.7139726.

[31] ISO, Robots and Robotic Devices — Vocabulary (ISO 8373:2016), International Organization for Standardization, 2016.

[32] ISO, Robots and Robotic Devices - Safety Requirements for Industrial Robots - Part 1: Robots (ISO 10218-1:2012), International Organization for Standardization, 2012.

[33] ISO, Robots and Robotic Devices – Safety Requirements for Industrial Robots – Part 2: Robot Systems and Integration (ISO 10218-2:2012), International Organization for Standardization, 2012.

[34] ISO, Robots and Robotic Devices — Collaborative Robots (ISO-15066:2016), International Organization for Standardization, 2016.

[35] A. De Santis, B. Siciliano, A. De Luca, A. Bicchi, An atlas of physical human-robot interaction, Mech. Mach. Theory 43 (3) (2008) 253–270, http://dx.doi.org/10.1016/j.mechmachtheory.2007.03.003.

[36] M. Safeea, P. Neto, R. Béarée, A quest towards safe human robot collaboration, in: K. Althoefer, J. Konstantinova, K. Zhang (Eds.), Towards Autonomous Robotic Systems, Springer International Publishing, Cham, 2019, pp. 493–495.

[37] J.H. Chen, K.T. Song, Collision-free motion planning for human-robot collaborative safety under cartesian constraint, IEEE ICRA (2018) 4348–4354, http://dx.doi.org/10.1109/ICRA.2018.8460185.

[38] C.T. Landi, F. Ferraguti, S. Costi, M. Bonfe, C. Secchi, Safety barrier functions for human-robot interaction with industrial manipulators, in: ECC 2019, EUCA, 2019, pp. 2565–2570, http://dx.doi.org/10.23919/ECC.2019.8796235.

[39] C. Scheurer, M.D. Fiore, S. Sharma, C. Natale, Industrial implementation of a multi-task redundancy resolution at velocity level for highly redundant mobile manipulators, IEEE ISR 2016 (2016) 109–117.

[40] Z. Liu, X. Wang, Y. Cai, W. Xu, Q. Liu, Z. Zhou, D.T. Pham, Dynamic risk assessment and active response strategy for industrial human-robot collaboration, Comput. Ind. Eng. 141 (141) (2020) 106302, http://dx.doi.org/10.1016/j.cie.2020.106302.

[41] A. Mohammed, B. Schmidt, L. Wang, Active collision avoidance for human–robot collaboration driven by vision sensors, Int. J. Comput. Integr. Manuf. 30 (9) (2017) 970–980, http://dx.doi.org/10.1080/0951192X.2016.1268269.

[42] S. Haddadin, A. De Luca, A. Albu-Schaffer, Robot collisions: A survey on detection, isolation, and identification, IEEE Trans. Robot. 33 (6) (2017) 1292–1312, http://dx.doi.org/10.1109/TRO.2017.2723903.

[43] P. Aivaliotis, S. Aivaliotis, C. Gkournelos, K. Kokkalis, G. Michalos, S. Makris, Power and force limiting on industrial robots for human-robot collaboration, Robot. Comput.-Integr. Manuf. 59 (2019) 346–360, http://dx.doi.org/10.1016/j.rcim.2019.05.001.

[44] L. Villani, J. De Schutter, Springer Handbook of Robotics, Springer International Publishing, Cham, 2016, pp. 195–2020, Ch. Force control, Vol. 2 of of Siciliano and Khatib [184], https://doi.org/10.1007/978-3-319-32552-1.

[45] M.C. Yip, D.B. Camarillo, Model-less hybrid position/force control: A minimalist approach for continuum manipulators in unknown, constrained environments, IEEE Robot. Autom. Lett. 1 (2) (2016) 844–851, http://dx.doi.org/10.1109/LRA.2016.2526062.

[46] A.C. Leite, F. Lizarralde, Liu Hsu, Hybrid adaptive vision—Force control for robot manipulators interacting with unknown surfaces, Int. J. Robot. Res. 28 (7) (2009) 911–926, http://dx.doi.org/10.1177/0278364909101932.

[47] P. Gierlak, M. Szuster, Adaptive position/force control for robot manipulator in contact with a flexible environment, Robot. Auton. Syst. 95 (2017) 80–101, http://dx.doi.org/10.1016/j.robot.2017.05.015.

[48] A.Q. Keemink, H. van der Kooij, A.H. Stienen, Admittance control for physical human–robot interaction, Int. J. Robot. Res. 37 (11) (2018) 1421–1444, http://dx.doi.org/10.1177/0278364918768950.

[49] F. Dimeas, N. Aspragathos, Fuzzy learning variable admittance control for human-robot cooperation, in: 2014 IEEE/RSJ Int. Conf. Intell. Robot. Syst., IEEE, 2014, pp. 4770–4775, http://dx.doi.org/10.1109/IROS.2014.6943240.

[50] I. Ranatunga, S. Cremer, D.O. Popa, F.L. Lewis, Intent aware adaptive admittance control for physical human-robot interaction, in: IEEE Int. Conf. Robot. Autom., vol. 2015-June, IEEE, Seattle, 2015, pp. 5635–5640, http://dx.doi.org/10.1109/ICRA.2015.7139988.

[51] J. Bae, K. Kim, J. Huh, D. Hong, Variable admittance control with virtual stiffness guidance for human–robot collaboration, IEEE Access 8 (2020) 117335–117346, http://dx.doi.org/10.1109/ACCESS.2020.3004872.

[52] F. Ficuciello, L. Villani, B. Siciliano, Variable impedance control of redundant manipulators for intuitive human–robot physical interaction, IEEE Trans. Robot. 31 (4) (2015) 850–863, http://dx.doi.org/10.1109/TRO.2015.2430053.

[53] F. Ficuciello, L. Villani, B. Siciliano, Impedance control of redundant manipulators for safe human-robot, Acta Polytech. Hungar. 13 (1) (2016) 223–238, http://dx.doi.org/10.12700/APH.13.1.2016.1.15.

[54] M. Laffranchi, N.G. Tsagarakis, D.G. Caldwell, Safe human robot interaction via energy regulation control, in: 2009 IEEE/RSJ Int. Conf. Intell. Robot. Syst., IEEE, 2009, pp. 35–41, http://dx.doi.org/10.1109/IROS.2009.5354803.

[55] G. Raiola, C.A. Cardenas, T.S. Tadele, T. De Vries, S. Stramigioli, Development of a safety- and energy-aware impedance controller for collaborative robots, IEEE Robot. Autom. Lett. 3 (2) (2018) 1237–1244, http://dx.doi.org/10.1109/LRA.2018.2795639.

[56] B. Vanderborght, A. Albu-Schaeffer, A. Bicchi, E. Burdet, D. Caldwell, R. Carloni, M. Catalano, O. Eiberger, W. Friedl, G. Ganesh, M. Garabini, M. Grebenstein, G. Grioli, S. Haddadin, H. Hoppner, A. Jafari, M. Laffranchi, D. Lefeber, F. Petit, S. Stramigioli, N. Tsagarakis, M. Van Damme, R. Van Ham, L. Visser, S. Wolf, Variable impedance actuators: A review, Robot. Auton. Syst. 61 (12) (2013) 1601–1614, http://dx.doi.org/10.1016/j.robot.2013.06.009.

[57] C. Ott, R. Mukherjee, Y. Nakamura, Unified impedance and admittance control, in: Proc. - IEEE Int. Conf. Robot. Autom., IEEE, 2010, pp. 554–561, http://dx.doi.org/10.1109/ROBOT.2010.5509861.

[58] M. Kimmel, M. Lawitzky, S. Hirche, 6D workspace constraints for physical human-robot interaction using invariance control with chattering reduction, IEEE Int. Conf. Intell. Robot. Syst. (2012) 3377–3383, http://dx.doi.org/10.1109/IROS.2012.6385906.

[59] M. Rauscher, M. Kimmel, S. Hirche, Constrained robot control using control barrier functions, IEEE Int. Conf. Intell. Robot. Syst. 2016-Novem (2016) 279–285, http://dx.doi.org/10.1109/IROS.2016.7759067.

[60] F. Dimeas, V.C. Moulianitis, N. Aspragathos, Manipulator performance constraints in human-robot cooperation, Robot. Comput. Integr. Manuf. 50 (2018) 222–233, http://dx.doi.org/10.1016/j.rcim.2017.09.015.

[61] H. Han, J. Park, Robot control near singularity and joint limit using a continuous task transition algorithm, Int. J. Adv. Robot. Syst. 10 (2013) 1–10, http://dx.doi.org/10.5772/56714.

[62] S. Hjorth, J. Lachner, S. Stramigioli, O. Madsen, D. Chrysostomou, An energy-based approach for the integration of collaborative redundant robots in restricted work environments, in: 2020 IEEE/RSJ International Conference on Intelligent Robots and Systems, IEEE, 2020, http://dx.doi.org/10.1109/IROS45743.2020.9341561.

[63] O. Khatib, Real-time obstacle avoidance for manipulators and mobile robots, in: 1985 IEEE International Conference on Robotics and Automation, vol. 2, 1985, pp. 500–505, http://dx.doi.org/10.1109/ROBOT.1985.1087247.

[64] F. Flacco, A. De Luca, O. Khatib, Control of redundant robots under hard joint constraints: Saturation in the null space, IEEE Trans. Robot. 31 (3) (2015) 637–654, http://dx.doi.org/10.1109/TRO.2015.2418582.

[65] J.D. Muñoz Osorio, F. Allmendinger, M.D. Fiore, U.E. Zimmermann, T. Ortmaier, Physical human-robot interaction under joint and cartesian constraints, ICRA (2019) 185–191, http://dx.doi.org/10.1109/ICAR46387.2019.8981579.

[66] A. Ajoudani, A.M. Zanchettin, S. Ivaldi, A. Albu-Schäffer, K. Kosuge, O. Khatib, Progress and prospects of the human–robot collaboration, Auton. Robots 42 (5) (2018) 957–975, http://dx.doi.org/10.1007/s10514-017-9677-2.

[67] E. Matheson, R. Minto, E.G. Zampieri, M. Faccio, G. Rosati, Human-robot collaboration in manufacturing applications: A review, Robotics 8 (4) (2019) 100, http://dx.doi.org/10.3390/robotics8040100.

[68] S. Maksymova, R. Matarneh, V. Lyashenko, N. Belova, Voice control for an industrial robot as a combination of various robotic assembly process models, J. Comput. Commun. (2017) http://dx.doi.org/10.4236/jcc.2017.511001.

[69] M.C. Bingol, O. Aydogmus, Performing predefined tasks using the human–robot interaction on speech recognition for an industrial robot, Eng. Appl. Artif. Intell. 95 (2020) 103903, http://dx.doi.org/10.1016/j.engappai.2020.103903.

[70] A. González-Docasal, C. Aceta, H. Arzelus, A. Álvarez, I. Fernández, J. Kildal, Towards a natural human-robot interaction in an industrial environment, in: Conversational Dialogue Systems for the Next Decade, Springer, 2020, pp. 243–255.

[71] L. Wang, R. Gao, J. Váncza, J. Krüger, X.V. Wang, S. Makris, G. Chryssolouris, Symbiotic human-robot collaborative assembly, CIRP Ann. 68 (2) (2019) 701–726, http://dx.doi.org/10.1016/j.cirp.2019.05.002.

[72] H. Liu, L. Wang, Gesture recognition for human-robot collaboration: A review, Int. J. Ind. Ergon. 68 (2018) 355–367, http://dx.doi.org/10.1016/j.ergon.2017.02.004.

[73] H. Hagiwara, Trends in HRC and their effects on human operators' sense of presence in manufacturing settings, in: Proceedings of the Human Factors and Ergonomics Society Annual Meeting, vol. 62, no. 1, 2018, pp. 1296–1300, http://dx.doi.org/10.1177/1541931218621297.

[74] P. Tsarouchi, S. Makris, G. Chryssolouris, Human–robot interaction review and challenges on task planning and programming, Int. J. Comput.-Integr. Manuf. 29 (8) (2016) 916–931, http://dx.doi.org/10.1080/0951192X.2015.1130251.

[75] I. Maurtua, I. Fernandez, A. Tellaeche, J. Kildal, L. Susperregi, A. Ibarguren, B. Sierra, Natural multimodal communication for human–robot collaboration, Int. J. Adv. Robot. Syst. 14 (4) (2017) 1729881417716043, http://dx.doi.org/10.1177/1729881417716043.

[76] S. Makris, P. Tsarouchi, D. Surdilovic, J. Krüger, Intuitive dual arm robot programming for assembly operations, CIRP Ann. 63 (1) (2014) 13–16, http://dx.doi.org/10.1016/j.cirp.2014.03.017.

[77] P. Neto, M. Simão, N. Mendes, M. Safeea, Gesture-based human-robot interaction for human assistance in manufacturing, Int. J. Adv. Manuf. Technol. 101 (1–4) (2019) 119–135, http://dx.doi.org/10.1007/s00170-018-2788-x.

[78] H. Liu, T. Fang, T. Zhou, Y. Wang, L. Wang, Deep learning-based multimodal control interface for human-robot collaboration, Procedia CIRP 72 (2018) 3–8.

[79] H. Liu, T. Fang, T. Zhou, L. Wang, Towards robust human-robot collaborative manufacturing: multimodal fusion, IEEE Access 6 (2018) 74762–74771, http://dx.doi.org/10.1109/ACCESS.2018.2884793.

[80] P. Gustavsson, A. Syberfeldt, R. Brewster, L. Wang, Human-robot collaboration demonstrator combining speech recognition and haptic control, Procedia CIRP 63 (2017) 396–401, http://dx.doi.org/10.1016/j.procir.2017.03.126.

[81] A. Mohammed, L. Wang, Brainwaves driven human-robot collaborative assembly, CIRP Ann. 67 (1) (2018) 13–16, http://dx.doi.org/10.1016/j.cirp.2018.04.048.

[82] S. Robla-Gomez, V.M. Becerra, J.R. Llata, E. Gonzalez-Sarabia, C. Torre-Ferrero, J. Perez-Oria, Working together: A review on safe human-robot collaboration in industrial environments, IEEE Access 5 (2017) 26754–26773, http://dx.doi.org/10.1109/ACCESS.2017.2773127.

[83] C. Jost, B. Le Pévédic, T. Belpaeme, C. Bethel, D. Chrysostomou, N. Crook, M. Grandgeorge, N. Mirnig, Human-Robot Interaction: Evaluation Methods and Their Standardization, vol. 12, Springer Nature, 2020.

[84] S. Berman, H. Stern, Sensors for gesture recognition systems, IEEE Trans. Syst. Man Cybern. C 42 (3) (2011) 277–290, http://dx.doi.org/10.1109/TSMCC.2011.2161077.

[85] D. Kumičáková, A. Rengevič, M. Císar, V. Tlach, Utilisation of kinect sensors for the design of a human-robot collaborative workcell, Adv. Sci. Technol. Res. J. 11 (2017) http://dx.doi.org/10.12913/22998624/80937.

[86] O. Mazhar, B. Navarro, S. Ramdani, R. Passama, A. Cherubini, A real-time human-robot interaction framework with robust background invariant hand gesture detection, Robot. Comput.-Integr. Manuf. 60 (2019) 34–48, http://dx.doi.org/10.1016/j.rcim.2019.05.008.

[87] F. Ferraguti, C.T. Landi, S. Costi, M. Bonfè, S. Farsoni, C. Secchi, C. Fantuzzi, Safety barrier functions and multi-camera tracking for human–robot shared environment, Robot. Auton. Syst. 124 (2020) 103388, http://dx.doi.org/10.1016/j.robot.2019.103388.

[88] X.V. Wang, X. Zhang, Y. Yang, L. Wang, A human-robot collaboration system towards high accuracy, Procedia CIRP 93 (2020) 1085–1090, http://dx.doi.org/10.1016/j.procir.2020.04.085.

[89] D. Bassily, C. Georgoulas, J. Guettler, T. Linner, T. Bock, Intuitive and adaptive robotic arm manipulation using the leap motion controller, in: ISR/Robotik 2014; 41st International Symposium on Robotics, VDE, 2014, pp. 1–7.

[90] P. Tsarouchi, A. Athanasatos, S. Makris, X. Chatzigeorgiou, G. Chryssolouris, High level robot programming using body and hand gestures, Procedia CIRP 55 (2016) 1–5, http://dx.doi.org/10.1016/j.procir.2016.09.020.

[91] J. de Gea Fernández, D. Mronga, M. Günther, T. Knobloch, M. Wirkus, M. Schröer, M. Trampler, S. Stiene, E. Kirchner, V. Bargsten, et al., Multimodal sensor-based whole-body control for human–robot collaboration in industrial settings, Robot. Auton. Syst. 94 (2017) 102–119, http://dx.doi.org/10.1016/j.robot.2017.04.007.

[92] E. Benli, Y. Motai, J. Rogers, Visual perception for multiple human–robot interaction from motion behavior, IEEE Syst. J. 14 (2) (2019) 2937–2948, http://dx.doi.org/10.1109/JSYST.2019.2958747.

[93] C. Gkournelos, P. Karagiannis, N. Kousi, G. Michalos, S. Koukas, S. Makris, Application of wearable devices for supporting operators in human-robot cooperative assembly tasks, Procedia CIRP 76 (2018) 177–182, http://dx.doi.org/10.1016/j.procir.2018.01.019.

[94] L. Piyathilaka, S. Kodagoda, Gaussian Mixture based HMM for human daily activity recognition using 3D skeleton features, in: 2013 IEEE 8th Conference on Industrial Electronics and Applications, ICIEA, IEEE, 2013, pp. 567–572, http://dx.doi.org/10.1109/ICIEA.2013.6566433.

[95] J. Berg, T. Reckordt, C. Richter, G. Reinhart, Action recognition in assembly for human-robot-cooperation using hidden markov models, Procedia CIRP 76 (2018) 205–210, http://dx.doi.org/10.1016/j.procir.2018.02.029.

[96] S. Sharma, S. Modi, P.S. Rana, J. Bhattacharya, Hand gesture recognition using Gaussian threshold and different svm kernels, in: International Conference on Advances in Computing and Data Sciences, Springer, 2018, pp. 138–147, http://dx.doi.org/10.1007/978-981-13-1813-9_14.

[97] S. Ji, W. Xu, M. Yang, K. Yu, 3D convolutional neural networks for human action recognition, IEEE Trans. Pattern Anal. Mach. Intell. 35 (1) (2012) 221–231, http://dx.doi.org/10.1109/TPAMI.2012.59.

[98] A. Roitberg, A. Perzylo, N. Somani, M. Giuliani, M. Rickert, A. Knoll, Human activity recognition in the context of industrial human-robot interaction, in: Signal and Information Processing Association Annual Summit and Conference (APSIPA), 2014 Asia-Pacific, IEEE, 2014, pp. 1–10, http://dx.doi.org/10.1109/APSIPA.2014.7041588.

[99] F. Mohammadi Amin, M. Rezayati, H.W. van de Venn, H. Karimpour, A mixed-perception approach for safe human–robot collaboration in industrial automation, Sensors 20 (21) (2020) 6347, http://dx.doi.org/10.3390/s20216347.

[100] J. Zhang, P. Li, T. Zhu, W.-A. Zhang, S. Liu, Human motion capture based on kinect and IMUs and its application to human-robot collaboration, in: 2020 5th International Conference on Advanced Robotics and Mechatronics, ICARM, IEEE, 2020, pp. 392–397, http://dx.doi.org/10.1109/ICARM49381.2020.9195342.

[101] S. Sheikholeslami, A. Moon, E.A. Croft, Cooperative gestures for industry: Exploring the efficacy of robot hand configurations in expression of instructional gestures for human–robot interaction, Int. J. Robot. Res. 36 (5–7) (2017) 699–720, http://dx.doi.org/10.1177/0278364917709941.

[102] B. Gleeson, K. MacLean, A. Haddadi, E. Croft, J. Alcazar, Gestures for industry intuitive human-robot communication from human observation, in: 2013 8th ACM/IEEE International Conference on Human-Robot Interaction, HRI, IEEE, 2013, pp. 349–356, http://dx.doi.org/10.1109/HRI.2013.6483609.

[103] N. Modi, J. Singh, A review of various state of art eye gaze estimation techniques, Adv. Comput. Intell. Commun. Technol. (2020) 501–510, http://dx.doi.org/10.1007/978-981-15-1275-9_41.

[104] O. Palinko, F. Rea, G. Sandini, A. Sciutti, Robot reading human gaze: Why eye tracking is better than head tracking for human-robot collaboration, in: 2016 IEEE/RSJ International Conference on Intelligent Robots and Systems, IROS, IEEE, 2016, pp. 5048–5054, http://dx.doi.org/10.1109/IROS.2016.7759741.

[105] H. Kim, Y. Ohmura, Y. Kuniyoshi, Using human gaze to improve robustness against irrelevant objects in robot manipulation tasks, IEEE Robot. Autom. Lett. (2020) http://dx.doi.org/10.1109/LRA.2020.2998410.

[106] K. Dufour, J. Ocampo-Jimenez, W. Suleiman, Visual–spatial attention as a comfort measure in human–robot collaborative tasks, Robot. Auton. Syst. 133 (2020) 103626, http://dx.doi.org/10.1016/j.robot.2020.103626.

[107] A. Moon, D.M. Troniak, B. Gleeson, M.K. Pan, M. Zheng, B.A. Blumer, K. MacLean, E.A. Croft, Meet me where i'm gazing: How shared attention gaze affects human-robot handover timing, in: Proceedings of the 2014 ACM/IEEE International Conference on Human-Robot Interaction, Association for Computing Machinery, New York, NY, USA, 2014, pp. 334–341, http://dx.doi.org/10.1145/2559636.2559656.

[108] A. Casalino, C. Messeri, M. Pozzi, A.M. Zanchettin, P. Rocco, D. Prattichizzo, Operator awareness in human–robot collaboration through wearable vibrotactile feedback, IEEE Robot. Autom. Lett. 3 (4) (2018) 4289–4296, http://dx.doi.org/10.1109/LRA.2018.2865034.

[109] G. Salvietti, M.Z. Iqbal, D. Prattichizzo, Bilateral haptic collaboration for human-robot cooperative tasks, IEEE Robot. Autom. Lett. 5 (2) (2020) 3517–3524, http://dx.doi.org/10.1109/LRA.2020.2975715.

[110] F. Bergner, E. Dean-Leon, G. Cheng, Efficient distributed torque computation for large scale robot skin, in: 2018 IEEE/RSJ International Conference on Intelligent Robots and Systems, IROS, 2018, pp. 1593–1599, http://dx.doi.org/10.1109/IROS.2018.8594144.

[111] G. Tang, P. Webb, J. Thrower, The development and evaluation of robot light skin: A novel robot signalling system to improve communication in industrial human–robot collaboration, Robot. Comput.-Integr. Manuf. 56 (2019) 85–94, http://dx.doi.org/10.1016/j.rcim.2018.08.005.

[112] E. Bottani, G. Vignali, Augmented reality technology in the manufacturing industry: A review of the last decade, IISE Trans. 51 (3) (2019) 284–310, http://dx.doi.org/10.1080/24725854.2018.1493244.

[113] J. Egger, T. Masood, Augmented reality in support of intelligent manufacturing–a systematic literature review, Comput. Ind. Eng. 140 (2020) 106195, http://dx.doi.org/10.1016/j.cie.2019.106195.

[114] S.T. Mortensen, D. Chrysostomou, O. Madsen, A novel framework for virtual recommissioning in reconfigurable manufacturing systems, in: 2017 22nd IEEE International Conference on Emerging Technologies and Factory Automation, ETFA, IEEE, 2017, pp. 1–4, http://dx.doi.org/10.1109/ETFA.2017.8247744.

[115] G. Michalos, P. Karagiannis, S. Makris, Ö. Tokçalar, G. Chryssolouris, Augmented reality (AR) applications for supporting human-robot interactive cooperation, Procedia CIRP 41 (2016) 370–375, http://dx.doi.org/10.1016/j.procir.2015.12.005.

[116] S. Rabah, A. Assila, E. Khouri, F. Maier, F. Ababsa, P. Maier, F. Mérienne, et al., Towards improving the future of manufacturing through digital twin and augmented reality technologies, Procedia Manuf. 17 (2018) 460–467, http://dx.doi.org/10.1016/j.promfg.2018.10.070.

[117] F. Ferraguti, F. Pini, T. Gale, F. Messmer, C. Storchi, F. Leali, C. Fantuzzi, Augmented reality based approach for on-line quality assessment of polished surfaces, Robot. Comput.-Integr. Manuf. 59 (2019) 158–167, http://dx.doi.org/10.1016/j.rcim.2019.04.007.

[118] O. Danielsson, A. Syberfeldt, R. Brewster, L. Wang, Assessing instructions in augmented reality for human-robot collaborative assembly by using demonstrators, Procedia CIRP 63 (2017) 89–94, http://dx.doi.org/10.1016/j.procir.2017.02.038.

[119] A. Argyrou, C. Giannoulis, A. Sardelis, P. Karagiannis, G. Michalos, S. Makris, A data fusion system for controlling the execution status in human-robot collaborative cells, Procedia CIRP 76 (2018) 193–198, http://dx.doi.org/10.1016/j.procir.2018.01.012.

[120] A. Luxenburger, J. Mohr, T. Spieldenner, D. Merkel, F. Espinosa, T. Schwartz, F. Reinicke, J. Ahlers, M. Stoyke, Augmented reality for human-robot cooperation in aircraft assembly, in: 2019 IEEE International Conference on Artificial Intelligence and Virtual Reality, AIVR, IEEE Computer Society, 2019, pp. 263–2633, http://dx.doi.org/10.1109/AIVR46125.2019.00061.

[121] P. Tavares, C.M. Costa, L. Rocha, P. Malaca, P. Costa, A.P. Moreira, A. Sousa, G. Veiga, Collaborative welding system using BIM for robotic reprogramming and spatial augmented reality, Autom. Constr. 106 (2019) 102825, http://dx.doi.org/10.1016/j.autcon.2019.04.020.

[122] Q. Wang, Y. Cheng, W. Jiao, M.T. Johnson, Y. Zhang, Virtual reality human-robot collaborative welding: A case study of weaving gas tungsten arc welding, J. Manuf. Process. 48 (2019) 210–217, http://dx.doi.org/10.1016/j.jmapro.2019.10.016.

[123] O. Kyjanek, B. Al Bahar, L. Vasey, B. Wannemacher, A. Menges, Implementation of an augmented reality AR workflow for human robot collaboration in timber prefabrication, in: M. Al-Hussein (Ed.), Proceedings of the 36th International Symposium on Automation and Robotics in Construction, ISARC, International Association for Automation and Robotics in Construction (IAARC), Banff, Canada, 2019, pp. 1223–1230, http://dx.doi.org/10.22260/ISARC2019/0164.

[124] R.S. Andersen, O. Madsen, T.B. Moeslund, H.B. Amor, Projecting robot intentions into human environments, in: 2016 25th IEEE International Symposium on Robot and Human Interactive Communication, RO-MAN, IEEE, 2016, pp. 294–301, http://dx.doi.org/10.1109/ROMAN.2016.7745145.

[125] H. Liu, L. Wang, An AR-based worker support system for human-robot collaboration, Procedia Manuf. 11 (2017) 22–30, http://dx.doi.org/10.1016/j.promfg.2017.07.124.

[126] S. Papanastasiou, N. Kousi, P. Karagiannis, C. Gkournelos, A. Papavasileiou, K. Dimoulas, K. Baris, S. Koukas, G. Michalos, S. Makris, Towards seamless human robot collaboration: integrating multimodal interaction, Int. J. Adv. Manuf. Technol. 105 (9) (2019) 3881–3897, http://dx.doi.org/10.1007/s00170-019-03790-3.

[127] M. Koppenborg, P. Nickel, B. Naber, A. Lungfiel, M. Huelke, Effects of movement speed and predictability in human–robot collaboration, Hum. Factors Ergon. Manuf. Serv. Ind. 27 (4) (2017) 197–209, http://dx.doi.org/10.1002/hfm.20703.

[128] E. Matsas, G.-C. Vosniakos, D. Batras, Prototyping proactive and adaptive techniques for human-robot collaboration in manufacturing using virtual reality, Robot. Comput.-Integr. Manuf. 50 (2018) 168–180, http://dx.doi.org/10.1016/j.rcim.2017.09.005.

[129] F. Chenf, B. Gao, M. Selvaggio, Z. Li, D. Caldwell, K. Kershaw, A. Masi, M. Di Castro, R. Losito, A framework of teleoperated and stereo vision guided mobile manipulation for industrial automation, 2016 IEEE International Conference on Mechatronics and Automation, IEEE ICMA 2016 (2016) 1641–1648, http://dx.doi.org/10.1109/ICMA.2016.7558810.

[130] M. Ostanin, S. Mikhel, A. Evlampiev, V. Skvortsova, A. Klimchik, Human-robot interaction for robotic manipulator programming in mixed reality, in: 2020 IEEE International Conference on Robotics and Automation, ICRA, IEEE, 2020, pp. 2805–2811, http://dx.doi.org/10.1109/ICRA40945.2020.9196965.

[131] A. Munoz, X. Mahiques, J.E. Solanes, A. Marti, L. Gracia, J. Tornero, Mixed reality-based user interface for quality control inspection of car body surfaces, J. Manuf. Syst. 53 (2019) 75–92, http://dx.doi.org/10.1016/j.jmsy.2019.08.004.

[132] TAPAS, Robotics-enabled logistics and assistive services for the transformable factory of the future, 2011-2014, EU project funded under the European Commission's Seventh Framework Programme grant no 260026. URL: http://www.tapas-project.eu/.

[133] CARLoS, Cooperative robot for large spaces manufacturing, 2014-2015, EU project funded under the European Commission's Seventh Framework Programme grant no 606363. URL: http://carlosproject.eu/.

[134] ACAT, Learning and execution of action categories acat project website, 2013-2016, EU project funded under the European Commission's Seventh Framework Programme grant no 600578. URL: http://www.acat-project.eu/.

[135] CARMEN, Center for avanceret robotbaseret automation (center for advanced robot-based automation), 2013-2017, National Danish research project funded by Innovation Fund Denmark. URL: http://innovationsfonden.dk/en/node/609.

[136] J.F. Buhl, R. Grønhøj, J.K. Jørgensen, G. Mateus, D. Pinto, J.K. Sørensen, S. Bøgh, D. Chrysostomou, A dual-arm collaborative robot system for the smart factories of the future, Procedia Manuf. 38 (2019) (2019) 333–340, http://dx.doi.org/10.1016/j.promfg.2020.01.043.

[137] F. Wallhoff, J. Blume, A. Bannat, W. Rösel, C. Lenz, A. Knoll, A skill-based approach towards hybrid assembly, Adv. Eng. Informatics 24 (3) (2010) 329–339, http://dx.doi.org/10.1016/j.aei.2010.05.013.

[138] C. Breazeal, K. Dautenhahn, T. Kanda, Springer Handbook of Robotics, Springer International Publishing, Cham, 2016, pp. 1941–1944, Ch. Socio-cognitive skills, Vol. 2 of Siciliano and Khatib [184], https://doi.org/10.1007/978-3-319-32552-1.

[139] C. Breazeal, K. Dautenhahn, T. Kanda, Springer Handbook of Robotics, Springer International Publishing, Cham, 2016, pp. 1946–1950, Ch. Social robots and communication skills, Vol. 2 of Siciliano and Khatib [184], https://doi.org/10.1007/978-3-319-32552-1.

[140] C. Paxton, A. Hundt, F. Jonathan, K. Guerin, G.D. Hager, Costar: Instructing collaborative robots with behavior trees and vision, in: 2017 IEEE Int. Conf. Robot. Autom., IEEE, 2017, pp. 564–571, http://dx.doi.org/10.1109/ICRA.2017.7989070, URL arXiv:1611.06145.

[141] K.R. Guerin, C. Lea, C. Paxton, G.D. Hager, A framework for end-user instruction of a robot assistant for manufacturing, in: 2015 IEEE Int. Conf. Robot. Autom., vol. 2015-June, IEEE, 2015, pp. 6167–6174, http://dx.doi.org/10.1109/ICRA.2015.7140065.

[142] C. Schou, J.S. Damgaard, S. Bogh, O. Madsen, Human-robot interface for instructing industrial tasks using kinesthetic teaching, in: 2013 44th Int. Symp. Robot. ISR 2013, 2013, http://dx.doi.org/10.1109/ISR.2013.6695599.

[143] M.J. Rosenstrauch, J. Kruger, Safe human-robot-collaboration-introduction and experiment using ISO/TS 15066, in: 2017 3rd Int. Conf. Control. Autom. Robot., IEEE, 2017, pp. 740–744, http://dx.doi.org/10.1109/ICCAR.2017.7942795.

[144] R.S. Andersen, C. Schou, J.S. Damgaard, O. Madsen, Using a flexible skill-based approach to recognize objects in industrial scenarios, in: 47th Int. Symp. Robot. ISR 2016, vol. 2016, 2016, pp. 399–406.

[145] M. Stenmark, M. Haage, E.A. Topp, J. Malec, Supporting semantic capture during kinesthetic teaching of collaborative industrial robots, Int. J. Semant. Comput. 12 (1) (2018) 167–186, http://dx.doi.org/10.1142/S1793351X18400093.

[146] G. Canal, E. Pignat, G. Alenya, S. Calinon, C. Torras, Joining high-level symbolic planning with low-level motion primitives in adaptive HRI: Application to dressing assistance, in: Proc. - IEEE Int. Conf. Robot. Autom., 2018, pp. 3273–3278, http://dx.doi.org/10.1109/ICRA.2018.8460606.

[147] J. Saukkoriipi, T. Heikkilä, J.M. Ahola, T. Seppälä, P. Isto, Programming and control for skill-based robots, Open Eng. 10 (1) (2020) 368–376, http://dx.doi.org/10.1515/eng-2020-0037.

[148] J. Huckaby, H. Christensen, Modeling robot assembly tasks in manufacturing using SysML, in; Proc. Jt. Conf. ISR 2014 - 45th Int. Symp. Robot. Robot. 2014 - 8th Ger. Conf. Robot. ISR/ROBOTIK 2014, 2014, pp. 743–749.

[149] C. Schou, R.S. Andersen, D. Chrysostomou, S. Bøgh, O. Madsen, Skill-based instruction of collaborative robots in industrial settings, Robot. Comput. Integr. Manuf. 53 (June 2016) (2018) 72–80, http://dx.doi.org/10.1016/j.rcim.2018.03.008.

[150] S. Vongbunyong, P. Vongseela, J. Sreerattana-Aporn, A process demonstration platform for product disassembly skills transfer, Procedia CIRP 61 (2017) 281–286, http://dx.doi.org/10.1016/j.procir.2016.11.197.

[151] F.J. Abu-Dakka, L. Rozo, D.G. Caldwell, Force-based learning of variable impedance skills for robotic manipulation, in: 2018 IEEE-RAS 18th Int. Conf. Humanoid Robot., vol. 2018-Novem, IEEE, 2018, pp. 1–9, http://dx.doi.org/10.1109/HUMANOIDS.2018.8624938.

[152] Z. Zhou, J. Liu, D.T. Pham, W. Xu, F.J. Ramirez, C. Ji, Q. Liu, Disassembly sequence planning: Recent developments and future trends, Proc. Inst. Mech. Eng. B 233 (5) (2019) 1450–1471, http://dx.doi.org/10.1177/0954405418789975.

[153] S. Behdad, L. Berg, J. Vance, D. Thurston, Immersive computing technology to investigate tradeoffs under uncertainty in disassembly sequence planning, J. Mech. Des. 136 (7) (2014) 1–9, http://dx.doi.org/10.1115/1.4025021.

[154] M. Alshibli, A. El Sayed, E. Kongar, T.M. Sobh, S.M. Gupta, Disassembly sequencing using tabu search, J. Intell. Robot. Syst. Theory Appl. 82 (1) (2016) 69–79, http://dx.doi.org/10.1007/s10846-015-0289-9.

[155] S. Vongbunyong, S. Kara, M. Pagnucco, Learning and revision in cognitive robotics disassembly automation, Robot. Comput. Integr. Manuf. 34 (2015) 79–94, http://dx.doi.org/10.1016/j.rcim.2014.11.003.

[156] G.Q. Jin, W.D. Li, S. Wang, X. Lu, Solution space generation for disassembly research on liquid crystal displays televisions, in: Proc. 2014 IEEE 18th Int. Conf. Comput. Support. Coop. Work Des. CSCWD 2014, 2014, pp. 35–40, http://dx.doi.org/10.1109/CSCWD.2014.6846813.

[157] Y. Wang, F. Lan, D.T. Pham, J. Liu, J. Huang, C. Ji, S. Su, W. Xu, Q. Liu, Z. Zhou, Automatic detection of subassemblies for disassembly sequence planning, in: Proc. 15th Int. Conf. Informatics Control. Autom. Robot., vol. 1, SCITEPRESS - Science and Technology Publications, 2018, pp. 104–110, http://dx.doi.org/10.5220/0006906601040110.

[158] K. Xia, L. Gao, L. Wang, W. Li, K.-M. Chao, A simplified teaching-learning-based optimization algorithm for disassembly sequence planning, in: 2013 IEEE 10th International Conference on E-Business Engineering, IEEE, 2013, pp. 393–398, http://dx.doi.org/10.1109/ICEBE.2013.60.

[159] W. Xu, Q. Tang, J. Liu, Z. Liu, Z. Zhou, D.T. Pham, Disassembly sequence planning using discrete bees algorithm for human-robot collaboration in remanufacturing, Robot. Comput. Integr. Manuf. 62 (September) (2020) http://dx.doi.org/10.1016/j.rcim.2019.101860.

[160] J. Liu, Z. Zhou, D.T. Pham, W. Xu, C. Ji, Q. Liu, Robotic disassembly sequence planning using enhanced discrete bees algorithm in remanufacturing, Int. J. Prod. Res. 56 (9) (2018) 3134–3151, http://dx.doi.org/10.1080/00207543.2017.1412527.

[161] K. Li, Q. Liu, W. Xu, J. Liu, Z. Zhou, H. Feng, Sequence planning considering human fatigue for human-robot collaboration in disassembly, Procedia CIRP 83 (2019) 95–104, http://dx.doi.org/10.1016/j.procir.2019.04.127.

[162] I. Rodriguez, K. Nottensteiner, D. Leidner, M. Durner, F. Stulp, A. Albu-Schaffer, Pattern recognition for knowledge transfer in robotic assembly sequence planning, IEEE Robot. Autom. Lett. 5 (2) (2020) 3666–3673, http://dx.doi.org/10.1109/LRA.2020.2979622.

[163] I. Rodriguez, K. Nottensteiner, D. Leidner, M. Kasecker, F. Stulp, A. Albu-Schäffer, Iteratively refined feasibility checks in robotic assembly sequence planning, IEEE Robot. Autom. Lett. 4 (2) (2019) 1416–1423, http://dx.doi.org/10.1109/LRA.2019.2895845.

[164] S. Vongbunyong, S. Kara, M. Pagnucco, Application of cognitive robotics in disassembly of products, CIRP Ann. - Manuf. Technol. 62 (1) (2013) 31–34, http://dx.doi.org/10.1016/j.cirp.2013.03.037.

[165] S. Vongbunyong, S. Kara, M. Pagnucco, Basic behaviour control of the vision-based cognitive robotic disassembly automation, Assem. Autom. 33 (1) (2013) 38–56, http://dx.doi.org/10.1108/01445151311294694.

[166] S. Vongbunyong, W.H. Chen, in: C. Herrmann, S. Kara (Eds.), Disassembly Automation, Springer, 2015, pp. 25–54, http://dx.doi.org/10.1007/978-3-319-15183-0_3.

[167] S. Vongbunyong, M. Pagnucco, S. Kara, Vision-based execution monitoring of state transition in disassembly automation, Int. J. Autom. Technol. 10 (5) (2016) 708–716, http://dx.doi.org/10.20965/ijat.2016.p0708.

[168] M. Bdiwi, A. Rashid, M. Putz, Autonomous disassembly of electric vehicle motors based on robot cognition, in: 2016 IEEE Int. Conf. Robot. Autom., IEEE, 2016, pp. 2500–2505, http://dx.doi.org/10.1109/ICRA.2016.7487404.

[169] D. Schneider, E. Schomer, N. Wolpert, A motion planning algorithm for the invalid initial state disassembly problem, in: 2015 20th Int. Conf. Methods Model. Autom. Robot. MMAR 2015, 2015, pp. 35–40, http://dx.doi.org/10.1109/MMAR.2015.7283702.

[170] S. Chen, J. Yi, H. Jiang, X. Zhu, Ontology and CBR based automated decision-making method for the disassembly of mechanical products, Adv. Eng. Informatics 30 (3) (2016) 564–584, http://dx.doi.org/10.1016/j.aei.2016.06.005.

[171] W. Figueiredo, A High-speed Robotic Disassembly System for the Recycling and Reuse of Cellphones (Master thesis), Massachusetts Institute of Technology, 2018, pp. 0–68.

[172] W.H. Chen, G. Foo, S. Kara, M. Pagnucco, Automated generation and execution of disassembly actions, Robot. Comput.-Integr. Manuf. 68 (February 2020) (2021) 102056, http://dx.doi.org/10.1016/j.rcim.2020.102056.

[173] Y. Zhang, H. Lu, D.T. Pham, Y. Wang, M. Qu, J. Lim, S. Su, Peg–hole disassembly using active compliance, R. Soc. Open Sci. 6 (8) (2019) http://dx.doi.org/10.1098/rsos.190476.

[174] J. Liu, Z. Zhou, D.T. Pham, W. Xu, J. Cui, C. Yang, Service platform for robotic disassembly planning in remanufacturing, J. Manuf. Syst. 57 (August) (2020) 338–356, http://dx.doi.org/10.1016/j.jmsy.2020.10.005.

[175] Q. Liu, Z. Liu, W. Xu, Q. Tang, Z. Zhou, D.T. Pham, Human-robot collaboration in disassembly for sustainable manufacturing, Int. J. Prod. Res. 57 (12) (2019) 4027–4044, http://dx.doi.org/10.1080/00207543.2019.1578906.

[176] Z. Liu, Q. Liu, W. Xu, Z. Liu, Z. Zhou, J. Chen, Deep learning-based human motion prediction considering context awareness for human-robot collaboration in manufacturing, Procedia CIRP 83 (2019) 272–278, http://dx.doi.org/10.1016/j.procir.2019.04.080.

[177] J. Huang, D.T. Pham, Y. Wang, M. Qu, C. Ji, S. Su, W. Xu, Q. Liu, Z. Zhou, A case study in human–robot collaboration in the disassembly of press-fitted components, Proc. Inst. Mech. Eng. B 234 (3) (2020) 654–664, http://dx.doi.org/10.1177/0954405419883060.

[178] W.H. Chen, K. Wegener, F. Dietrich, A robot assistant for unscrewing in hybrid human-robot disassembly, in: 2014 IEEE Int. Conf. Robot. Biomimetics, IEEE ROBIO 2014, 2014, pp. 536–541, http://dx.doi.org/10.1109/ROBIO.2014.7090386.

[179] R. Li, C. Ji, Q. Liu, Z. Zhou, D.T. Pham, J. Huang, Y. Tan, M. Qu, Y. Wang, M. Kerin, K. Jiang, S. Su, Unfastening of hexagonal headed screws by a collaborative robot, IEEE Trans. Autom. Sci. Eng. (2020) 1–14, http://dx.doi.org/10.1109/TASE.2019.2958712.

[180] J. Jungbluth, W. Gerke, P. Plapper, An intelligent agent-controlled and robot-based disassembly assistant, IOP Conf. Ser.: Mater. Sci. Eng. 235 (1) (2017) http://dx.doi.org/10.1088/1757-899X/235/1/012005.

[181] J. Jungbluth, W. Gerke, P. Plapper, Recent progress toward intelligent robot assistants for non-destructive recent progress toward intelligent robot assistants for non- destructive disassembly, in: 2. RACIR – Robotix-Academy Conference for Industrial Robotics 2018, 2018, pp. 11–20, URL http://hdl.handle.net/10993/37793.

[182] A. Axenopulos, G.T. Papadopoulos, D. Giakoumis, I. Kostavelis, A. Papadimitriou, S. Sillaurren, L. Bastida, O.S. Oguz, D. Wollherr, E. Garnica, V. Vouloutsi, P.F. Verschure, D. Tzovaras, P. Daras, A hybrid human-robot collaborative environment for recycling electrical and electronic equipment, in: 2019 IEEE SmartWorld, Ubiquitous Intelligence & Computing, Advanced & Trusted Computing, Scalable Computing & Communications, Cloud & Big Data Computing, Internet of People and Smart City Innovation (SmartWorld/SCALCOM/UIC/ATC/CBDCom/IOP/SCI), IEEE, 2019, pp. 1754–1759, http://dx.doi.org/10.1109/SmartWorld-UIC-ATC-SCALCOM-IOP-SCI.2019.00312.

[183] Y. Ding, W. Xu, Z. Liu, Z. Zhou, D.T. Pham, Robotic task oriented knowledge graph for human-robot collaboration in disassembly, Procedia CIRP 83 (2019) 105–110, http://dx.doi.org/10.1016/j.procir.2019.03.121.

[184] B. Siciliano, O. Khatib (Eds.), Springer Handbook of Robotics, vol. 2, Springer International Publishing, Cham, 2016, http://dx.doi.org/10.1007/978-3-319-32552-1.

PAPER B

An Energy-based Approach for the Integration of Collaborative Redundant Robots in Restricted Work Environments

written by
Sebastian Hjorth, Johannes Lachner, Stefano Stramigioli, Ole Madsen and Dimitrios Chrysostomou

The paper has been published in: *IEEE/RSJ International Conference on Intelligent Robots and Systems* © 2020 IEEE. Reprinted; with permission; from Sebastian Hjorth, Johannes Lachner, Stefano Stramigioli, Ole Madsen and Dimitrios Chrysostomou; An Energy-based Approach for the Integration of Collaborative Redundant Robots in Restricted Work Environments; IEEE/RSJ International Conference on Intelligent Robots and Systems, 10/2020

2020 IEEE/RSJ International Conference on Intelligent Robots and Systems (IROS)
October 25-29, 2020, Las Vegas, NV, USA (Virtual)

An Energy-based Approach for the Integration of Collaborative Redundant Robots in Restricted Work Environments

Sebastian Hjorth [†] *, Johannes Lachner [‡§], Stefano Stramigioli [‡], Ole Madsen [†] and Dimitrios Chrysostomou [†]
[†]Department of Materials and Production
Aalborg University, Aalborg, Denmark
* Corresponding author E-mail: sshj@mp.aau.dk
[‡]Faculty of Electrical Engineering, Mathematics and Computer Science
University of Twente, Enschede, Netherlands
[§]Kuka Deutschland GmbH, Zugspitzstraße 140, 86165 Augsburg, Deutschland

***Abstract*—To this day, most robots are installed behind safety fences, separated from the human. New use-case scenarios demand for collaborative robots, e.g. to assist the human with physically challenging tasks. These robots are mainly installed in work-environments with limited space, e.g. existing production lines. This brings certain challenges for the control of such robots. The presented work addresses a few of these challenges, namely: stable and safe behaviour in contact scenarios; avoidance of restricted workspace areas; prevention of joint limits in automatic mode and manual guidance. The control approach in this paper extents an Energy-aware Impedance controller by repulsive potential fields in order to comply with Cartesian and joint constraints. The presented controller was verified for a KUKA LBR iiwa 7 R800 in simulation as well as on the real robot.**

***Index Terms*—Workspace restriction, Redundant manipulators, Collaborative robots, Impedance Control, Artificial potential fields, Energy-aware robotics.**

I. Introduction

In recent years the number of collaborative robots has increased and will continue to rise in multiple work environments, especially in industrial and medical settings [1], [2]. These collaborative robots (e.g. KUKA LBR iiwa, ABB YuMi and FANUC CRX) are no longer restricted to only operate in a static and well-defined environment behind a fence, such as classic serial manipulators (e.g. KUKA KR6 and Fanuc M16iB) are. Hereby, these robots share their workspace with humans and support/share various complex tasks with them, such as: positioning an object in a more ergonomic position for the workforce [3], place or remove sub-components on the product while an operator works on a different part on the same product [4].

As the mentioned examples show, the implementation possibilities of collaborative robots are plentiful. However, all these possibilities bring up a number of challenges [5]. Two of them are:

- Safe physical Human Robot interaction (pHRI): the operator can share one workspace with the robot and if necessary interfere with its operation
- Integration in areas with limited space, e.g. in existing production lines

These challenges result in constraints for the robotic system, given by the workspace and the manipulator itself. In areas with limited space, pHRI is unavoidable and even wanted, Therefore, it should be possible for the human co-worker to distort the execution of the robot task. Moreover, there are Cartesian constraints in the workspace where the robot should be kept out of. As in those areas clamping situations in case of an unintended collision could occur. Robot given constraints are e.g. singularities, self collisions and joint limits. If any of these constraints are violated, the manipulator stops its movement and must be reinitialized. In an efficient pHRI scenario, interacting without stability problems, due to singularities and joint limit violations, have to be ensured. Moreover, appropriate joint limit avoidance strategies reduce the risk of robot self collisions.

Different control strategies have been developed over the years to meet these challenges. These control strategies are implemented on different control levels, e.g. position, velocity, force and torque level. However, most of them focus only on some of these challenges.

The work [6]–[8] focus on the avoidance of pHRIs, by either adapting the manipulator's trajectory or Nullspace, while relying on external sensors (e.g. cameras and depth sensors). In [9], a closed-loop-inverse-kinematic control approach on velocity level is implemented that respects the manipulator's joint limits as well as Cartesian obstacles. The method proposed in [10] saturates the manipulator's Nullspace. It combines the stack of task approach with quadratic programming in order to keep the manipulator within a set of hard-constraints for the joint positions, velocities, and accelerations. This approach can also be used to restricting the manipulator's workspace. The approaches proposed in [11], [12] focus on an admittance control strategy to limit the manipulator's workspaces for planned/guided interactions only. Because of their non compliant behaviour in planned or unplanned contact, the controller in [6]–[12] show drawbacks for their use in pHRI.

For redundant manipulators, [13] proposes six-dimensional Cartesian workspace constrains using an invariance control

978-1-7281-6212-6/20/$31.00 ©2020 IEEE

scheme in combination with a discrete-time Euler solver to reduce oscillations at the Cartesian constraint, as the discrete-time implementations of the invariance control suffers from so called chattering. In [14], a combination of impedance control, control-barrier-functions and quadratic programming was successfully used to enforce Cartesian workspace-restrictions for a redundant robot. Both approaches presented in [13] and [14] solely focus on the enforcement of Cartesian workspace constraints of the end-effector and do not include the constrains in the manipulator's joint space.

The work in [15] presents an Operational Space Control framework to handle joint limits and singularities. However, this framework does not include Cartesian constraints. One closely related work is [16]. It extends the Operational Space Control framework by hard constraints and transforming the algorithm in [10] to torque level.

None of the above presented approaches observe the energy in the robotic system or the energy exchange with its environment. However, this is a crucial aspect to ensure robot stability and safe pHRI.

The formalism presented in this paper will focus on an energy-based control strategy in order to tackle the aforementioned challenges. This will be done by combining the Energy-aware reactive control scheme presented in [17], [18] with the concept of artificial potential fields introduced in [19]. Compared to the related work this formalism has a clear advantage: it enables an autonomous adaption of the manipulator's compliant behaviour without external sensory input. The implemented Energy-aware control scheme observes, monitors and limits the energy introduced to the manipulator by the controller and its energy exchange with environment. This ensures a safe interaction since the energy exchange is limited to a specified threshold. As mentioned in [16], common problems of the potential field approach are occurring oscillations when a link moves along the activation zone of a constraint. In our work this drawback can be minimized by regulating the energy in the robot system. To summarize, the main contributions of the proposed work are:

- Cartesian workspace restriction and joint limit avoidance, valid for all links/joints
- Energy-based formulation of the control strategy ensures stable and safe robot behaviour
- Verification of the implemented control strategy on a redundant manipulator in simulation and the real world.

The remainder of the paper is structured as follows: Section II provides a general overview over the presented control strategy. In Section III the theory of the implemented control strategy is introduced. In Section IV the experimental results are shown while Section V concludes the findings of the experimental results.

Notation: Small bold letters and capital bold letters indicate vectors and matrices respectively. The transpose of $\mathbf{x}$ is represented as $\mathbf{x}^\top$. The wrench of frame c in respect to frame j expressed in i is indicated by $\mathbf{w}_c^{i,j}$. $\widehat{\mathbf{x}}$ is the skew-symmetric matrix representation of $\mathbf{x}$. $\mathbf{I}_f$ represents an identity matrix of dimension f.

II. Concept

Reactive control schemes merge the planning and execution phase of the robot [20]. Compared to traditional control schemes, these controllers provide a greater flexibility in terms of handling interactions with its environment, e.g. the human co-worker. An impedance controller is a reactive controller that can be described as a mass-spring-damper system with adjustable parameters [21]. Instead of controlling just a single state variable, an impedance controller creates a dynamic relationship between the different state variables, by controlling the impedance of the robotic system [22]. Therefore, it is possible to describe any interaction with such a system as an energy exchange between the manipulator and its environment.

The robot's equation of motion is given by

$$\mathbf{M}(\mathbf{q})\ddot{\mathbf{q}} + \bar{\mathbf{C}}(\mathbf{q},\dot{\mathbf{q}})\dot{\mathbf{q}} + \bar{\mathbf{G}}(\mathbf{q}) = \boldsymbol{\tau}^\top, \tag{1}$$

with $\mathbf{q} \in \mathbb{R}^n$ being the generalized joint positions and $\mathbf{M}(\mathbf{q}) \in \mathbb{R}^{n\times n}$ being the positive-definite mass matrix. $\bar{\mathbf{C}}(\mathbf{q},\dot{\mathbf{q}})\dot{\mathbf{q}} \in \mathbb{R}^n$ represents the centrifugal and Coriolis torques, $\bar{\mathbf{G}}(\mathbf{q}) \in \mathbb{R}^n$ the gravitational torques and $\boldsymbol{\tau}^\top \in \mathbb{R}^n$ the control torques, respectively. Hereby, n denotes the number of joints. The joint torques on the right hand side of (1) can be decompose to

$$\boldsymbol{\tau}^\top = \boldsymbol{\tau}_{\text{Control}}^\top - \boldsymbol{\tau}_{\text{CC}}^\top + \boldsymbol{\tau}_{\text{JLA}}^\top + \underbrace{\boldsymbol{\tau}_{\text{Coriolis}}^\top}_{\bar{\mathbf{C}}(\mathbf{q},\dot{\mathbf{q}})\dot{\mathbf{q}}} + \underbrace{\boldsymbol{\tau}_{\text{Gravity}}^\top}_{\bar{\mathbf{G}}(\mathbf{q})}, \tag{2}$$

with $\boldsymbol{\tau}_{\text{Control}}^\top$ being the control torques of the robot task, $\boldsymbol{\tau}_{\text{CC}}^\top$ incorporating the Cartesian workspace restrictions, $\boldsymbol{\tau}_{\text{JLA}}^\top$ representing the torques to avoid joint limits and $\boldsymbol{\tau}_{\text{Coriolis}}^\top$ and $\boldsymbol{\tau}_{\text{Gravity}}^\top$ being the compensation torques for Coriolis and Gravity.

An overview of the implemented control structure with all components of (2) can be seen in Fig. 1.

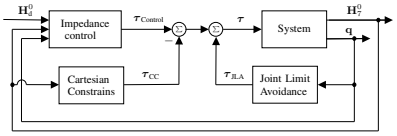

Fig. 1. The overall structure of the implemented control strategy.

III. Methods

The following section describes the mathematical derivation of the torque commands for the robot motion (III-A), including the Cartesian (III-B) and joint limit (III-C) constraints.

A. Control scheme

The presented controller includes methods such as Energy shaping and Damping injection [17]. These methods counteract autonomously the non-linear behavior of a normal Impedance controller, by observing the energy introduced to the manipulator and its power exchanged in contact with the environment [23], [24].

The resulting joint torques $\boldsymbol{\tau}_{\text{Control}}^{\top}$ of (2) can be decomposed to

$$\boldsymbol{\tau}_{\text{Control}}^{\top} = \boldsymbol{\tau}_{\text{Motion}}^{\top} - \boldsymbol{\tau}_{\text{Damping}}^{\top}, \tag{3}$$

where $\boldsymbol{\tau}_{\text{Motion}}^{\top} \in \mathbb{R}^n$ and $\boldsymbol{\tau}_{\text{Damping}}^{\top} \in \mathbb{R}^n$ are the torques generated by the motion generating springs and by the damping term, respectively.

1) Mathematical description of the motion generating springs: A wrench $\mathbf{w}_K^{7,7} \in se^*(3)$ generates the motion of the end-effector based on the end-effector's current transformation $\mathbf{H}_7^0 \in SE(3)$ and its desired goal transformation $\mathbf{H}_d^0 \in SE(3)$:

$$\mathbf{w}_K^{7,7\top} = \begin{bmatrix} \mathbf{f}_K^{7,7\top} \\ \mathbf{m}_K^{7,7\top} \end{bmatrix} = \begin{bmatrix} \mathbf{K}_t & \mathbf{K}_c \\ \mathbf{K}_c^{\top} & \mathbf{K}_r \end{bmatrix} \Delta\boldsymbol{\chi}, \tag{4}$$

with $\Delta\boldsymbol{\chi}^{\top} = \begin{bmatrix} \Delta\mathbf{o}_K^{7,7\top} & \Delta\boldsymbol{\theta}_K^{7,7\top} \end{bmatrix} \in se(3)$ being the infinitesimal body twist displacement, which can be extracted from $\left(\mathbf{H}_K^7\right)^{-1}\dot{\mathbf{H}}_K^7$ [23]. The elements $\mathbf{K}_t,\ \mathbf{K}_r \in \mathbb{R}^{3\times3}$ represent the stiffness for translation and rotation of the spring and $\mathbf{K}_c \in \mathbb{R}^{3\times3}$ is the decoupling between these two terms. In order to describe $\mathbf{w}_K^{7,7}$ purely in terms of energy, the force $\mathbf{f}_K^{7,7} \in \mathbb{R}^{1\times3}$ and momentum $\mathbf{m}_K^{7,7} \in \mathbb{R}^{1\times3}$ are formulated as

$$\begin{aligned} \widehat{\mathbf{f}}_K^{7,7} = &- \mathbf{R}_d^7 as\big(\mathbf{G}_t\widehat{\mathbf{p}}_7^d\big)\mathbf{R}_7^d - as\big(\mathbf{G}_t\mathbf{R}_d^7\widehat{\mathbf{p}}_7^d\mathbf{R}_7^d\big) \\ &- 2as\big(\mathbf{G}_c\mathbf{R}_7^d\big) \end{aligned} \tag{5}$$

and

$$\begin{aligned} \widehat{\mathbf{m}}_K^{7,7} = &- 2as\big(\mathbf{G}_r\mathbf{R}_7^d\big) - as\big(\mathbf{G}_t\mathbf{R}_d^7\widehat{\mathbf{p}}_7^d\mathbf{R}_7^d\big) \\ &- 2as\big(\mathbf{G}_c\widehat{\mathbf{p}}_7^d\mathbf{R}_7^d\big). \end{aligned} \tag{6}$$

Where $\mathbf{p}_7^d \in \mathbb{R}^3$ is the translation between the end-effector and its desired position and $\mathbf{G}_{r,t,c}$ are the co-stiffnesses for the translational spring, the rotational spring and the coupling terms, respectively. The operator $as()$ returns the anti-symmetric part of a square matrix. The co-stiffnesses are introduced for the convention between $\Delta\boldsymbol{\chi}$ and the Rotation matrices $\mathbf{R} \in SO(3)$:

$$\mathbf{G}_{r,t,c} = \frac{1}{2}tr\big(\mathbf{K}_{r,t,c}\big)\mathbf{I}_3 - \mathbf{K}_{r,t,c}. \tag{7}$$

The elastic wrench $\mathbf{w}_K^{7,7\top}$ can be mapped to the inertial reference frame by the adjoint coordinate transformation $Ad_{\mathbf{H}_0^7}^{\top} \in \mathbb{R}^{6\times6}$,

$$\mathbf{w}_K^{0,7\top} = Ad_{\mathbf{H}_0^7}^{\top}\mathbf{w}_K^{7,7\top}. \tag{8}$$

The joint torques $\boldsymbol{\tau}_{\text{Motion}}^{\top}$ are calculated with the transposed of the spatial geometric Jacobian $\mathbf{J}_7^{0,0}(\mathbf{q}) \in \mathbb{R}^{6\times n}$ (9).

$$\boldsymbol{\tau}_{\text{Motion}}^{\top} = \mathbf{J}_7^{0,0\top}(\mathbf{q})\mathbf{w}_K^{0,7\top} \tag{9}$$

2) Energy Scaling: In the concept of Energy-aware control, the energy of the system is scaled in order to assign a strict minimum in the desired configuration [25]. The energy-based safety metric demands a limit on the total energy of the system. The total energy stored in system is $E_{\text{total}} = T_{\text{total}} + U_{\text{total}}$, with $T_{\text{total}} \in \mathbb{R}$ being the kinetic energy and $U_{\text{total}} \in \mathbb{R}$ being the potential due to spatial springs [26]. Based on E_{total} and a chosen maximum energy $E_{\max}$ which the system is allowed to store, a scaling parameter $\lambda \in \mathbb{R}$ is computed:

$$\lambda = \begin{cases} 1 & \text{if } E_{\text{total}} \leqslant E_{\max} \\ \frac{E_{\max} - T_{\text{total}}}{U_{\text{total}}} & \text{otherwise.} \end{cases} \tag{10}$$

with

$$\begin{aligned} U_{\text{total}} = &-tr\big(\mathbf{G}_r\mathbf{R}_7^d\big) + \Big(-\frac{1}{4}tr\big(\widehat{\mathbf{p}}_7^d\mathbf{G}_t\widehat{\mathbf{p}}_7^d\big) \\ &-\frac{1}{4}tr\big(\widehat{\mathbf{p}}_7^d\mathbf{R}_7^d\mathbf{G}_r\mathbf{R}_d^7\widehat{\mathbf{p}}_7^d\big)\Big) + tr\big(\mathbf{G}_c\mathbf{R}_d^7\widehat{\mathbf{p}}_7^d\big) \end{aligned} \tag{11}$$

As the potential energy stored in the spatial springs U_{total} are proportional to the Co-stiffness $\mathbf{G}_{r,t,c}$ [23], it is sufficient to scale $\mathbf{G}_{r,t,c}$:

$$\mathbf{G}_{r,t,c} \leftarrow \lambda\mathbf{G}_{r,t,c}. \tag{12}$$

Therefore, the motion generating wrench $\mathbf{w}_K^{0,7\top}$ applied at the robot end-effector is changed.

3) Damping injection: Next to the energy in the system, the power of the robot must be monitored and if necessary limited. Therefore, the *damping injection* method is used. Whenever the power resulting from the manipulator's motion

$$P_{\text{motion}} = \big(\mathbf{J}_7^{0,0}(\mathbf{q})^{\top}\mathbf{w}_K^{0,7\top} - \mathbf{B}_{\text{init}}\dot{\mathbf{q}}\big)^{\top}\dot{\mathbf{q}} \tag{13}$$

exceeds a maximal power threshold $P_{\max}$ the damping torque in (3) is increased:

$$\boldsymbol{\tau}_{\text{Damping}}^{\top} = \beta\mathbf{B}_{\text{init}}\dot{\mathbf{q}}; \quad \mathbf{B}_{\text{init}} \in \mathbb{R}^{n\times n}. \tag{14}$$

Hereby, the scaling factor $\beta \in \mathbb{R}$ is defined as:

$$\beta = \begin{cases} 1 & \text{if } P_{\text{motion}} \leqslant P_{\max} \\ \frac{\left(\mathbf{J}_7^{0,0}(\mathbf{q})^{\top}\mathbf{w}_K^{0,7\top}\right)^{\top}\dot{\mathbf{q}} - P_{\max}}{\dot{\mathbf{q}}^{\top}\mathbf{B}_{\text{init}}\dot{\mathbf{q}}} & \text{otherwise.} \end{cases} \tag{15}$$

Note that the initial damping $\mathbf{B}_{\text{init}}$ should be monitored with eq. (15), once the robot starts moving toward the desired transformation $\mathbf{H}_d^0$. In this case $P_{\text{motion}} > 0$. Once the human stops and handguides the robot the damping is kept at $\mathbf{B}_{\text{init}}$.

B. Cartesian constraints

In this work, a modified version of an artificial repulsive potential field is introduced in order to implement workspace constraints. As the work does not focus on the path planning itself, but rather on the restriction of the manipulator's Cartesian workspace, the focus will be limited to repulsive artificial potential fields for the remainder of the work.

To keep the respective links of the manipulator within the predefined Cartesian constraints C_j, a repelling wrench $\mathbf{w}_{C_j}^{i,i}$ is introduced:

$$\mathbf{w}_{C_j}^{i,i\top} = \begin{bmatrix} \mathbf{f}_{C_j}^{i,i\top} \\ \mathbf{m}_{C_j}^{i,i\top} \end{bmatrix}. \tag{16}$$

Its deveriation is based on the concepts presented in [27] and its component can be calulated by

$$\widehat{\mathbf{f}}_{C_j}^{i,i} = -as\big(\mathbf{Q}_{C_j,t_i}\mathbf{R}_{C_j}^{i}\widehat{\mathbf{p}}_{i}^{C_j}\mathbf{R}_{i}^{C_j}\big) - \mathbf{R}_{C_j}^{i}as\big(\mathbf{Q}_{C_j,t_i}\widehat{\mathbf{p}}_{i}^{C_j}\big)\mathbf{R}_{i}^{C_j} \tag{17}$$

and

$$\widehat{\mathbf{m}}_{C_j}^{i,i} = -as\big(\mathbf{Q}_{C_j,t_i}\mathbf{R}_{C_j}^{i}\widehat{\mathbf{p}}_{i}^{C_j}\widehat{\mathbf{p}}_{i}^{C_j}\mathbf{R}_{i}^{C_j}\big). \tag{18}$$

Note that since only the translational motion is of interest, it is only necessary to express (17) and (18) in dependency of the translational Co-stiffness $\mathbf{Q}_{C_j,t_i}$. However, because of the non isotropic spring, the co-stiffness $\mathbf{Q}_{C_j,t_i}$ also generates a repelling moment. Hereby, $\mathbf{Q}_{C_j,t_i} = \frac{1}{2}tr(\mathbf{L}_{C_j,t_i})\mathbf{I}_3 - \mathbf{L}_{C_j,t_i}$, with $\mathbf{L}_{C_j,t_i} \in \mathbb{R}^{3\times3}$ being the spring stiffness of the wrench $\mathbf{w}_{C_j}^{i,i\,\top}$. This repelling force is directly dependent on a repulsive potential field, which is defined by the potential function

$$\sigma_{C_j,i} = \begin{cases} \frac{1}{\gamma}\left(\frac{1}{d_{i,C_j}(\mathbf{q})} - \frac{1}{x_j}\right)^{\gamma} & \text{if } d_{i,C_j}(\mathbf{q}) \le x_j \\ 0 & \text{otherwise,} \end{cases} \tag{19}$$

where $\gamma > 0$ represents the generated potential. The shortest Euclidean distance between the points $\mathbf{p}_i^0 \in \mathbb{R}^3$ and its projection onto the constraint $\mathbf{p}_{i,C_j}^0 \in \mathbb{R}^3$ is given by $d_{i,C_j}(\mathbf{q}) \in \mathbb{R}$. The activation distance of the constraint is denoted $x_j \in \mathbb{R}$.

This function serves as a transition function between the free and restricted motion and is defined as a non-negative smooth surface for any given joint configuration $\mathbf{q}$. The resulting potential $\sigma_{C_j,i} \in \mathbb{R}$ increases towards infinity as the i^{th} constraint link of the manipulator approach the constraint C_j. These Cartesian constraints also referred to as *virtual walls* can be described by any smooth manifold $C \cong \mathbb{R}^3$.

The potential $\sigma_{C_j,i}$ is then used to scale the translational co-stiffnesses $\mathbf{Q}_{C_j,t_i}$ used for the computation of the repelling force $\mathbf{w}_{C_j}^{i,i}$ (16) described in (17) and (18) as seen in (20).

$$\mathbf{Q}_{C_j,t_i} \leftarrow \sigma_{C_j,i}\mathbf{Q}_{C_j,t_i} \tag{20}$$

In order to being able to express the repelling wrench $\mathbf{w}_{C_j}^{i,i\,\top}$ generated by constraint C_j acting on the i^{th} link in the inertial reference 0-frame, it can be mapped with the help of the adjoint coordinate transformation $Ad_{\mathbf{H}_0^i}^{\top}$:

$$\mathbf{w}_{C_j}^{0,i\,\top} = Ad_{\mathbf{H}_0^i}^{\top}\mathbf{w}_{C_j}^{i,i\,\top}. \tag{21}$$

All link and constraint specific wrenches, expressed in the inertial reference frame, can be mapped to their equivalent joint torque representation by

$$\boldsymbol{\tau}_{\text{CC}}^{\top} = \Big(\sum_{i=1}^{n}\big(\sum_{j=1}^{z}\mathbf{J}_i^{0,0\,\top}(\mathbf{q})\mathbf{w}_{C_j}^{0,i\,\top}\big)\Big), \tag{22}$$

where $\mathbf{J}_i^{0,0}(\mathbf{q})$ is the spatial geometric Jacobian for the i^{th} link and z the number of constraints acting on the i^{th} link. Both, (9) and (22), describe the mapping of the desired Cartesian behaviour into the robot's joint space. At this point one advantage for the control of kinematically redundant robots can be seen. The controller enables stable transitions of the robot in and out of singularities, since no inversions of the Jacobian matrix occurs.

C. Joint limit avoidance

The concept of *joint limit avoidance* has strong similarities to the concept of Cartesian constraints: once a joint comes in a critical area, a repelling torque is generated that forces the joint to stay within the predefined limits. In the remainder of this section, the mathematical description of this control scheme will be based on a single joint; for an in-depth description of multiple joints see [19].

The difference between the current position of joint q_i and its lower/upper joint limits $\underline{q}_{i,\text{limit}}/\bar{q}_{i,\text{limit}}$ serve as input for a function, that generates a torque into the opposite direction of the active constraint:

$$\tau_{\text{JLA}_i} = \begin{cases} \frac{\Omega}{\underline{q}_i^2}\left(\frac{1}{\underline{q}_i} - \frac{1}{\underline{q}_{i,J}}\right) & \text{if } \underline{q}_i \le \underline{q}_{i,J} \\ -\frac{\Omega}{\bar{q}_i^2}\left(\frac{1}{\bar{q}_i} - \frac{1}{\bar{q}_{i,J}}\right) & \text{if } \bar{q}_i \le \bar{q}_{i,J} \\ 0 & \text{otherwise.} \end{cases} \tag{23}$$

Note that the repelling torques $\boldsymbol{\tau}_{\text{JLA}}^{\top} \in \mathbb{R}^n$ not only depended on the distance between q_i and its minimal/maximal bounds, but also on a distance $\underline{q}_{i,J}/\bar{q}_{i,J}$ at which the constraints turn active and the scaling factor $\Omega > 0$. The distances $\underline{q}_i$ and $\bar{q}_i$ can be calculated by

$$\begin{aligned} \underline{q}_i &= q_i - \underline{q}_{i,\text{limit}} \\ \bar{q}_i &= \bar{q}_{i,\text{limit}} - q_i\ . \end{aligned} \tag{24}$$

IV. Experimental Results

The performance of the presented control framework is evaluated both in simulation using MATLAB and on the real robot KUKA LBR iiwa 7 R800. The robot is controlled via an external PC and communicates with KUKA's Fast-Research-Interface (FRI) [28]. For the validation, two different test scenarios are presented: firstly, the behaviour at the Cartesian constraint is shown in simulation and on the real robot (IV-A); secondly, the joint-limit-avoidance in a compliant state was tested on the physical system (IV-B). Table I shows the parameters of the implemented reactive control scheme and the constraints of all experiments. The maximum contact energy threshold E_{max} in our experiments was chosen according to the ISO/TS 15066:2016 [29] specified range of $0.52 - 2.5$J and the maximal power threshold P_{max} was chosen based on previous positive results of [18].

A. Cartesian constraint Experiment

To verify the concept of Cartesian constraints, the experiment was split into two tests. In the first experiment the manipulators end-effector is forced to violate two constraints simultaneously. In the second experiment multiple links of the manipulator are simultaneously forced into a single constraint.

1) Multi Cartesian constraints: In this test, the manipulator moves along a predefined trajectory. The respective virtual walls C_1 and C_2 are positioned in in a way that, on its path, the robot will violate these constrains. The experimental set-up and the predefined trajectory can be seen in Fig. 2.

The activation distance $d_{7,C_{1/2}}$ of the constraints C_1 and C_2

TABLE I
CONTROL VARIABLES USED DURING THE DIFFERENT EXPERIMENTS.

Reactive control scheme			
Translational spring stiffness	$\mathbf{K}_t$	$2000 \cdot \mathbf{I}_3$	
Rotational spring stiffness	$\mathbf{K}_r$	$100 \cdot \mathbf{I}_3$	
Coupling spring stiffness	$\mathbf{K}_c$	$0 \cdot \mathbf{I}_3$	
max. allowed Energy	$E_{\max}$	2 J	
max. allowed Power	$P_{\max}$	0.5 W	
inital Damping coeff.	$\mathbf{B}$	$5 \cdot \mathbf{I}_7$	
Cartesian constraint Experiment			
Virtual wall 1	C_1	$\begin{bmatrix}0.5\\1\\0\end{bmatrix}, \begin{bmatrix}0.5\\1\\0.9\end{bmatrix}, \begin{bmatrix}0.5\\-1\\0\end{bmatrix}, \begin{bmatrix}0.5\\-1\\0.9\end{bmatrix}$	m
Virtual wall 2	C_2	$\begin{bmatrix}0.5\\1\\0.9\end{bmatrix}, \begin{bmatrix}0.5\\1\\0.9\end{bmatrix}, \begin{bmatrix}-1\\-1\\0.9\end{bmatrix}, \begin{bmatrix}-1\\1\\0.9\end{bmatrix}$	m
Virtual wall 3	C_3	$\begin{bmatrix}0.5\\1\\0.1\end{bmatrix}, \begin{bmatrix}0.5\\1\\0.1\end{bmatrix}, \begin{bmatrix}-1\\-1\\0.1\end{bmatrix}, \begin{bmatrix}-1\\1\\0.1\end{bmatrix}$	m
Translational spring stiffness	$\mathbf{L}_{C_j,\mathrm{t_i}}$	$10 \cdot \mathbf{I}_3$	
activation distance	$d_{0,C_{1/2/3}}$	0.05m	
exponential	γ	2	
Joint Limit Avoidance Experiment			
upper activation limit	$\bar{q}_{i,J}$	0.2 rad	
lower activation limit	$\underline{q}_{i,J}$	0.2 rad	
scaling factor	Ω	0.025	

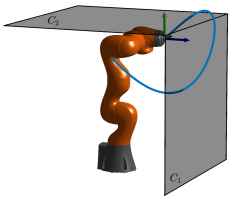

Fig. 2. The setup of the "Multi Cartesian constraint" test consists of a trajectory $\mathbf{H}_d^0(t)$ indicated as a blue line . As well as the constraints C_1/C_2 visualized as grey planes, which are placed respectively along the z-axis and x-axis in reference of the robots inertial reference frame.

was chosen to be 0.05m in order to have a sufficient buffer, such that the constraint is not being violated. The exponential of the transition function γ was set to 2, as it was stated in [19]. The initial spring stiffnesses of the repelling springs $\mathbf{L}_{C_{1/2},\mathrm{t}_7}$ are chosen to be 10 as early testing has shown that it is a sufficient value to keep the manipulator within the Cartesian constraints.

The resulting Cartesian motion of the manipulator's end-effector can be seen in Figs. 3a and 3b, for the simulation and real robot, respectively. It can be seen that the end-effector's movement deviates from the desired path when crossing the respective activation distance $d_{7,C_{1/2}}$ at time $t = 6\text{s}/t = 2\text{s}$. While the end-effector follows the trajectory along the constraint C_2, it encounters the constraint C_1 at time $t = 5.5\text{s}$ for the simulation and $t = 5\text{s}$ for the real-world test. At time $t = 8\text{s}$ the robot no longer violates the virtual wall C_2 and the end-effector moves back on the z-component of the trajectory. However, in both scenarios the end-effector is only able to track the trajectory with an offset, until the trajectory no longer violates the constraint C_1 at $t = 15\text{s}$ and $t = 14\text{s}$. This behaviour results from the implemented energy scaling method described in III-A2. Here, two benefits of the implemented control framework can be seen: the robot respects all Cartesian constraints while complying with the predefined energy and power for interaction. Moreover, thanks to energy scaling, no oscillations occur while moving along the constraints of C_1 and C_2, nor in the transition phase between C_1 and C_2, between 5-8s (cf. red zone in Fig. 3).

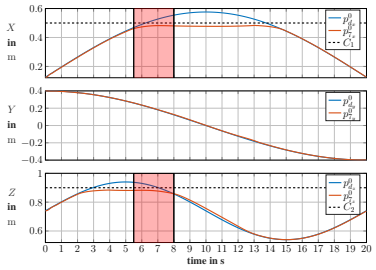

(a)

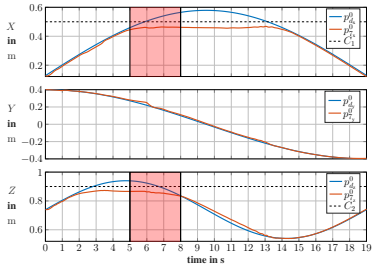

(b)

Fig. 3. The relationship of the trajectory and end-effector position for the simulation and real-world test are shown in (a) and (b), respectively. The virtual wall C_1 and C_2 only restricts the movements of the end-effector along the x-axis and z-axis of the base frame. The y-axis has no restriction.

With the energy E_{total} never exceeding the threshold E_{max} as seen in Fig. 4.

2) Multiple link restriction: This test validates the behaviour of manipulator when multiple links encounter a Cartesian constraints at the same point in time. The virtual walls C_3 is positioned in such a way that link 4, 6 and 7 can reach the constraint. Figure 5 shows how the manipulator is maneuvered until all three axes reaching the constraint.

In Fig. 6 it can be observed that even when multiple joints are pulled/pushed against the virtual wall for a period of 5.5s (cf. red zone in Fig. 6a), none of the respective links violate the constraint C_3. When all the respective links have crossed their respective activation distance d_{i,C_3} at around time $t = 11.5\text{s}$, the respective scaling factor $\sigma_{C_3,i}$ of the spring is increased and a repulsive force $\mathbf{w}_{C_3}^{0,i}$ is generated.

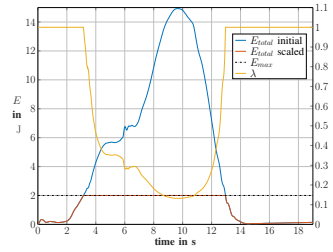

Fig. 4. The total energy E_{total} during the real-world Mutli-Cartesian constraint test. It can also be seen how λ limits E_{total} to E_{max}.

Fig. 5. The experimental setup for the "Multiple link restriction" test, where links 4, 6 and 7 forced towards the constraint C_3 visualized as a grey plane.

This shows another benefit of the implemented controller: when the energy threshold is violated through pulling/pushing on the robot structure, the stiffness of the spatial spring is decreased and the robot can be freely moved. Once the robot is released, it automatically approaches back on the desired trajectory while complying with the specified safe energy threshold.

B. Joint limit avoidance

This experiment validates the behavior of the implemented joint limit avoidance strategy when approaching one or multiple joint limits. By exceeding the maximal specified energy threshold, the manipulator was brought into compliant state and multiple joints where manually forced into the repecitve joint limit (joints 2, 4 and 6). None of these joints violated these limits, even though all axes where manually pushed into the limit simultaneously over a period of 7s (cf. red zone in Fig. 7). When a joint reaches its respective activation-area by crossing over the upper/lower activation limit $\underline{q}_{i,J}/\bar{q}_{i,J}$, a torque in opposing direction is generated. Figure 7 depicts that the torque τ_{JLA_i} increases as the distance to the constraint $\underline{q}_i/\bar{q}_i$ decreases and vise versa. This correlation can be seen when comparing the individual joint position q_i and the respective generated torques τ_{JLA_i}. None of these joints show an oscillatory behaviour (cf. red zone in Fig. 7). For redundant manipulators, benefits through the combination of

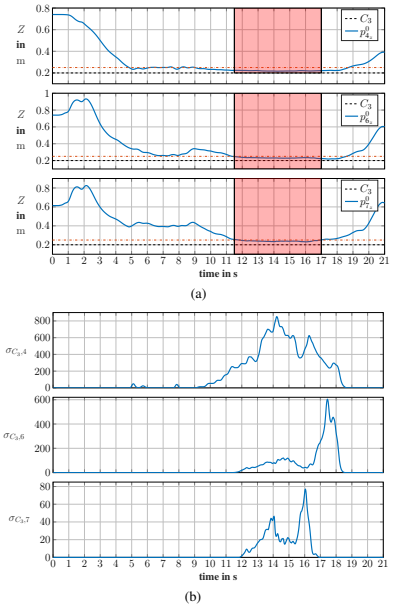

(a)

(b)

Fig. 6. The Cartesian position along the base frames z-axis for body 4, 6 and the 7 are shown in (a) and the respective repulsive field in (b).The virtual wall C_3 only restricts the movements of the links along the z-axis of the base frame. x-axis and y-axis are not restricted. The red dash dotted line in (a) indicates the distance at which the constraint activates or deactivates.

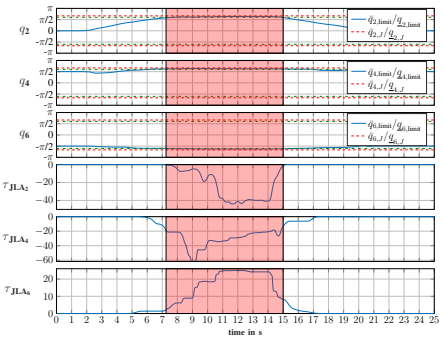

Fig. 7. The joint position of joints 2, 4, 6 and the torques generated by the implemented joint limit avoidance feature are visualized. The area marked in red indicates the time interval in which all joints encounter there respective limits simultaneously.

the energy-aware control scheme and the joint limit avoidance algorithm can be seen. When the energy threshold is violated

during a pHRI, the stiffness of the spatial spring is decreased and the nullspace of the manipulator autonomously adapts through the repelling torques of the joint limit avoidance algorithm.

V. Conclusions

This paper presents an energy-based control formalism for the integration of collaborative redundant robots in restricted work environments. It extends the concept of artificial potential fields by combining it with an Energy-aware reactive control scheme. The presented control framework is capable of handling planned and unplanned pHRI within a workspace with restricted areas. Therefore, no external sensors are needed.

The results of the experiments can be summarized as follows:

- In an unplanned collision, the presented controller reacts in a compliant manner, without exceeding predefined energy thresholds. After contact, the robot automatically re-positions on the trajectory.
- During pHRI, the robot can manually be guided by the human. The presented controller keeps the robot from violating its joint limits. This also holds, when multiple joints encounter their limits. No oscillatory behaviour could be monitored, when approaching the activation zone of the potential field.
- Restricted work environments yield Cartesian constraints for the robot. The controller was tested in scenarios with multiple restricted areas, where multiple links encountered Cartesian constraints. No oscillatory behaviour could be monitored, when approaching the activation zone of the potential field, nor in the transition phase between multiple constraints.

One drawback of the presented controller is that all relevant constraint parameters have to be tuned manually. If the manipulator is forced far from its desired configuration, the stiffness of the spatial spring are scaled close to 0. If the manipulator encounters joint limit constraint on its way back, the desired pose will not be reached without manual guidance. However, in true pHRI scenarios the human co-worker can assist in such cases.

In future work a safe recovery motion planner for handling such events could investigate. Furthermore, an extensive comparison between this work and other approaches, e.g. nullspace saturation algorithms could be done. Also the presented controller could be extended to incorporate more complex shaped Cartesian constraints. Lastly, the effects of the scaling functions in eq. (10) and eq. (15) and the effect of the repulsive forces on the passivity of the system have to be investigated, as for a passive robot, the energy and power thresholds can also be adapted online.

References

[1] A. M. Zanchettin, E. Croft, H. Ding, and M. Li, "Collaborative Robots in the Workplace," *IEEE Robotics and Automation Magazine*, vol. 25, no. 2, pp. 16–17, 2018.

[2] A. Ajoudani, A. M. Zanchettin, S. Ivaldi, A. Albu-Schäffer, K. Kosuge, and O. Khatib, "Progress and prospects of the human–robot collaboration," *Autonomous Robots*, vol. 42, no. 5, pp. 957–975, 2018.

[3] W. Kim, J. Lee, L. Peternel, N. Tsagarakis, and A. Ajoudani, "Anticipatory Robot Assistance for the Prevention of Human Static Joint Overloading in Human-Robot Collaboration," *IEEE RA-L*, vol. 3, no. 1, pp. 68–75, 2018.

[4] C. Schou, R. S. Andersen, D. Chrysostomou, S. Bøgh, and O. Madsen, "Skill-based instruction of collaborative robots in industrial settings," *Robotics and Computer-Integrated Manufacturing*, vol. 53, pp. 72–80, 2018.

[5] A. De Santis, B. Siciliano, A. De Luca, and A. Bicchi, "An atlas of physical human-robot interaction," *Mechanism and Machine Theory*, vol. 43, no. 3, pp. 253–270, 2008.

[6] J. H. Chen and K. T. Song, "Collision-Free Motion Planning for Human-Robot Collaborative Safety under Cartesian Constraint," *IEEE ICRA*, pp. 4348–4354, 2018.

[7] C. T. Landi, F. Ferraguti, S. Costi, M. Bonfe, and C. Secchi, "Safety barrier functions for human-robot interaction with industrial manipulators," *ECC 2019*, pp. 2565–2570, 2019.

[8] F. Chen, P. Di, J. Huang, H. Sasaki, and T. Fukuda, "Evolutionary artificial potential field method based manipulator path planning for safe robotic assembly," *IEEE MHS*, pp. 92–97, 2009.

[9] C. Scheurer, M. D. Fiore, S. Sharma, and C. Natale, "Industrial implementation of a multi-task redundancy resolution at velocity level for highly redundant mobile manipulators," *IEEE ISR*, vol. 2016, pp. 109–117, 2016.

[10] F. Flacco, A. De Luca, and O. Khatib, "Control of Redundant Robots under Hard Joint Constraints: Saturation in the Null Space," *IEEE Trans. Robot.*, vol. 31, no. 3, pp. 637–654, 2015.

[11] P. Chotiprayanakul, D. K. Liu, D. Wang, and G. Dissanayake, "A 3-dimensional force field method for robot collision avoidance in complex environments," *ISARC*, pp. 139–145, 2007.

[12] K. P. Tee, R. Yan, and H. Li, "Adaptive admittance control of a robot manipulator under task space constraint," *IEEE ICRA*, no. 1, pp. 5181–5186, 2010.

[13] M. Kimmel, M. Lawitzky, and S. Hirche, "6D Workspace Constraints for Physical Human-Robot Interaction using Invariance Control with Chattering Reduction," *IEEE IROS*, pp. 3377–3383, 2012.

[14] M. Rauscher, M. Kimmel, and S. Hirche, "Constrained Robot Control Using Control Barrier Functions," *IEEE IROS*, pp. 279–285, 2016.

[15] H. Han and J. Park, "Robot control near singularity and joint limit using a continuous task transition algorithm," *Int. J. Adv. Robot. Syst.*, vol. 10, pp. 1–10, 2013.

[16] J. D. Muñoz Osorio, F. Allmendinger, M. D. Fiore, U. E. Zimmermann, and T. Ortmaier, "Physical Human-Robot Interaction under Joint and Cartesian Constraints," *ICRA*, pp. 185–191, 2019.

[17] S. Stramigioli, "From differential manifolds to interactive robot control," Ph.D. dissertation, University of Twente, 12 1998.

[18] G. Raiola, C. A. Cardenas, T. S. Tadele, T. De Vries, and S. Stramigioli, "Development of a Safety- and Energy-Aware Impedance Controller for Collaborative Robots," *IEEE RA-L*, vol. 3, no. 2, pp. 1237–1244, 2018.

[19] O. Khatib, "Real-time obstacle avoidance for manipulators and mobile robots," vol. 2, 1985, pp. 500–505.

[20] O. Khatib, L. Sentis, J. Park, and J. Warren, "Whole-body dynamic behavior and control of human-like robots." *Int. J. of Humanoid Robotics*, vol. 10, pp. 29–43, 03 2004.

[21] O. Khatib and B. Siciliano, *Handbook of Robotics*. Springer, 2008.

[22] N. Hogan, "Impedance control: An approach to manipulation. part i, ii, iii," vol. 107, 07 1984, pp. 304 – 313.

[23] S. Stramigioli, *Modeling and IPC Control of Interactive Mechanical Systems - A Coordinate-Free Approach*. Springer, 2001.

[24] C. Ott, *Cartesian Impedance Control of Redundant and Flexible-Joint Robots*. Springer, Berlin, Heidelberg, 2008.

[25] C. F. Cristian Secchi, Stefano Stramigioli, *Control of Interactive Robotic Interfaces*. Springer, 2007.

[26] T. Tadele, "Human-friendly robotic manipulators: safety and performance issues in controller design," Ph.D. dissertation, University of Twente, 11 2014.

[27] E. D. Fasse and C. M. Gosselin, "On the spatial impedance control of gough-stewart platforms," pp. 1749–1754 vol.2, May 1998.

[28] G. Schreiber, A. Stemmer, and R. Bischoff, "The fast research interface for the kuka lightweight robot," in *IEEE ICRA*, 2010, pp. 15–21.

[29] "ISO/TS 15066:2016 robots and robotic devices — collaborative robots," 2016. [Online]. Available: https://www.iso.org/standard/62996.html

PAPER C

Design of an Energy-Aware Cartesian Impedance Controller for Collaborative Disassembly

written by
Sebastian Hjorth, Edoardo Lamon, Dimitrios Chrysostomou, Arash Ajoudani

The paper has been published in: *IEEE/RSJ International Conference on Robotics and Automation* © 2023 IEEE Reprinted; with permission; from Sebastian Hjorth, Edoardo Lamon, Dimitrios Chrysostomou and Arash Ajoudani; Design of an Energy-Aware Cartesian Impedance Controller for Collaborative Disassembly; IEEE/RSJ International Conference on Robotics and Automation, 6/2023

2023 IEEE International Conference on Robotics and Automation (ICRA 2023)
May 29 - June 2, 2023. London, UK

Design of an Energy-Aware Cartesian Impedance Controller for Collaborative Disassembly

Sebastian Hjorth[1], Edoardo Lamon[2], Dimitrios Chrysostomou[1], and Arash Ajoudani[2]

***Abstract*— Human-robot collaborative disassembly is an emerging trend in the sustainable recycling process of electronic and mechanical products. It requires the use of advanced technologies to assist workers in repetitive physical tasks and deal with creaky and potentially damaged components. Nevertheless, when disassembling worn-out or damaged components, unexpected robot behaviors may emerge, so harmless and symbiotic physical interaction with humans and the environment becomes paramount. This work addresses this challenge at the control level by ensuring safe and passive behaviors in unplanned interactions and contact losses. The proposed algorithm capitalizes on an energy-aware Cartesian impedance controller, which features energy scaling and damping injection, and an augmented energy tank, which limits the power flow from the controller to the robot. The controller is evaluated in a real-world flawed unscrewing task with a Franka Emika Panda and is compared to a standard impedance controller and a hybrid force-impedance controller. The results demonstrate the high potential of the algorithm in human-robot collaborative disassembly tasks.**

I. Introduction

In the last decade, the European Union has started to promote the implementation of circular economy business models (CEBMs) across different manufacturing areas [1], [2]. CEBMs envision the adoption of take-back programs, efficient disassembly, and requalification processes [3]. To make such business models financially, environmentally, and socially viable, companies must recover as many undamaged components as possible. However, various challenges, for example, high variability in the condition of post-use parts, poor information about returned products, high product complexity, increasing quality requirements on recovered materials and components, and pressure on costs and efficiency, strongly limit the wide exploitation of effective disassembly processes [4].

To face the variability and uncertainties of the products' state [5], human-in-the-loop solutions such as human-robot collaborative disassembly (HRCD) cells, in which humans and robots support each other to complete a given non-destructive disassembly task, started to be conceived [6] (an example for an HRCD cell can be seen in Figure 1.).

[1]Dept. of Materials and Production, Aalborg University, Aalborg, Denmark. sshj@mp.aau.dk

[2]Human-Robot Interfaces and Interaction, Istituto Italiano di Tecnologia, Genoa, Italy. edoardo.lamon@iit.it

This research was partly supported by EU's SMART EUREKA programme S0218-chARmER, Innovation Fund Denmark (Grant no. 9118-00001B), by the EU's H2020-WIDESPREAD project no. 857061 "Networking for Research and Development of Human Interactive and Sensitive Robotics Taking Advantage of Additive Manufacturing – R2P2", and by EU's Horizon 2020 research and innovation programme under Grant Agreement No. 871237 (SOPHIA).

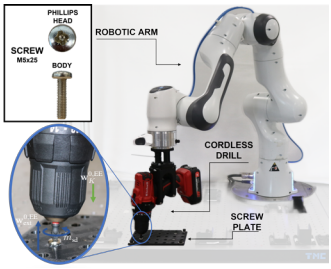

Fig. 1. Experimental setup: a manipulator, equipped with a cordless drill unfastens screws on the screw plate placed on the same workbench. The robot controller can drive the drill through a microcontroller.

Nonetheless, when it comes to physical human-robot interaction (pHRI), implementing such HRCD solutions demands high safety standards. Due to their design, collaborative-enabled robots can attain control strategies that regulate the level of compliance [7], enabling them to interact safely with unstructured environments [8]. These features are of great importance in HRCD, which presents a high risk of unpredictable events occurring due to the variability and uncertainties of the product's state. In particular, when separating two sub-assemblies, the breakage of the fasting component could lead to a contact loss between the robot's end-effector and the component, which, in turn, might result in damaged components, tools and, in the worst case, human harm.

A common fastening method that does not require destructive disassembly is screwing. However, since the product has reached its end of life, the screw condition can significantly affect the disassembly process [9]. Several control strategies for HRCD have been proposed in the literature, but only a few could deal with the realistic flawed conditions mentioned above. The work done by [10] focuses on the unscrewing of components on lithium-ion car batteries and the mechanism for changing the tool bit autonomously. It concluded that complained control schemes (i.e. impedance controller) are necessary to enable safe and direct pHRI. The work presented in [11], [12] focuses on the unfastening of screws with an external hexagonal-shaped head utilizing a KUKA LBR iiwa. Unscrewing is achieved with the help of a standard Cartesian impedance control scheme in combination with a custom nut-runner, which encloses the hexagonal-shaped screw head. Another unscrewing strategy for screws with a hexagonal shaped screw head was proposed in [13], where

screw location and orientation are detected and the unscrewing makes use of a standard Cartesian impedance controller and a conventional 2-fingers gripper. In [14], an unscrewing robotic system for the automatic disassembly of electronic devices was developed. The work investigated force and torque profiles used by humans when unscrewing Phillips and internal hex screws, to design a control strategy and tool that minimizes slippage. The proposed strategy was deployed on a position-controlled UR3 equipped with a force/torque sensor in combination with a purpose-built screwdriver with passive compliance along the tool z-axis. The drawback of using a position-controlled robot is that in case of collision, the robot's only safety mechanism is the emergency stop, which can result in a dangerous quasi-static contact scenario (e.g., clamping). Nevertheless, none of the above presented approaches considers the robot's behavior when an unpredicted faulty situation occurs during the unscrewing due to either a broken screw or failed engagement during the unscrewing process. In this context, observing, monitoring, and limiting the amount of energy and power flow that the controller is allowed to inject into the manipulator is crucial to a successful interaction. Additionally, the energy exchange between the manipulator and its environment would result in a safer task execution [15], not only by ensuring a passive behavior, but also by reducing the controller's action in potential faults. Different control schemes that could allow the limitation of the energy and power flow are presented in [15]–[17]. Therefore, the presented formalism will focus on an energy-aware control strategy with the aim to tackle the aforementioned challenges. The formalism is an extension of an energy-aware Cartesian impedance controller presented in [17], [18] in combination with a task-based energy tank and a power flow regulation mechanism proposed by [19]. Moreover, the controller's performance is evaluated and compared with the controller proposed in the literature through a set of experiments. These experiments assess the controller's ability to handle external disturbances and minimize the impact force and energy exchange with the environment. To summarize, the novel contributions of the manuscript are the following:

- The design of an energy-aware Cartesian impedance controller that uses a global energy tank with power limitation.
- An experimental comparison of the proposed energy-aware Cartesian impedance controller with a hybrid force-impedance controller [19], and a standard Cartesian impedance controller [20], in a faulty unscrewing task with a stripped screw head.

II. Problem Statement

In this paper, we examine an HRCD task with a redundant manipulator, focusing on the behavior in case of contact loss during the unscrewing. Such a scenario can occur due to a stripped screw head, corrosion, or screw damaged inside that is not detectable by external inspection (e.g., damaged threads or broken shaft) or due to a pHRI. The generalized approach for the unscrewing operation is to generate enough momentum $\mathbf{m}_z$ on the screw so that the screw rotates around its longitudinal axis, thus generating a vertical upward force $\mathbf{w}_{\text{ext}}^{0,\text{EE}}$. In order to ensure the engagement of the screwdriver bit during the unscrewing process, it is crucial to apply a force $\mathbf{w}_K^{0,\text{EE}}$ onto the screw throughout the entire unscrewing process. Common approaches to generate such force are standard Cartesian impedance and hybrid Cartesian force-impedance controllers. In case of a contact loss during the unscrewing process due to one of the scenarios mentioned above, the force applied at the screwdriver might cause the bit to hit the screwed product, damage the two components of the screwed product, or harm the operator. A graphical visualization of a successful and a failed unscrewing operation is depicted in Figure 2.

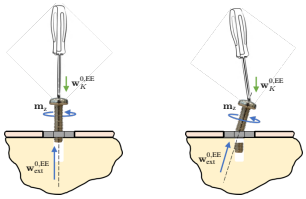

Fig. 2. Illustration of two different unscrewing scenarios. Left-hand side: a successful unscrewing operation. Right-hand side: a possible scenario for contact loss due to the screw shaft breakage during the unscrewing operation.

III. Methodology

A. Energy Aware-Impedance Controller

This control scheme presents a method that autonomously counteracts the possible non-linear behavior of the impedance model in contact scenarios [20], with the help of the energy shaping and damping injection techniques, firstly introduced in [21]. These concepts are utilized to monitor and limit the total energy of the system, as well as the power of the robot. In [17], [18], the same control strategy was successfully implemented on a kinematically redundant manipulator, whose control torques $\boldsymbol{\tau}_{\text{Control}}^{\top} \in \mathbb{R}^n$ are defined in a quasi-static condition as

$$\boldsymbol{\tau}_{\text{Control}}^{\top} = \boldsymbol{\tau}_{\text{Spring}}^{\top} - \boldsymbol{\tau}_{\text{Damp}}^{\top}, \tag{1}$$

where $\boldsymbol{\tau}_{\text{Spring}}^{\top} \in \mathbb{R}^n$ and $\boldsymbol{\tau}_{\text{Damp}}^{\top} \in \mathbb{R}^n$ are respectively generated by Cartesian springs and dampers. For a more detailed explanation of the notation hereafter, please refer to [18]. The torques $\boldsymbol{\tau}_{\text{Spring}}^{\top}$ are generated by the elastic wrench $\mathbf{w}_K^{\text{EE,EE}^{\top}} \in se^*(3)$, which can be expressed as

$$\mathbf{w}_K^{\text{EE,EE}^{\top}} = \begin{bmatrix} \mathbf{f}_K^{\text{EE,EE}^{\top}} \\ \mathbf{m}_K^{\text{EE,EE}^{\top}} \end{bmatrix} = \begin{bmatrix} \mathbf{K}_t & \mathbf{K}_c \\ \mathbf{K}_c^{\top} & \mathbf{K}_r \end{bmatrix} \Delta\boldsymbol{\eta} \tag{2}$$

where $\Delta\boldsymbol{\eta} \in se(3)$ describes the infinitesimal body twist displacement [16], the diagonal matrices $\mathbf{K}_r \in \mathbb{R}^{3\times3}$, $\mathbf{K}_t \in \mathbb{R}^{3\times3}$ hold the stiffness values for the rotational, translation springs, and $\mathbf{K}_c \in \mathbb{R}^{3\times3}$ describes the decoupling between these two terms. Force $\mathbf{f}_K^{\text{EE,EE}} \in \mathbb{R}^{1\times3}$ and momentum $\mathbf{m}_K^{\text{EE,EE}} \in \mathbb{R}^{1\times3}$ can be formulated in terms of energy by

basing their formulation on the end-effector's current transformation $\mathbf{H}^0_{\text{EE}} \in SE(3)$ and its desired goal transformation $\mathbf{H}^0_d \in SE(3)$ in the following way:

$$\begin{aligned}\widehat{\mathbf{f}}^{\text{EE,EE}}_K &= -\mathbf{R}^{\text{EE}}_d as\big(\mathbf{G}_t\widehat{\mathbf{p}}^d_{\text{EE}}\big)\mathbf{R}^d_{\text{EE}} - as\big(\mathbf{G}_t\mathbf{R}^{\text{EE}}_d\widehat{\mathbf{p}}^d_{\text{EE}}\mathbf{R}^d_{\text{EE}}\big) \\ &\quad - 2as\big(\mathbf{G}_c\mathbf{R}^d_{\text{EE}}\big) \\ \widehat{\mathbf{m}}^{\text{EE,EE}}_K &= -2as\big(\mathbf{G}_r\mathbf{R}^d_{\text{EE}}\big) - as\big(\mathbf{G}_t\mathbf{R}^{\text{EE}}_d\widehat{\mathbf{p}}^d_{\text{EE}}\widehat{\mathbf{p}}^d_{\text{EE}}\mathbf{R}^d_{\text{EE}}\big) \\ &\quad - 2as\big(\mathbf{G}_c\widehat{\mathbf{p}}^d_{\text{EE}}\mathbf{R}^d_{\text{EE}}\big),\end{aligned} \tag{3}$$

with $\mathbf{p}^d_{\text{EE}} \in \mathbb{R}^3$, $\mathbf{R}^{\text{EE}}_d \in SO(3)$ describe the translation and rotation between the end-effector's current and its desired configuration. $\mathbf{G}_{r,t,c} \in \mathbb{R}^{3\times3}$ are co-stiffnesses of the rotational spring, translational spring and coupling term [17], [18], [22] and $as()$ represents the asymmetric part of the matrix. Safety is dealt with two different controller features: (i) monitoring the total amount of energy stored in the system with the help of energy scaling and (ii) limiting the power of the system with the damping injection method, if necessary. The energy scaling method enforces a limit on the total energy of the system based on an energy-based safety metric $\overline{E}_{\text{total}}$. The total energy stored in the system can be expressed as $E_{\text{total}} = T_{\text{total}} + U_{\text{total}}$ where $T_{\text{total}} \in \mathbb{R}$ is the kinetic co-energy and $U_{\text{total}} \in \mathbb{R}$ the potential energy due to spatial springs [22]. In the event of a pHRI that results in a displacement of the end-effector, such that the statement $E_{\text{total}} > \overline{E}_{\text{total}}$ becomes true, one computes the following scaling parameter:

$$\lambda = \begin{cases} 1 & \text{if } E_{\text{total}} \leqslant \overline{E}_{\text{total}} \\ \frac{\overline{E}_{\text{total}} - T}{U_{\text{total}}} & \text{otherwise.} \end{cases} \tag{4}$$

As seen in [17] U_{total} is proportional to the co-stiffness $\mathbf{G}_{r,t,c}$. Therefore, by scaling $\mathbf{G}_{r,t,c}$ with $\lambda \in \mathbb{R}$ in the following way $\mathbf{G}_{r,t,c} \leftarrow \lambda\mathbf{G}_{r,t,c}$, the wrench generated by the springs $\mathbf{w}^{0,\text{EE}\top}_K$ is directly affected. This results in the motion generating torques from the Cartesian springs $\boldsymbol{\tau}^\top_{\text{Spring}} = \mathbf{J}(\mathbf{q})\mathbf{w}^{0,\text{EE}\top}_{\text{K}}$, where $\mathbf{w}^{0,\text{EE}\top}_K = Ad^\top_{\mathbf{H}^{\text{EE}}_0}\mathbf{w}^{\text{EE,EE}\top}_K$ with $Ad^\top_{\mathbf{H}^{\text{EE}}_0} \in \mathbb{R}^{6\times6}$ being the adjoint coordinate transformation. However, as the energy of the robot is manipulated directly, it is vital to ensure the passivity of the system. The enforcement of the passivity will be discussed in Section III-B. After limiting the total energy of the robot, the robot's power must also be overseen, as the power describes the instantaneous energy transferred when the robot makes contact with its environment. For this purpose, the damping injection method monitors the power resulting from the manipulator's motion $P_{\text{motion}} \in \mathbb{R}$:

$$P_{\text{motion}} = \big(\mathbf{J}(\mathbf{q})^\top\mathbf{w}^{0,\text{EE}\top}_K - \mathbf{B}_{\text{init}}\dot{\mathbf{q}}\big)^\top\dot{\mathbf{q}}, \tag{5}$$

with $\mathbf{B}_{\text{init}} \in \mathbb{R}^{n\times n}$ being the initial positive definite damping matrix. As soon as the robot starts moving towards a desired transformation $\mathbf{H}^0_d$, P_{motion} is monitored. In the event of P_{motion} exceeding the chosen power limit $\overline{P}_{\text{motion}} \in \mathbb{R}$, the scaling parameter $\beta \in \mathbb{R}$ is calculated:

$$\beta = \begin{cases} 1 & \text{if } P_{\text{motion}} \leqslant \overline{P}_{\text{motion}} \\ \frac{\left(\mathbf{J}^{0,0}_{\text{EE}}(\mathbf{q})^\top\mathbf{w}^{0,\text{EE}\top}_K\right)^\top\dot{\mathbf{q}} - \overline{P}_{\text{motion}}}{\dot{\mathbf{q}}^\top\mathbf{B}_{\text{init}}\dot{\mathbf{q}}} & \text{otherwise,} \end{cases} \tag{6}$$

multiplying β with the initial damping matrix $\mathbf{B}_{\text{init}}$, resulting in the damping term:

$$\boldsymbol{\tau}^\top_{\text{Damp}} = \beta\mathbf{B}_{\text{init}}\dot{\mathbf{q}}. \tag{7}$$

Hence, in the scenario in which P_{motion} exceeds $\overline{P}_{\text{motion}}$, the increase of β has a direct effect on the damping term.

B. Energy Tank Integration

The previously described methods ensure the robot's safety by manipulating the robot's energy; however, manipulating the system's energy can result in a passivity-violating behavior. Therefore, it is necessary to limit the amount of energy that the controller is allowed to inject into the system. Furthermore, to this aim, latest research, such as [19], [23]–[26] also highlights that one has to limit the rate of energy injected by the controller. The augmented energy tank described in [19] prevents the energy of the system from suddenly increasing within a single time step, thereby ensuring that the system stays stable. As mentioned in [27], the stored energy in an impedance-controlled robot can be expressed as a storage function $S = S_{\text{c}} + S_{\text{r}} \in \mathbb{R}$, which is composed of the storage functions of the controller and the robot. S_{r} is passive as the robot's energy is physically bounded from below [28]. This results in S being passive if S_{c} is passive with respect to the possible violating ports. The power flow of the possible violating ports with respect to the energy storage function S_{c} can be expressed as:

$$\dot{S}_{\text{c}} + P_{\text{dissipation}} + P_{\text{task}} = 0, \tag{8}$$

where $P_{\text{dissipation}} \in \mathbb{R}$ is the power flow due to the dissipation, and $P_{\text{task}} = -\mathbf{w}^{0,\text{EE}}_K\dot{\mathbf{x}} \in \mathbb{R}$ describes the power demand of the task and $\dot{\mathbf{x}} \in \mathbb{R}^6$ denotes the spatial end-effector velocity. The passivity of the overall system can be achieved by augmenting the storage function S_{c} with an energy tank E_{tank} bounded by upper and lower bounds $\overline{E}_{\text{tank}}$/$\underline{E}_{\text{tank}}$. The power flow of the new storage function can be expressed as

$$\dot{S}_{\text{c}} + \dot{E}_{\text{tank}} \leq 0, \tag{9}$$

where

$$\dot{E}_{\text{tank}} = P_{\text{task}}. \tag{10}$$

However, as pointed out in [19], a rapid increase of the system energy even with a bounding E_{tank} unstable behavior can occur. Therefore, the authors proposed to limit the positive power flow in the system through the following formalism:

$$P_{\text{task}} = \begin{cases} \gamma k P_{\text{task}} & \text{if } P_{\text{task}} \leq 0 \\ j P_{\text{task}} & \text{otherwise,} \end{cases} \tag{11}$$

where k and j ensure that the upper and lower bounds of E_{tank} are not violated. They are defined in such a way that the control system neither injects or takes out energy from the tank if the respective bound is reached.

$$\begin{aligned} k &= \begin{cases} 0 & \text{if } P_{\text{task}} \leq 0 \wedge E_{\text{tank}} \leq \underline{E}_{\text{tank}} \\ 1 & \text{otherwise} \end{cases} \\ j &= \begin{cases} 0 & \text{if } P_{\text{task}} \geq 0 \wedge E_{\text{tank}} \geq \overline{E}_{\text{tank}} \\ 1 & \text{otherwise} \end{cases} \end{aligned} \tag{12}$$

Additionally, the rate at which the controller can inject energy into the system is limited by:

$$\gamma = \begin{cases} \frac{\underline{P}_{\text{tank}}}{P_{\text{task}}} & \text{if } P_{\text{task}} < \underline{P}_{\text{tank}} \leq 0 \\ 1 & \text{otherwise.} \end{cases} \tag{13}$$

Where γ is defined as a ratio between the maximal allowed power flow $\underline{P}_{\text{tank}}$ and the originally calculated power flow P_{task} from the controller to the system. Integrating the above-described energy tank dynamic for the previously presented energy-aware Cartesian impedance controller, the energy scaling variable can be reformulated as

$$\lambda = \begin{cases} 1 & \text{if } E_{\text{total}} \leqslant \overline{E}_{\text{total}} \wedge k \neq 0 \\ \lambda(t-1) & \text{if } k = 0 \wedge P_{\text{task}} \leq 0 \\ \frac{\overline{E}_{\text{total}} - T}{U_{\text{total}}} & \text{otherwise.} \end{cases} \tag{14}$$

In case the energy tank is empty ($k = 0$), λ is hindered from increasing again after an interaction occurs, thereby keeping the $\mathbf{G}_{r,t,c}$ constant, which results in a standard Cartesian impedance controller with constant gains. This will reduce the controller's performance; however, it does not hinder λ from being further scaled down in order to ensure the safety metric $\overline{E}_{\text{total}}$ is not violated. Additionally, to ensure that λ does not increase when the energy tank is drained, it is important to ensure that λ does not rise too fast and result in an unstable behavior of the manipulator. Therefore, as previously mentioned, it is necessary to limit the energy that can be drained from the tank (P_{task}). Hence, applying the constraint γ, the power flow from the tank to the system results in the following $\boldsymbol{\tau}_{\text{Spring}}^{\top}$:

$$\boldsymbol{\tau}_{\text{Spring}}^{\top} = \gamma \mathbf{J}^{\top}(\mathbf{q}) \mathbf{w}_K^{0,\text{EE}\,\top} \tag{15}$$

After limiting the amount of energy that can be injected into the system through the energy scaling variable λ, the damping injection terms must be modified as follows:

$$P_{\text{motion}} = \left(\gamma \left(\mathbf{J}(\mathbf{q})^{\top} \mathbf{w}_K^{0,\text{EE}\,\top} \right) - \mathbf{B}_{\text{init}} \dot{\mathbf{q}} \right)^{\top} \dot{\mathbf{q}} \tag{16}$$

$$\beta = \begin{cases} 1 & \text{if } P_{\text{motion}} \leqslant \overline{P}_{\text{motion}} \\ \dfrac{\left(\gamma \left(\mathbf{J}(\mathbf{q})^{\top} \mathbf{w}_K^{0,\text{EE}\,\top} \right) \right)^{\top} \dot{\mathbf{q}} - \overline{P}_{\text{motion}}}{\dot{\mathbf{q}}^{\top} \mathbf{B}_{\text{init}} \dot{\mathbf{q}}} & \text{otherwise.} \end{cases} \tag{17}$$

As γ restricts the power flow to the system, it also has a direct effect on P_{motion} resulting in the following control law:

$$\tau_{\text{Control}}^{\top} = \gamma \mathbf{J}^{\top}(\mathbf{q}) \mathbf{w}_K^{0,\text{EE}\,\top} - \beta \mathbf{B}_{\text{init}} \dot{\mathbf{q}}. \tag{18}$$

IV. Experimental Results

The energy-aware Cartesian impedance controller was tested in a proof-of-concept unscrewing experiment with a stripped screw by comparing its performance with state-of-art approaches, i.e., a standard Cartesian impedance controller [20] and a Cartesian hybrid force-impedance controller with power limitation [19]. The setup consists of a Franka Emika Panada manipulator equipped with a cordless drill, a screw head fixture (screw plate), and an M5×25 Phillips head screw, as seen in Figure 1. The cordless drill is equipped with a microcontroller that communicates with the robot controller via ROS interface. The experiment can be divided into two different phases: 1) unscrewing, and 2) interaction with a human. For our use-case, it is assumed that the position of the screw is known a priori, similarly to the work of [11] who discusses an exploration method for successful tool insertion. The unscrewing phase starts with the tool-center-point (TCP) being already inserted in the screw head and begins to increase the force along the TCPs z-axis until it reaches the engagement force $\mathbf{f}_{\text{engage},z}$. For the standard and the presented energy-aware Cartesian impedance controller, $\mathbf{f}_{\text{engage},z}$ is achieved by moving the desired transformation $\mathbf{H}_d^0$ along the z-axis in the negative direction, thereby preventing the screw bit from slipping. As soon as $\mathbf{f}_{\text{engage},z}$ is reached, the drill starts, and simultaneously, the desired TCP pose is translated along the z-axis mentioned above in a positive direction to maintain $\mathbf{w}_{ext,z}^{0,EE}$ approximately constant. With the hybrid force-impedance controller, such mechanism is ensured by the force loop of the z-axis. To systematically generate contact loss, we use a simulated broken shaft, i.e., a screw $10\ \text{mm}$ shorter than expected by the robot motion planner. In this way, the controller still exerts some force while the shaft comes out from the plate. For this reason, due to $\mathbf{w}_K^{0,\text{EE}}$, the screw slips, hence losing the contact between the screw and the drill bit and the robot end-effector moves in z direction towards its current $\mathbf{H}_d^0$ and eventually hits the table. To further evaluate the suitability of the controller in human-populated environments, after the unscrewing phase, the robot's end-effector was disturbed by a human in the interaction phase. Snapshots of the experiment are available

TABLE I

Control parameters used during the different experiments.

Cartesian Impedance controller		
Translational spring stiffness	$\mathbf{K}_t$	$900 \cdot \mathbf{I}_3$
Rotational spring stiffness	$\mathbf{K}_r$	$40 \cdot \mathbf{I}_3$
Coupling spring stiffness	$\mathbf{K}_c$	$0 \cdot \mathbf{I}_3$
Hybrid Force-Impedance controller		
Translational spring stiffness	$\mathbf{K}_t$	$100 \cdot \mathbf{I}_3$
Rotational spring stiffness	$\mathbf{K}_r$	$10 \cdot \mathbf{I}_3$
Coupling spring stiffness	$\mathbf{K}_c$	$0 \cdot \mathbf{I}_3$
Desired force	$\mathbf{w}_{\text{desired},z}$	$-\mathbf{f}_{\text{engage},z}$
Energy-Aware Impedance controller		
Translational spring stiffness	$\mathbf{K}_t$	$900 \cdot \mathbf{I}_3$
Rotational spring stiffness	$\mathbf{K}_r$	$40 \cdot \mathbf{I}_3$
Coupling spring stiffness	$\mathbf{K}_c$	$0 \cdot \mathbf{I}_3$
Max. allowed energy	$\overline{E}_{\text{total}}$	0.7J
Max. allowed power	$\overline{P}_{\text{motion}}$	0.5W
Initial damping	$\mathbf{B}$	$5 \cdot \mathbf{I}_7$
Energy Tank & Others		
Engagement force	$\mathbf{f}_{\text{engage},z}$	15N
Max. allowed power to be extracted	$\underline{P}_{\text{tank}}$	-0.175W
Max. Energy level in the tank	$\overline{E}_{\text{tank}}$	5J
Min. Energy level in the tank	$\underline{E}_{\text{tank}}$	0.5J
Initial Energy level in the tank	E_{tank}	3J

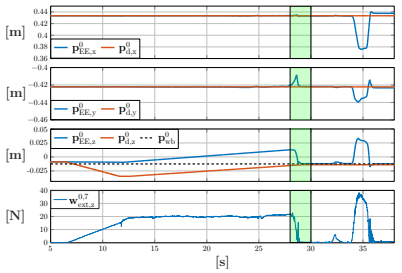

Fig. 3. Visualizes the observable quantities of the Cartesian impedance controller. The difference between current $\mathbf{p}^0_{\text{EE}}$ and desired position $\mathbf{p}^0_{\text{d}}$ as well as the workbench position $\mathbf{p}^0_{\text{wb}}$ and the linear z-component of the external force applied on the TCP $\mathbf{w}^{0,EE}_{ext,z}$.

in Figure 5. The control parameters chosen for each control scheme are shown in Table I. The force value 15 N was chosen based on an initial investigation which has shown that a screw tightened with 3 Nm needs approximately 15-20 N of force applied to avoid slippage. The maximum energy threshold $\overline{E}_{\text{total}}$ was selected according to ISO/TS 15066:2016 [29] that specified a range of 0.52 - 2.5 J, the value for $\overline{P}_{\text{motion}}$ and the threshold for the power limit on the energy tank $\underline{P}_{\text{tank}}$ were picked according to earlier results in [17], [18] and in [24], respectively.

A. Standard Cartesian Impedance Controller

As mentioned above, to generate the force required to perform the unscrewing process, $\mathbf{p}^0_{d,z}$ was moved incrementally below the screw head until $\mathbf{w}^{0,\text{EE}}_{K,z}$ reaches the desired force (Table I). This change along the z-axis results in an increase in the external force applied, as seen in the time period $7-12.5$ s in Figure 3. The time period between $12.5-28$ s marks the unscrewing phase, where the incremental change along the z-axis is changed in a direction such that $\mathbf{w}^{0,EE}_{ext,z}$ is kept within the acceptable working range. Focusing on the external force, one can see how force decreases due to the missing counter force by the screw, which drives the robot to hit the workbench with an impact force of 15 N before the equilibrium pose of the controller reaches the surface (highlighted with a green area). In the interaction phase, which starts immediately afterwards, the robot's end effector is displaced by pHRI at 32 s where the spatial spring generated a force of 37 N to counteract the disturbance. Once the end effector has reached its maximal displacement of 0.34 m, it is released, and the robot moves back towards its desired configuration and hits the workbench a second time with 18 N.

B. Hybrid Force-Impedance Controller

In the case of the hybrid controller, the force that is necessary to enable the the screw to be unscrewed is generated by the force control part. Therefore, it is not necessary to manipulate the desired pose $\mathbf{H}^0_d$, as seen in Figure 4. After 5 s, the desired force of 20 N is reached and the unscrewing phase

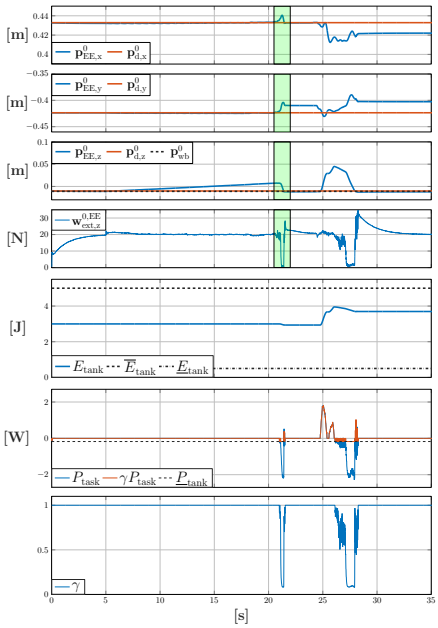

Fig. 4. Visualizes the observable quantities of the hybrid force impedance controller. The difference between current $\mathbf{p}^0_{\text{EE}}$ and desired position $\mathbf{p}^0_{\text{d}}$ as well as the workbench position $\mathbf{p}^0_{\text{wb}}$, the linear z-component of the external force applied on the TCP $\mathbf{w}^{0,EE}_{ext,z}$ and the energy tank E_{tank} and its power flow P_{task}.

begins, which lasts until 21 s. After the contact loss, the robot gets accelerated by the force controller in order to maintain the desired force. Even though the restrictions on the implemented energy tank already reduce the rate by which the controller can inject energy into the system (see Figure 4), the resulting force is still significant (approx. 26 N). In the interaction phase, which begins immediately afterwards, the robot end-effector is displaced by pHRI at 24.5 s. During the displacement of the robot, one can see how the force response tries to adapt to the applied force. When the end effector is released, the tank's power limit takes effect, thereby reducing the force response; however, even though the robot makes contact with the work surface with a significant impact force (approx. 34 N).

C. Energy-Aware Controller

The unscrewing task here follows the same procedure as the standard Cartesian impedance controller, where the equilibrium's pose has to be incrementally moved along the screw's longitudinal axis. The desired force is reached after 10 s (Figure 6), and the equilibrium pose is again translated in an upward direction during the unscrewing phase. At

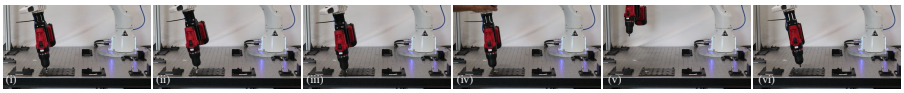

Fig. 5. Snapshots of the experiment with the energy-aware impedance controller. A video of the experiments is available in the multimedia extension and at https://www.youtube-nocookie.com/embed/SgYFHMlEl0k. From left to right: (i) unscrewing, (ii) contact loss, (iii) impact with table, (iv) pHRI, (v) end of the pHRI, (vi) second impact with table.

the point of contact loss (26 s), the end effector starts to move towards its equilibrium pose thereby making contact with the workbench at 29 s without a significant impact force (approx. 1.2 N). A similar behavior can be observed during the interaction phase, where the end effector hits the workbench after the end of the disturbance without resulting in a significant impact force (approx. 2.6 N). This can be attributed to the effect of the spring energy scaling and the power flow regulation based on the power limit in the energy tank. When λ decreases, the stiffness of the spring also decreases and thereby reduces the energy in the system; however, when λ increases again, energy is injected back into the system; if this injection is not kept in check, it can result in unstable and non-passive behavior. Therefore, the rate at which energy can be injected must be monitored and limited. When comparing the response of λ and γ, one can see that at every instant when λ increases, γ decreases. As in (15), γ directly affects the rate at which energy can be injected into the system, that is, it regulates how fast λ can increase at each time step. Additionally, the energy tank also ensures that λ can only be increased if there is energy in the tank ($E_{\text{tank}} > \underline{E}_{\text{tank}}$). If the energy tank is depleted, λ remains constant.

V. Discussion & Conclusions

This work presents an energy-based control formalism in combination with an augmented energy tank to ensure the passivity of the system. To the best of the authors knowledge, such a formalism has not been applied to a disassembly task before. The capabilities of the formalism to handle contact loss and pHRI are evaluated on an unscrewing task. Additionally, its performance was compared to a standard Cartesian impedance controller as well as a hybrid force-impedance controller. When it comes to applying and tracking a constant force onto the screw, the force-impedance control outperforms the standard Cartesian impedance controller and the energy-aware controller; however, in case of a contact loss, it generates the highest impact force among the compared controllers. On the other hand, the Cartesian impedance controller is intrinsically passive, but, due to the task requirements in terms of force and, thus, stiff behavior, a significant impact force is generated, which is not in compliance with pHRI. The presented formalism introduces an energy-aware scaling mechanism to the Cartesian impedance controller, as well as a power flow regulated energy tank, which ensures the passivity of the system. Therefore, enabling the manipulator to react in a compliant manner in the scenario of contact loss or pHRI, the manipulator stays within its predefined energy thresholds.

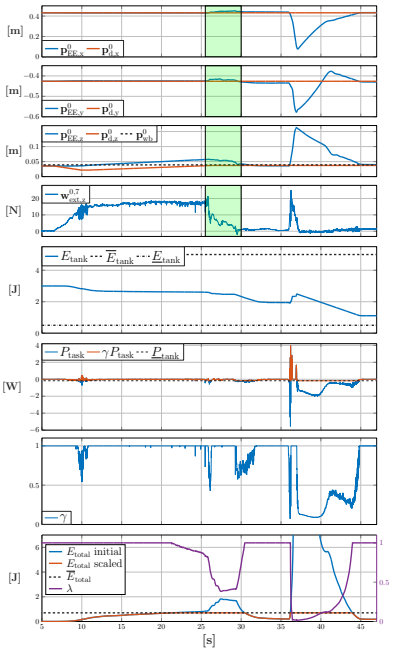

Fig. 6. Visualizes the observable quantities of the energy-aware impedance controller. The difference between current $\mathbf{p}^0_{\text{EE}}$ and desired position $\mathbf{p}^0_{\text{d}}$, as well as the workbench position $\mathbf{p}^0_{\text{wb}}$, the linear z-component of the external force applied on the TCP $\mathbf{w}^{0,EE}_{ext,z}$, the energy tank E_{tank} and its power flow P_{task} as well as the energy scaling of the total energy E_{total}.

Notably, during the pHRI, a larger displacement could be achieved whilst reducing the impact force between the tool and the robot (up to 92%), given the same initial end-effector impedance values as the classic Cartesian impedance controller. Moreover, when facing comparable disturbances, such as in the contact loss scenario, the impact force is reduced by up to 91% and 95% for the Cartesian Impedance and the hybrid force impedance controller respectively. One drawback of the presented control formalism is the parameterization of the power flow limit, i.e. the size of the energy tank must be designed manually. In the direction, in [23] the power flow formulation depends on the remaining energy in the tank.

REFERENCES

[1] E. Commission, "Circular Economy Action Plan," European Commission, Tech. Rep., 2015.

[2] European Environment Agency, "Recycling industry can boost the European economy," p. 2020, 2020. [Online]. Available: https://www.eea.europa.eu/highlights/recycling-industry-can-boost-the

[3] T. E. Graedel, J. Allwood, J.-P. Birat, B. K. Reck, S. F. Sibley, G. Sonnemann, M. Buchert, and C. Hagelüken, *UNEP (2011) Recycling Rates of Metals – A Status Report, A Report of the Working Group on the Global Metal Flows to the International Resource Panel.* International Resource Panel, 2011.

[4] T. Tolio, A. Bernard, M. Colledani, S. Kara, G. Seliger, J. Duflou, O. Battaia, and S. Takata, "Design, management and control of demanufacturing and remanufacturing systems," *CIRP Ann. - Manuf. Technol.*, vol. 66, no. 2, pp. 585–609, 2017.

[5] K. Elo and E. Sundin, "Automatic dismantling challenges in the structural design of LCD TVs," *Procedia CIRP*, vol. 15, pp. 251–256, 2014.

[6] S. Hjorth and D. Chrysostomou, "Human–robot collaboration in industrial environments: A literature review on non-destructive disassembly," *Robotics and Computer-Integrated Manufacturing*, vol. 73, p. 102208, 2022.

[7] J. Zhao, A. Giammarino, E. Lamon, J. M. Gandarias, E. D. Momi, and A. Ajoudani, "A hybrid learning and optimization framework to achieve physically interactive tasks with mobile manipulators," *IEEE Robotics and Automation Letters*, vol. 7, no. 3, pp. 8036–8043, 2022.

[8] A. Pereira, M. Baumann, J. Gerstner, and M. Althoff, "Improving efficiency of human-robot coexistence while guaranteeing safety: Theory and user study," *IEEE Transactions on Automation Science and Engineering*, pp. 1–14, 2022.

[9] S. Vongbunyong and W. H. Chen, *Disassembly Automation: Automated Systems with Cognitive Abilities*, ser. Sustainable production, life cycle engineering and management. Cham: Springer International Publishing AG, 2015.

[10] W. H. Chen, K. Wegener, and F. Dietrich, "A robot assistant for unscrewing in hybrid human-robot disassembly," *2014 IEEE Int. Conf. Robot. Biomimetics, IEEE ROBIO 2014*, pp. 536–541, 2014.

[11] R. Li, C. Ji, Q. Liu, Z. Zhou, D. T. Pham, J. Huang, Y. Tan, M. Qu, Y. Wang, M. Kerin, K. Jiang, and S. Su, "Unfastening of Hexagonal Headed Screws by a Collaborative Robot," *IEEE Trans. Autom. Sci. Eng.*, pp. 1–14, 2020.

[12] J. Huang, D. T. Pham, R. Li, M. Qu, Y. Wang, M. Kerin, S. Su, C. Ji, O. Mahomed, R. Khalil, D. Stockton, W. Xu, Q. Liu, and Z. Zhou, "An experimental human-robot collaborative disassembly cell," *Computers & Industrial Engineering*, vol. 155, p. 107189, 2021.

[13] A. Rastegarpanah, R. Ner, R. Stolkin, and N. Marturi, "Nut unfastening by robotic surface exploration," *Robotics*, vol. 10, no. 3, 2021.

[14] D. Mironov, M. Altamirano, H. Zabihifar, A. Liviniuk, V. Liviniuk, and D. Tsetserukou, "Haptics of screwing and unscrewing for its application in smart factories for disassembly," in *International Conference on Human Haptic Sensing and Touch Enabled Computer Applications*. Springer, 2018, pp. 428–439.

[15] J. Lachner, F. Allmendinger, E. Hobert, N. Hogan, and S. Stramigioli, "Energy budgets for coordinate invariant robot control in physical human–robot interaction," *The International Journal of Robotics Research*, vol. 40, no. 8-9, pp. 968–985, 2021.

[16] S. Stramigioli, *Modeling and IPC Control of Interactive Mechanical Systems - A Coordinate-Free Approach*. Springer, 2001.

[17] G. Raiola, C. A. Cardenas, T. S. Tadele, T. de Vries, and S. Stramigioli, "Development of a safety- and energy-aware impedance controller for collaborative robots," *IEEE Robotics and Automation Letters*, vol. 3, no. 2, pp. 1237–1244, 2018.

[18] S. Hjorth, J. Lachner, S. Stramigioli, O. Madsen, and D. Chrysostomou, "An energy-based approach for the integration of collaborative redundant robots in restricted work environments," in *2020 IEEE/RSJ International Conference on Intelligent Robots and Systems (IROS)*. IEEE, 2020, pp. 7152–7158.

[19] E. Shahriari, L. Johannsmeier, E. Jensen, and S. Haddadin, "Power flow regulation, adaptation, and learning for intrinsically robust virtual energy tanks," *IEEE Robotics and Automation Letters*, vol. 5, no. 1, pp. 211–218, 2019.

[20] C. Ott, *Cartesian Impedance Control of Redundant and Flexible-Joint Robots*. Springer, Berlin, Heidelberg, 2008.

[21] S. Stramigioli, "From differential manifolds to interactive robot control," Ph.D. dissertation, University of Twente, 12 1998.

[22] T. Tadele, "Human-friendly robotic manipulators: safety and performance issues in controller design," Ph.D. dissertation, University of Twente, 11 2014.

[23] Y. Michel, C. Ott, and D. Lee, "Safety-aware hierarchical passivity-based variable compliance control for redundant manipulators," *IEEE Transactions on Robotics*, 2022.

[24] N. Ramuzat, S. Boria, and O. Stasse, "Passive inverse dynamics control using a global energy tank for torque-controlled humanoid robots in multi-contact," *IEEE Robotics and Automation Letters*, vol. 7, no. 2, pp. 2787–2794, 2022.

[25] B. Gerlagh, F. Califano, S. Stramigioli, and W. Roozing, "Energy-aware adaptive impedance control using offline task-based optimization," in *2021 20th International Conference on Advanced Robotics (ICAR)*. IEEE, 2021, pp. 187–194.

[26] F. Califano, D. van Dijk, and W. Roozing, "A task-based post-impact safety protocol based on energy tanks," *IEEE Robotics and Automation Letters*, vol. 7, no. 4, pp. 8791–8798, 2022.

[27] J. Lachner, F. Allmendinger, S. Stramigioli, and N. Hogan, "Shaping impedances to comply with constrained task dynamics," *IEEE Transactions on Robotics*, 2022.

[28] S. Stramigioli, "Energy-aware robotics," in *Mathematical Control Theory I*, M. K. Camlibel, A. A. Julius, R. Pasumarthy, and J. M. Scherpen, Eds. Cham: Springer International Publishing, 2015, pp. 37–50.

[29] "ISO/TS 15066:2016 robots and robotic devices — collaborative robots," 2016. [Online]. Available: https://www.iso.org/standard/62996.html

PAPER D

Enabling passivity for Cartesian workspace restrictions

written by
Sebastian Hjorth, Johannes Lachner, Arash Ajoudani, Dimitrios Chrysostomou;

The paper has been submitted to: *IEEE International Conference on Robotics and Automation 2024*

ISSN (online): 2446-1636
ISBN (online): 978-87-7573-663-8

AALBORG UNIVERSITY PRESS